UNIVERSITY OF TROMSØ UIT

FACULTY OF SCIENCE AND TECHNOLOGY
DEPARTMENT OF GEOLOGY

Petrogenesis and tectonic setting of the mafic-ultramafic rock association from NW Senja, West Troms Basement Complex

Nadezda Priyatkina

GEO-3900 Master's Thesis in Geology

February 2013

Abstract

The studied mafic-ultramafic rock association occurs within Archean tonalitic gneisses and metasupracrustal suites of the Astridal belt belonging to the West Troms Basement Complex in the northwestern part of the Senja Island. The rock association appears in lens-shaped bodies, up to 200 m long, which are oriented conformal to the major metamorphic fabric of the host rock. The rock association is made up by interlayered units of green spinel-bearing olivine orthopyroxene-hornblendite, hornblende peridotite, olivine hornblendite, hornblendite and amphibolite (metagabbroic rock). Microscope studies and whole rock geochemical data indicate that the ultramafic rocks represent a single magmatic series of mafic and ultramafic olivine-amphibole cumulates, which have been significantly affected by metamorphism. Igneous mineral and whole rock trace element data indicate MORB affinity of the cumulates and suggest their emplacement in oceanic rift or rifted continental margin setting. The studied cumulates may represent a crustal remnant of the Paleoproterozic Svecofennian ocean. The rocks were metamorphosed together with the supracrustal suites of the Astridal belt during the major Svecofennian event about 1.74 Ga ago as indicated by a U-Pb age of metamorphic zircons from the metagabbroic rock belonging to the studied suite.

Acknowledgment

This study was made possible through the Quota Scholarship Scheme, which is a funding scheme sponsored by the Norwegian Ministry of Education and Research. I would like to thank Kåre Kullerud (UiT) for introducing geology of NW Senja to me, his great support during field work, help with analytical procedures and with interpretation of data. This thesis would have been impossible also without Kåre Kullerud's patience to correct my written English. Many thanks to Fernando Corfu (UiO) for great debates on Senja geology and processing of U-Pb zircon dating and Steffen Bergh for discussions of field observations and introducing to me constraints on structural and tectonic evolution of the Astridal belt. Productive advices from Pritam Nasipuri (UiT), Erling Ravna (UiT), Oliver Pluemper (UiO), Valery Ivanikov (SPbSU) enabled to understand the origin of the studied rocks. Finally, I would like to thank my friend Anna Pryadunenko, who was embracing my work and my love to ultramafic rocks.

Nadya Priyatkina,

30 January 2013.

Contents

Introduction

The West Troms Basement Complex (WTBC), which is the northwesternmost part of the Precambrian basement of the Fennoscandian shield, is a key area for making up new constraints on the Precambrian evolution of the Fennoscandian shield. Furthermore, many valuable ore deposits are hosted by Archean and Paleoproterozoic suites in Finland and NW Russia (e.g. Lahtinen et al., 2005). The comparison and correlation of major rock associations of the WTBC along the strike to the major geological units of the southeastern parts of Fennoscandia may bring valuable scientific input in development of ore prospecting activities in northern Norway.

Bergh et al. (2010) presented the first full overview for the region based mainly on structural investigations. The main age constraints are suggested by Corfu et al. (2003). However, there are still a lot of rock associations of uncertain age and origin, such as some of the supracrustal belts occurring within the Archean basement gnesisses of WTBC. The evolution of the Archean continental margin, as well as the position of the suture zone between the Archean and Svecofennian zone in WTBC also remains uncertain. Therefore, petrological studies of the ultramafic and mafic rocks, which are widespread within the Astridal supracrustal belt of presumed Paleoproterozoic age, and also within the adjacent Archean basement gneisses, will be of significant importance for understanding the tectonic setting of the supracrustal belts in the western part of WTBC, e.g. Senja Shear Belt. The understanding of the tectonic setting of the Senja ultramafics may also provide a link between the Astridal belt and some generation of the Paleoproterozoic supracrustal formations in Finland and NW Russia.

The studied layered mafic-ultramafic suite from NW Senja is probably not the best opportunity for the above mentioned research purpose, because the rocks occur as dismembered bodies within an area of amphibolite facies metamorphism. The high degree of metamorphic alteration and tectonic modification of the contacts to the host rock complicates the interpretation of the petrogenesis. However, this case is relevant for a methodological aspect of research. Many researchers pointed out the difficulties associated with the genetic interpretation of ultramafic rocks, as they can represent continental or oceanic mantle, or oceanic crust. Further, they may represent early subduction-related cumulates or other types of layered intrusions (e.g. Moores, 1973; Coleman, 1971, Moores and Raymond, 1972; Wyllie, 1967), or even be produced through dehydration reactions of chlorite- and serpentine-rich rocks through progressive metamorphism (e.g. Evans, 1977; Khedr and Arai, 2011; Vance and Dungan, 1977). Indeed, rocks

showing similar rock-forming mineral assemblages to the Senja ultramafics are relatively widespread in various orogenic belts and have been reported from the Vammala Nickel Belt, Finland (Peltonen, 1995) and several other occurrences (e.g. Desmarais, 1981; Paktunc, 1984; Tracy et al, 1984; Berger et al., 2012). Such rocks have often been referred to as “metamorphosed ultramafics” and some authors (e.g. Berger et al., 2012) pointed out the uncertainty of the origin for some of the rock-forming mineral assemblages, basically whether they are metamorphic or igneous. Thus, the second purpose for this project is to figure out the petrogeneses of the studied rocks.

Thus, the present study aims to (1) reveal the petrogensis and protolith characteristics of the mafic-ultramafic suite from NW Senja, (2) establish its age and tectonic setting, and (3) suggest possible implications for the tectonic position of the Astridal belt within the WTBC and the entire Fennoscandian shield. To solve these questions, a number of studies such as field investigations including detailed mapping, microscope studies, whole rock geochemical analysis, mineral chemistry analyses and U-Pb zircon dating have been carried out.

Chapter 1. Geological setting

The Island of Senja belongs to the West Troms Basement Complex (WTBC), which is exposed west of the Caledonian nappes and represents a part of the Precambrian rock association making up the Fennoscandian shield (Fig.1.1). The WTBC comprises the following major rock units: 1) Neoarchaean gneisses of various compositions, 2.89-2.56 Ga; 2) Neoarchaean and Palaeoproterozoic supracrustal rocks, 2.85-1.97 Ga; 3) Early Palaeoproterozoic mafic dyke swarms (2.4-2.22 Ga) and 4) Svecofennian igneous suites, 1.8-1.76 Ga (Fig. 1.2., Bergh et al, 2011).

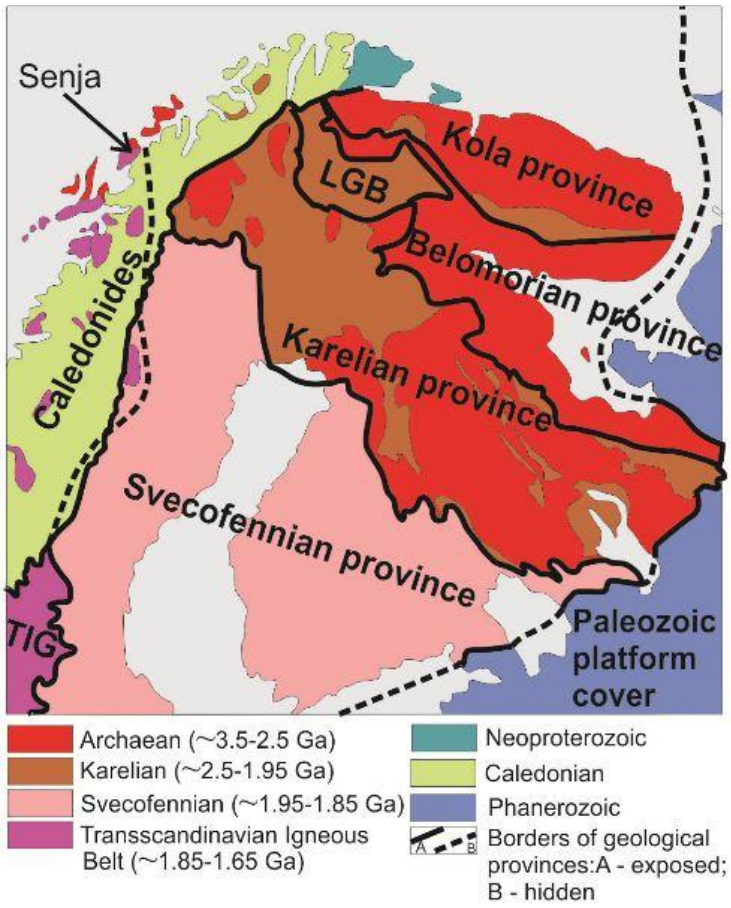

Fig.1.1. Location of the Island of Senja on the map showing the major tectonic units of the Fennoscandian shield, simplified after Koistinen et al. (2001), Gaal and Gorbatchev (1987).

The Island of Senja is located along the continuation of the boundary between the Achaean and Svecofennian domains of the Fennoscandian shield (Fig.1.1). The southwestern part of the island is dominated by intrusive rocks of 1.8-1.77 Ga, related to the Transscandinavian Igneous Belt. The northeastern part of Senja is represented by the more than 30 km wide Senja shear belt (Fig.1.2) and comprises Achaean basement gneisses (2.8 - 2.75 Ga, Kullerud et al., 2006) and lens-shaped inliers of folded Paleoproterozoic metasupracrustals (Astridal, Torsnes and Svanfjellet

belts). The latter are represented by mafic volcanic rocks and mainly terrigenous sedimentary successions. Recent results of U-Pb zircon dating from a gabbro in the Mjelde-Skorelvatn belt and of detrital zircon dating from a metapsammite in the Torsnes belt yield the ages of 1992±2 Ma and up to 1970±14 Ma of an intrusive event and maximum age of deposition respectively (Myhre et al, 2011). Bergh et al. (2010) proposed for the neighboring Astridal belt - the area of this study - the same age based on similarities in architecture of two belts and their lithological characteristics.

The studied layered mafic-ultramafic rock association occurs both within the Archean basement gneisses and the Astridal supracrustal belt (Fig.1.3), which is 2-4 km wide and strikes in NW-SE direction, and is exposed for nearly 20 km along strike. It consists of greenschist- to amphibolite facies volcanic and siliciclastic rocks, tuffaceous rocks, conglomerates, marbles, micaschists (garnet-rich in the north) and metapsammites in the south (Fareth 1983; Pedersen 1997). Whithin the Astridal belt, primary depositional contacts between gneisses and supracrustal rocks have never been observed due to their tectonic modification (Bergh et al, 2011).

Based on structural observations as well as isotope data, the deformation and medium grade metamorphism of the Astridal belt, as well as for the entire WTBC, has been inferred to reflect mainly a Svecofennian tectono-thermal event with much less significant Caledonian overprint (Bergh et al., 2010). Deformation of the Astridal belt is characterized by (1) gently, NW-plunging and NE-vergent isoclinal folds and probable thrusts, (2) tight, moderately north-plunging macro-folds that refolded the earlier folds and (3) late stage subvertical folds accompanied by steep, mostly sinistral strike-slip shear zones (Pedersen, 1997; Bergh et al., 2010), implying a multiphase deformation history of the Astridal supracrustal belt. The major amphibolite facies metamorphic event has been related to the first stage of deformation and occurred nearly 1760-1740 Ma ago, while later deformation has been accompanied mostly by emplacement of granite pegmatites (Fernando Corfu, personal communication 2012; this study).

The most detailed sampling during the present study has been done along the southwestern shore of Baltsfjord within the supracrustal zone, which for the first time is described here. Additional scattered field investigations and sampling have been carried out in other parts of NE Senja (Fig.1.3). All observation points and sample locations are shown on topographic maps in Appendix 1.

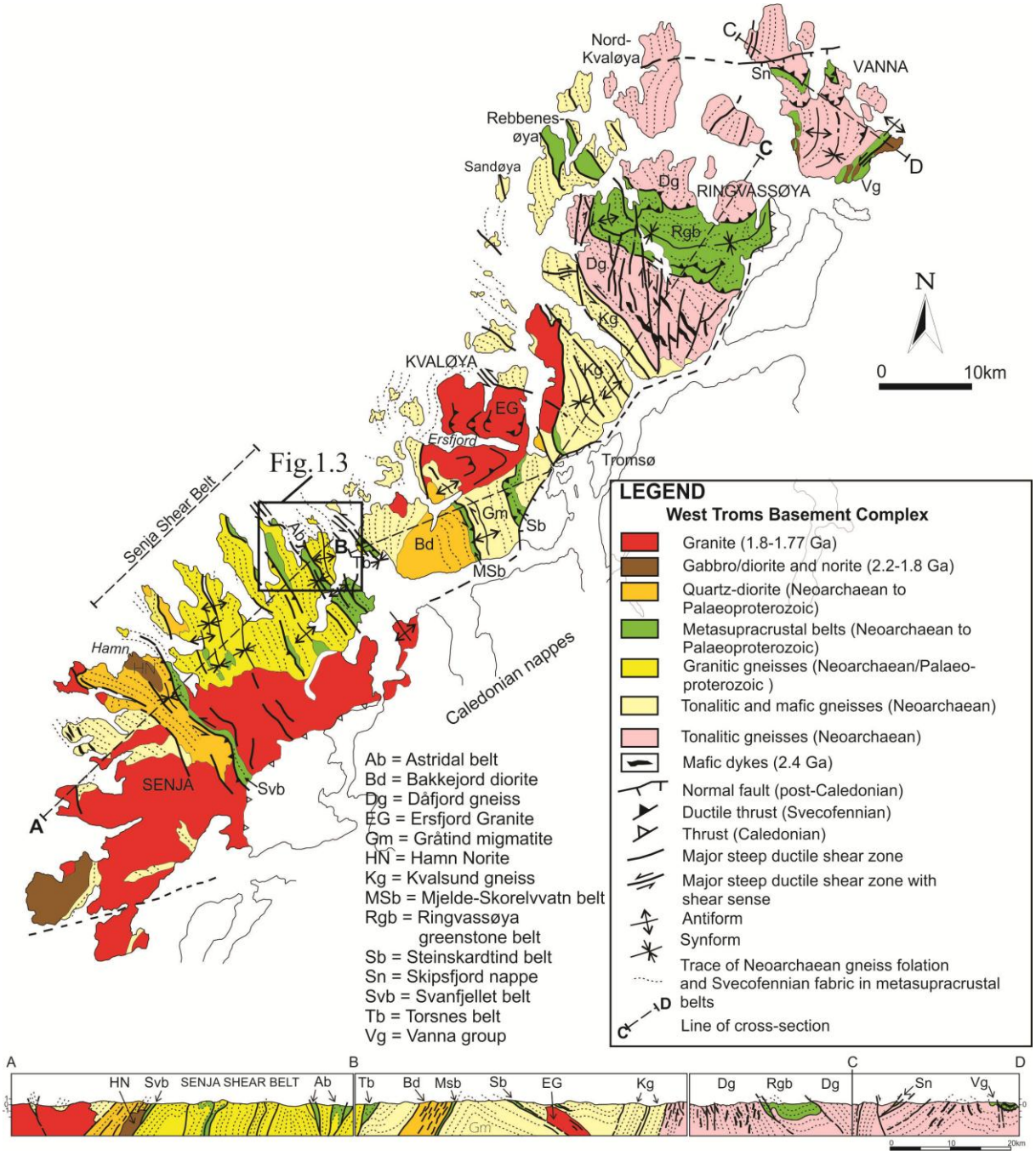

Fig.1.2. Regional geologic-tectonic map and cross-section of the West Troms Basement Complex (from Bergh et al., 2010)

.

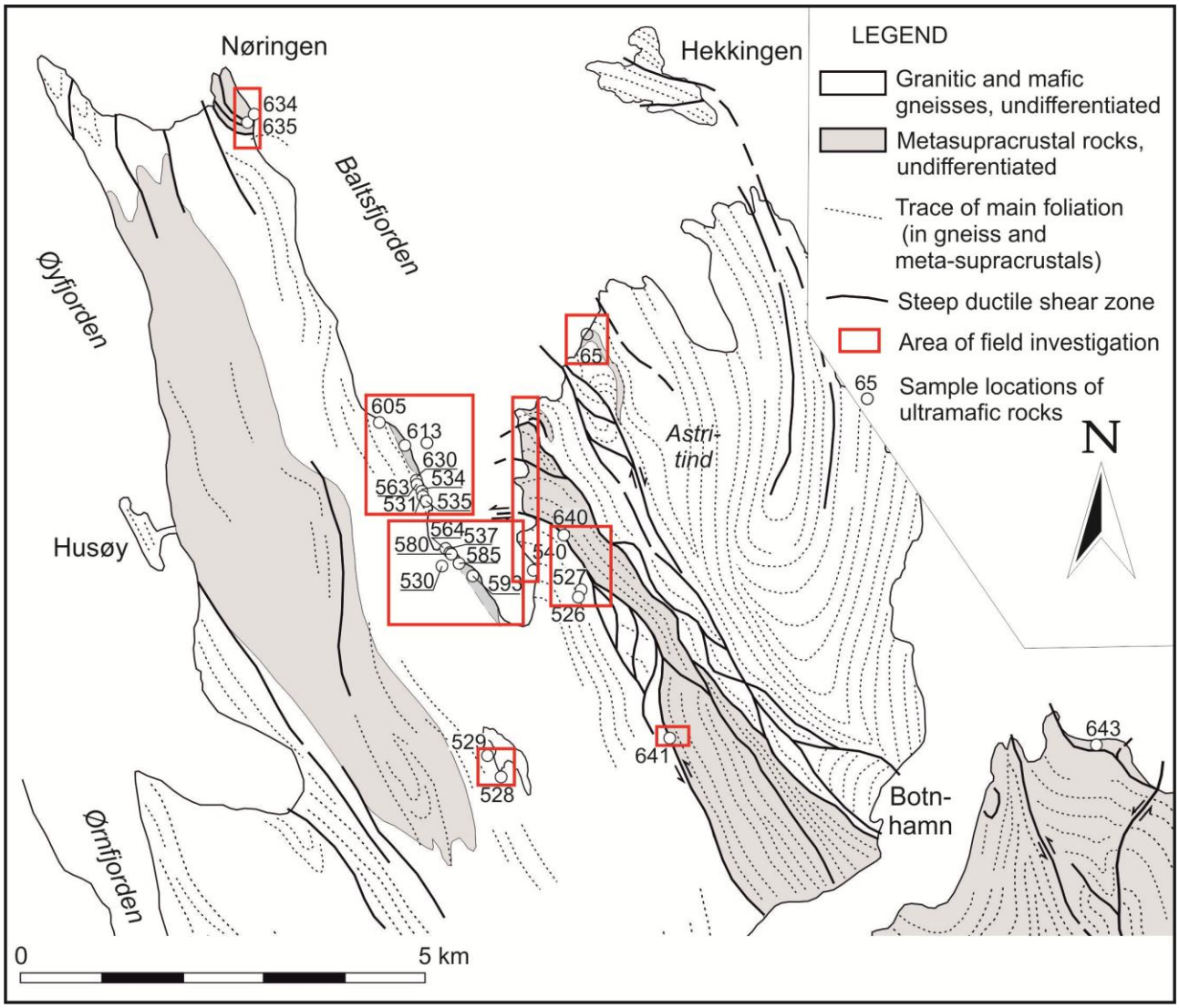

Fig.1.3. Schematic map simplified and partly modified after Bergh et al. (2010) showing the main areas of sampling and field investigations.

Chapter 2. Field occurrence of the layered mafic-ultramafic association

2.1. Relation to other lithological units of the Astridal belt

Geological maps of the main part of the Astridal belt have been composed by Pedersen (1997). His maps cover the eastern shore of Baltsfjord, as well as the Nøringen area. In this study the poorly studied southwestern shore of Baltsfjord has been mapped in detail (Fig.2.1.1.). Field observations indicated the presence of both basement and supracrustal rock associations in this area, comparable to those observed by Pedersen (1997) and Bergh et al. (2010). Thus, the newly described supracrustal zone might be considered as a part of the Astridal belt that makes a turn (F3-fold) from the main section westwards and merges back into a NNW-SSE trend.

The following major lithological unites have been documented:

1) **Tonalitic gneiss**

The basement gneiss outcropping at the southwestern shore and further inland is represented by a massive light pinkish plagioclase-dominating variety. The gneiss encloses a set of amphibolitized mafic dyke-like bodies. The thickness of the mafic enclaves varies from a few tens of cm to 1-1.5 m. Bodies occurring both conformal to strike of the entire structure (point 536, Fig.2.1.1, Fig.2.1.2) and slightly folded (northeast of map sheet A at Fig.2.1.1) have been documented. Any intrusive relationship between the gneiss and the amphibolite enclaves cannot be documented, due to tectonic modification of the contacts.

Fig.2.1.2. Tonalitic gneiss with amphibolite dyke-like enclaves, western shore of Baltsfjord (locality 536).

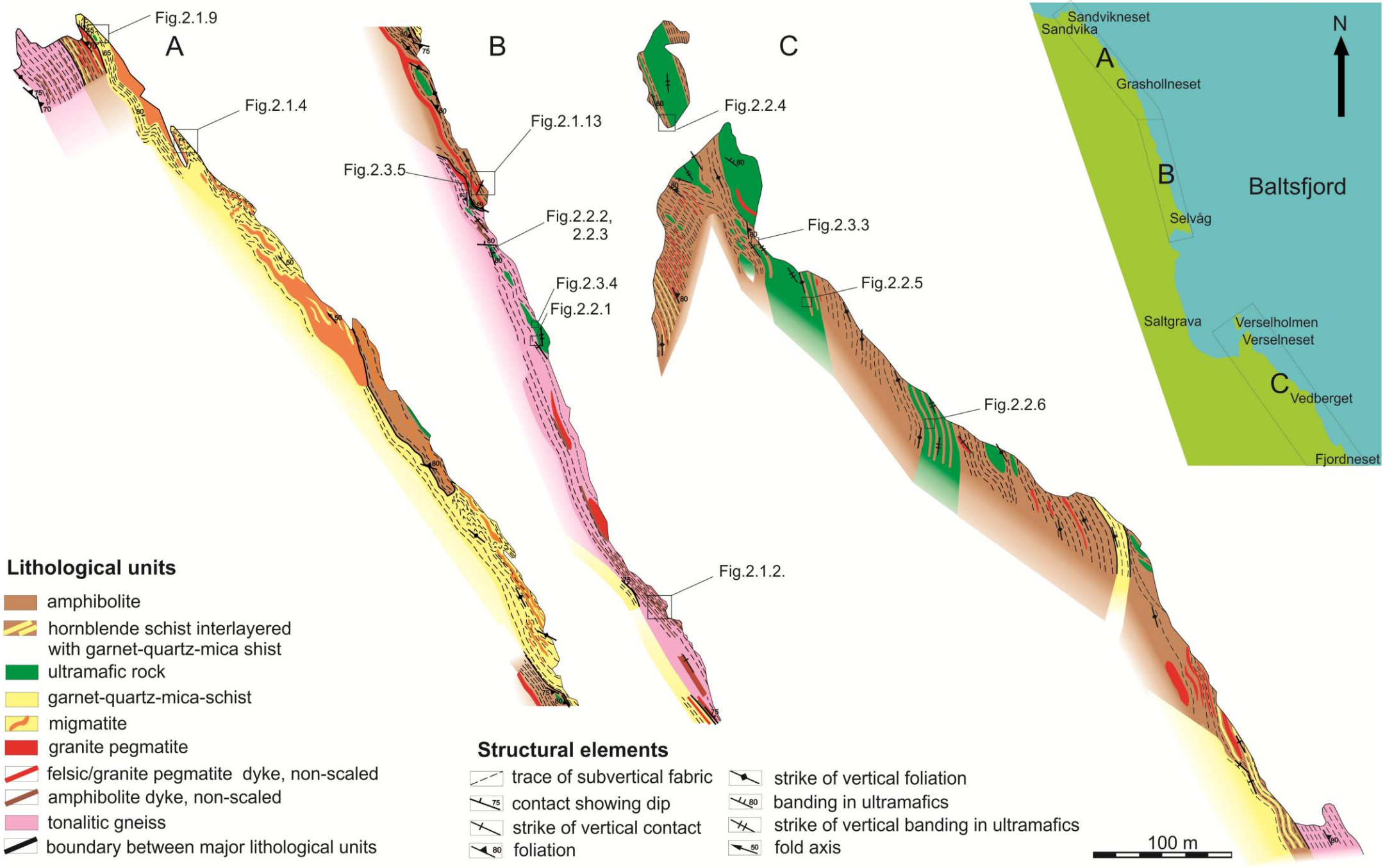

Fig.2.1.1. Detailed map of the supracrustal zone at the western shore of Baltsfjord. Frames with numbers of figures show locations of field photographs.

2) Supracrustal volcanic-sedimentary association

This lithological group includes metavolcanic rocks, metapelite and metaarkose represented respectively by amphibolite and hornblende schist showing volcanoclasic textures, garnet-quartz-mica schist and quartz-mica schist. On the eastern shore of Baltsfjord the metasedimentary succession includes also various calc-silicate metamorphic rocks.

On the eastern shore of Baltsfjord the thickness of the supracrustal suite approaches 1 km and increases further inland. The metasedimentary rocks overall show steeply dipping foliation and are often tightly folded. The supracrustal succession elsewhere is separated from the basement gneiss by tectonically modified contacts making it impossible to document its deposition on top of the gneiss. Within the metasedimentary units, primary lithological contacts are commonly well preserved: interlayering in scale of centimeters to meters between quartz-hornblende-biotite schist, quartz-garnet-mica schist, quartz-mica schist can be observed (Fig.2.1.3).

Fig.2.1.3. Lithological contact between garnet-mica schist (lower part of the photo) and hornblende schist (upper part of the photo) at Nøringen (locality 637).

On the western shore of Baltsfjord the metasedimentary succession is represented by a terrigenous association, which is strongly predominated by garnet-quartz-mica schist (Fig.2.1.1). The metasedimentary rock occurs as several steeply dipping sequences with

thickness of 2 - 40 meters. The contacts between the metasedimentary units and the basement are tectonically modified, while the contacts to amphibolite and hornblende schist are commonly gradual. In the southwestern part of the mapped area (Fig. 2.1.1, map sheet A) garnet-quartz-mica schist forms the thickest (40 m) enclave. The main subvertical metamorphic fabric shows N-NNW strike, which is typical for the entire structure. The fabric is complicated by tight parasitic folds with hinges dipping towards NW with common dip angles of 45-50˚ (Fig.2.1.4). Migmatization (Fig.2.1.4) occurs within most intensively sheared part of the metasedimentary unit in this area.

Fig.2.1.4. Migmatized garnet-mica schist, western shore of Baltsfjord (locality 606).

In most cases, both amphibolite and hornblende schist are spatially associated with metasedimentary successions (Fig.2.1.1.). Some of the amphibolites outcropping at Nøringen and on the easterm shore of Baltsfjord (e.g. locality 644, 514) show clearly pronounced volcanoclastic textures (Fig.2.1.5) indicated by the presence of strained light-colored clasts of felsic composition. However, in many other cases, amphibolite spatially associated with metasedimentary rocks shows textures that much more uncertain can be interpreted as volcanoclastic (Fig.2.1.6), or even massive textures. Particularly, on the western shore of Baltsfjord, it is complicated to decide whether the amphibolite represented intrusive or supracrustal rocks prior to deformation and metamorphism.

Fig. 2.1.5. Amphibolite displaying clear volcanoclastic texture at Nøringen, locality 644.

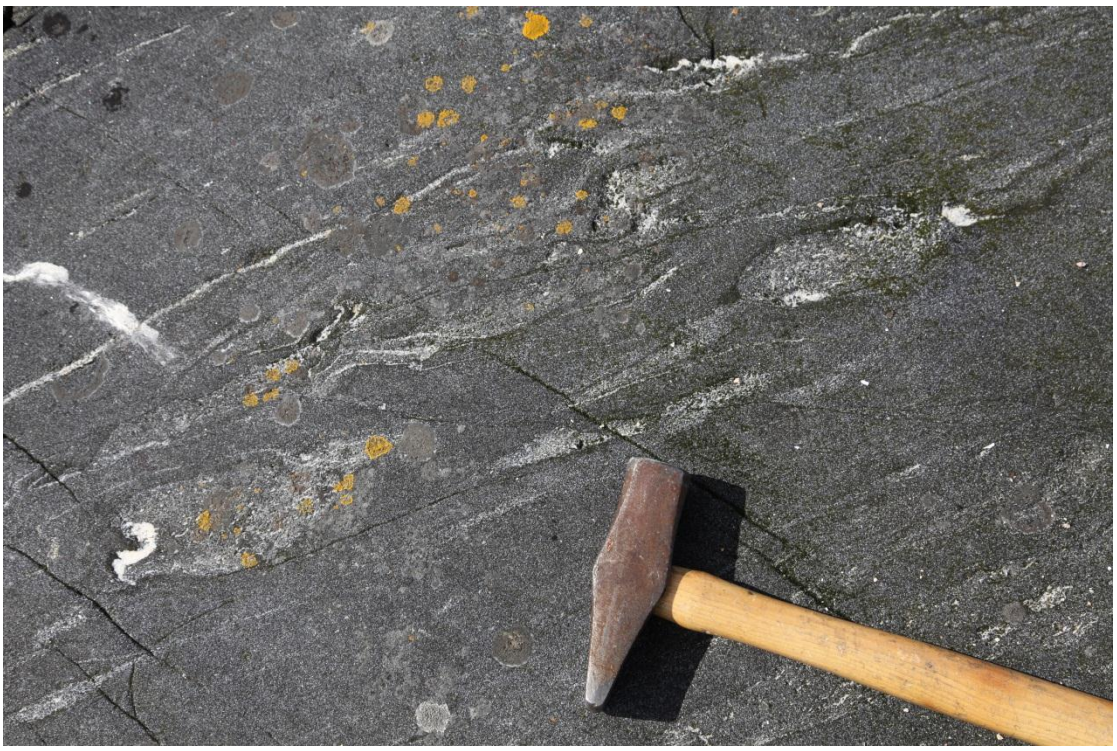

Fig.2.1.6. Amphibolite displaying volcanoclastic texture, eastern shore of Baltsfjord, locality 516.

3) Layered mafic-ultramafic rock association

The studied mafic-ultramafic rock association occurs both within the Archean basement gneiss (Fig. 2.1.7) and the Astridal supracrustal units. The ultramafic rock is always preserved as podiform bodies up to 200 m long, which tend to form chains striking in NW direction. The largest lenses, which occur within the tonalitic gneisses, are commonly homogenous and made up of ultramafic olivine-pyroxene-amphibole rock only, and do not include mafic amphibolite or hornblendite. In all observed cases, the contacts to the host gneiss are tectonically modified (Fig.2.1.8), making it impossible to define relative structural and consequently age relationships between gneiss and ultramafic lenses.

*Fig.2.1.7. Lenses of ultramafic rock (at the right side below the top) and amphibolite (at the top) within tonalitic gneisses (*Kåre Kullerud, pers. comm. 2012*), Astritind. Red dashed lines mark the contacts of lenses.*

Fig. 2.1.8. Tectonically modified contact between tonalitic gneiss and a lens of olivine pyroxene-hornblendite (locality 530).

Along the western shore of Baltsfjord the ultramafic rock occurs as lenses of various size (from 4-5 m up to 100 m long) within gneisses (Fig.2.1.7, Fig.2.1.8) and metasedimentary rocks (Fig. 2.1.9), but in most cases the ultramafic rock is closely associated with massive amphibolite (Fig.2.1.1, 2.1.10, 2.1.11, 2.1.12).

Fig. 2.1.9. A lens of ultramafic olivine-amphibole rock within migmatized garnet-mica schist (locality 605).

The orientation of the lenses is conformal to the major structural planar fabric of the host rock and the series of lenses form chains. Figure 2.1.10 clearly shows that extremely competent ultramafic olivine-amphibole rock forms boudins bounded by fault contacts, which is “floating” in the less competent amphibolitic matrix.

Fig. 2.1.10. Boudin of ultramafic olivine-rich rock within mafic amphibolite (locality 633).

At the localities 65-90 on the eastern shore of Baltsfjord, where deformation is more intense and complicated, smaller lenses are multiply folded (Fig.2.1.11, 2.1.12). The fold hinges predominantly dip steeply towards north.

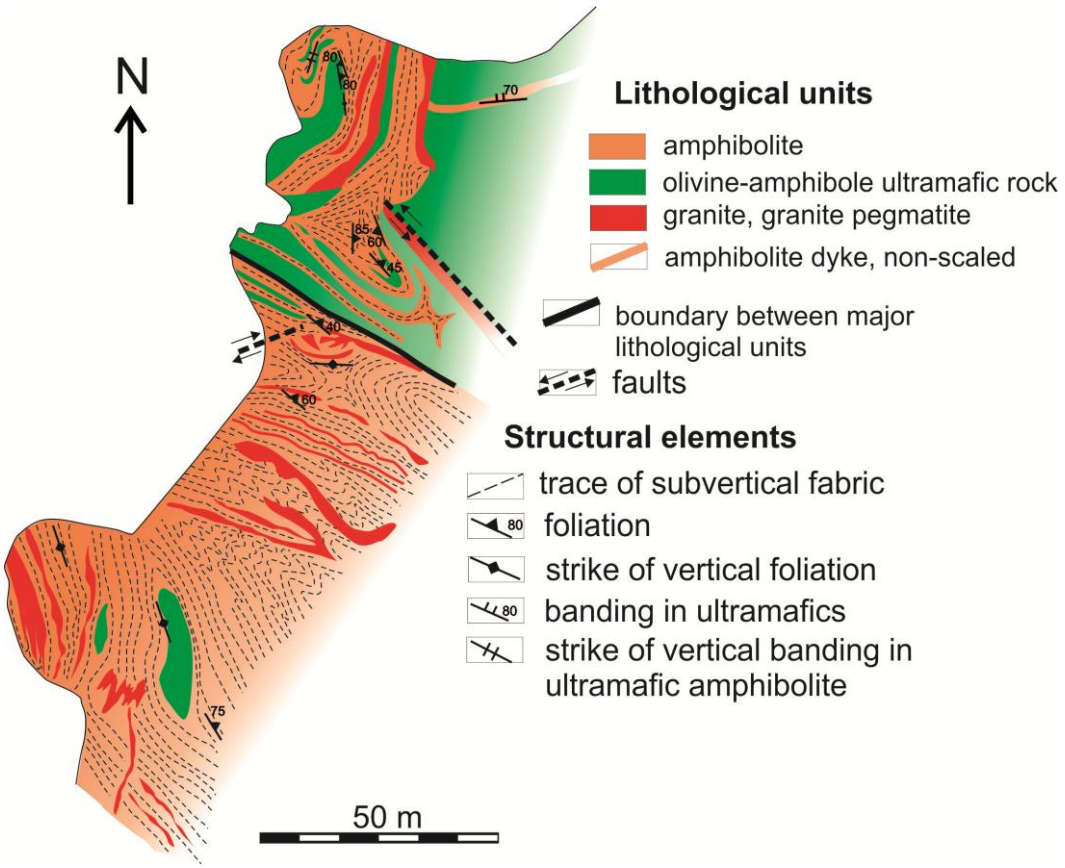

Fig. 2.1.11. A detail map showing structural relationships between major lithological units on the eastern shore of Baltsfjord (localities 65-90).

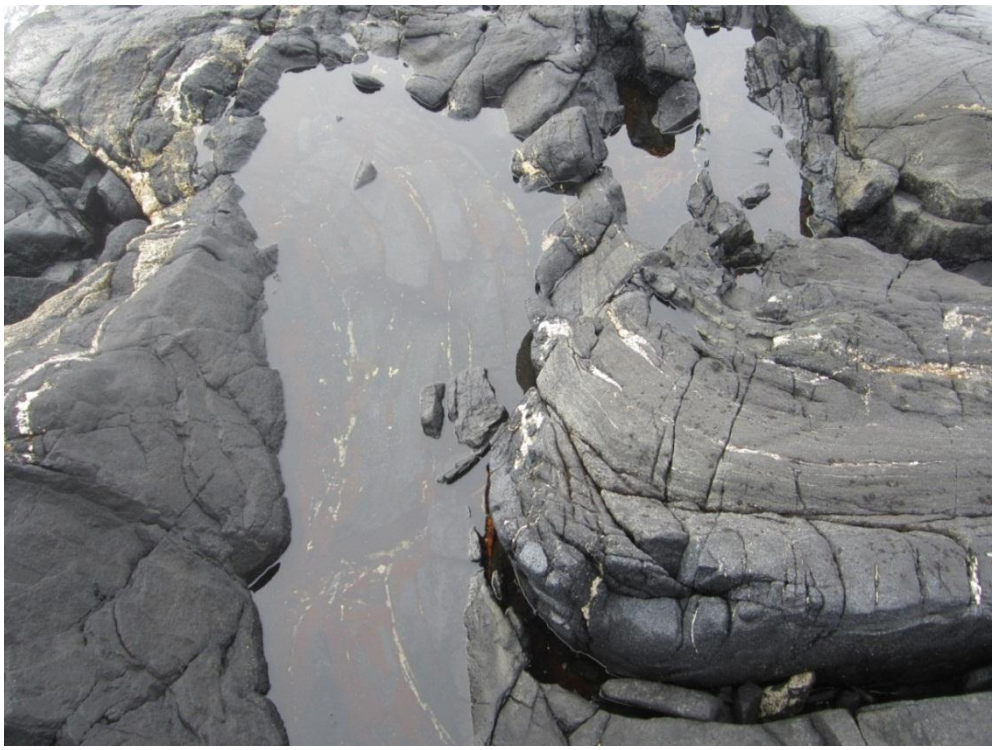

Fig. 2.1.12. Folded olivine-amphibole rock, at the eastern shore of Baltsfjord (locality 0782).

4) Late granite pegmatites and felsic dykes

There are several generations of felsic rocks documented both on the eastern and western shores of Baltsfjord (Fig.2.1.1, 2.1.11). Medium-grained granite dykes deformed in the same style as the host supracrustal units are inferred to represent the first generation of felsic rocks. Their emplacement was synchronous to F1 deformation and their U-Pb zircons and titanite age of 1758 Ma (Fernando Corfu, personal communication 2012) coincides well with the age of the main Svecofennian orogenic event. There are also numerous granite pegmatites observed both on the eastern and western shore of Baltsfjord, which cross-cut the early deformation fabrics, but are sheared as well (Fig.2.1.13). U-Pb zircon dating of such a pegmatite shown in Fig.2.1.13 yielded an age of 1630-1600 Ma (Fernando Corfu, personal communication 2012) implying that post-Svecofennian shearing F3 and magmatism took place in this area.

Fig. 2.1.13. Two generations of felsic rocks in relation to the host amphibolite, on the western shore of Baltsfjord (locality 560).

2.2. Field occurrence of mafic-ultramafic association

Field observations indicate that there are two major varieties of ultramafic enclaves occurring within tonalitic gneisses of the basement and supracrustal units of the Astridal belt. The first type is represented by largely homogenous lenses, showing laterally variable modal igneous banding or patched texture. On weathered surfaces, banding/patches appear as light brownish stripes/spots entirely composed orthopyroxene, or rich in orthopyroxene (Fig.2.2.1 and 2.2.2 respectively). Dark greenish parts of the rock are rich in amphibole, olivine and contain green spinel as well. Structural measurements indicate that the orientation of the banding is generally parallel or slightly oblique to the orientation of the entire lens and the metamorphic fabric of the host rocks (see Fig.2.1.1).

The second macroscopic variety has been documented in detail both on the western and eastern shore of Baltsfjord (Fig.2.1.1, 2.1.11). It is represented by a modally layered association of both mafic and ultramafic rocks. The layers are formed by several rock types: 1) the earlier mentioned spot-textured rock composed of spinel, orthopyroxene, olivine and amphibole, 2) a dark greenish laminated rock composed of olivine and amphibole, 3) a non-foliated black rock entirely composed of hornblende, 4) foliated mafic amphibolite, dominated by plagioclase and amphibole, and 5) rare interlayers represented by non-foliated glimmerite.

The thickness of the layers varies commonly from several centimeters (Fig.2.2.4) to several meters (Fig.2.2.3, 2.2.5). The former case give a reason to exclude any kind of metasomatic origin of layering, if it is assumed that a homogenous ultramafic rock was emplaced into a gabbroic host rock. Some of the layers have constant composition and thickness along the strike, so that they can be followed for several meters or even tens of meters (Fig.2.2.3, 2.2.4, 2.2.5). It has also been observed that layered mafic-ultramafic bodies sometimes form discordant contacts between layers and consequently showing variable thickness (Fig.2.2.5).

The contacts within layered intrusive bodies are commonly referred to as gradational if the phase change from the composition of one layer to the neighbouring occurs through the distance of more than one grain diameter, while the change within a distance of approximately one grain diameter corresponds to a sharp contact between layers (Irvine, 1982). Both cases have been observed for the studied mafic-ultramafic bodies. Sharp contacts are more abundant (Fig.2.2.4) than typical gradational contacts when a shift from olivine-rich to pure hornblendite layers occurs through gradual increase of amphibole content compared to that of olivine (Fig.2.2.3).

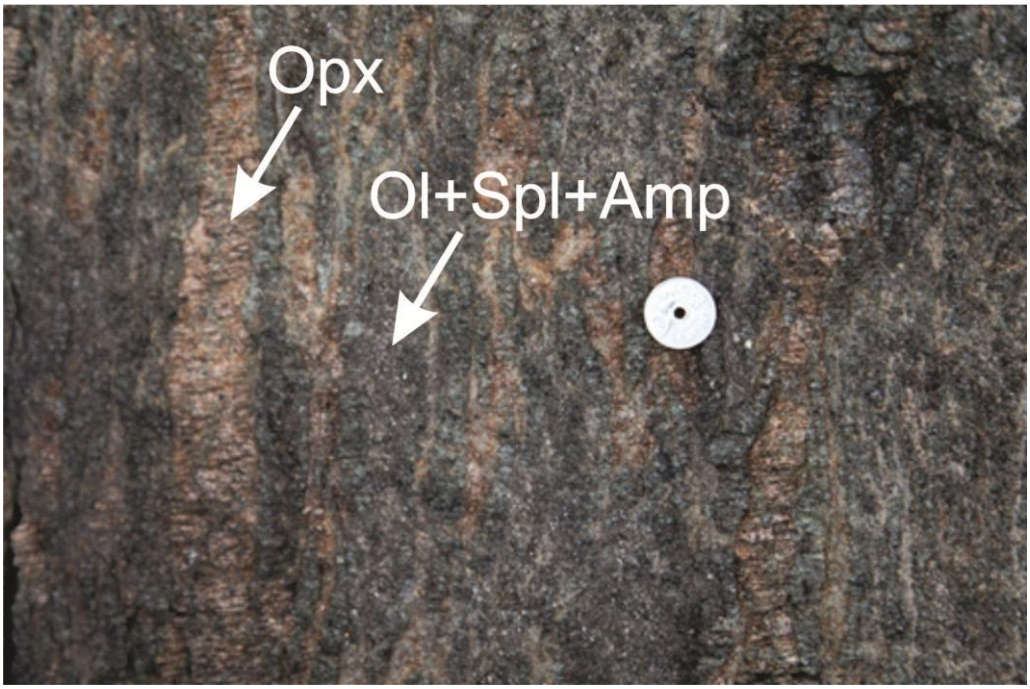

Fig.2.2.1. Thin modal igneous banding in the ultramafic rock (locality 545). The following abbreviations for mineral names are used: Opx- ortopyroxene, Ol – olivine, Spl - spinel, Amp – amphibole (Whitney and Evans, 2010).

Fig.2.2.2. Spot-textured ultramafic rock (locality 554). Abbreviations for mineral names are the same as in Fig.2.2.1.

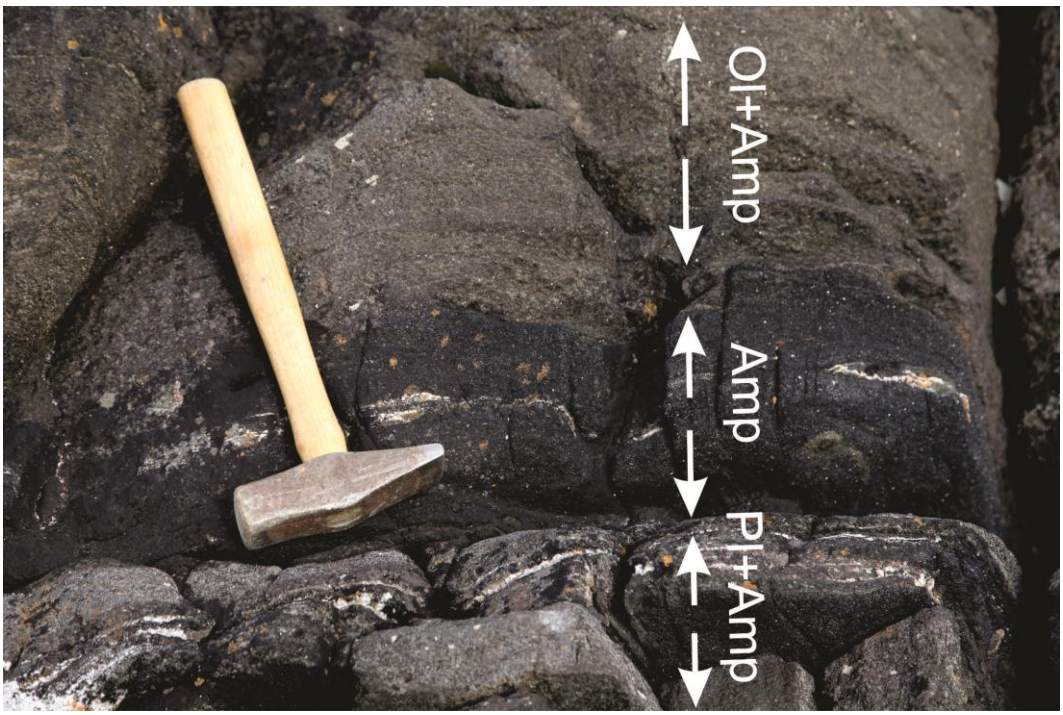

Fig.2.2.3. Modal layering in mafic-ultramafic lens (locality 554). Pl- plagioclase, the other abbreviations for mineral names are the same as in Fig.2.2.1.

Fig.2.2.4. Thin modal layering in mafic-ultramafic lens (locality 564).

Fig.2.2.5. Gradational phase contact between layers within a mafic-ultramafic body (locality 539). Bt – biotite, all other abbreviations for mineral names are the same as in Fig.2.2.1.

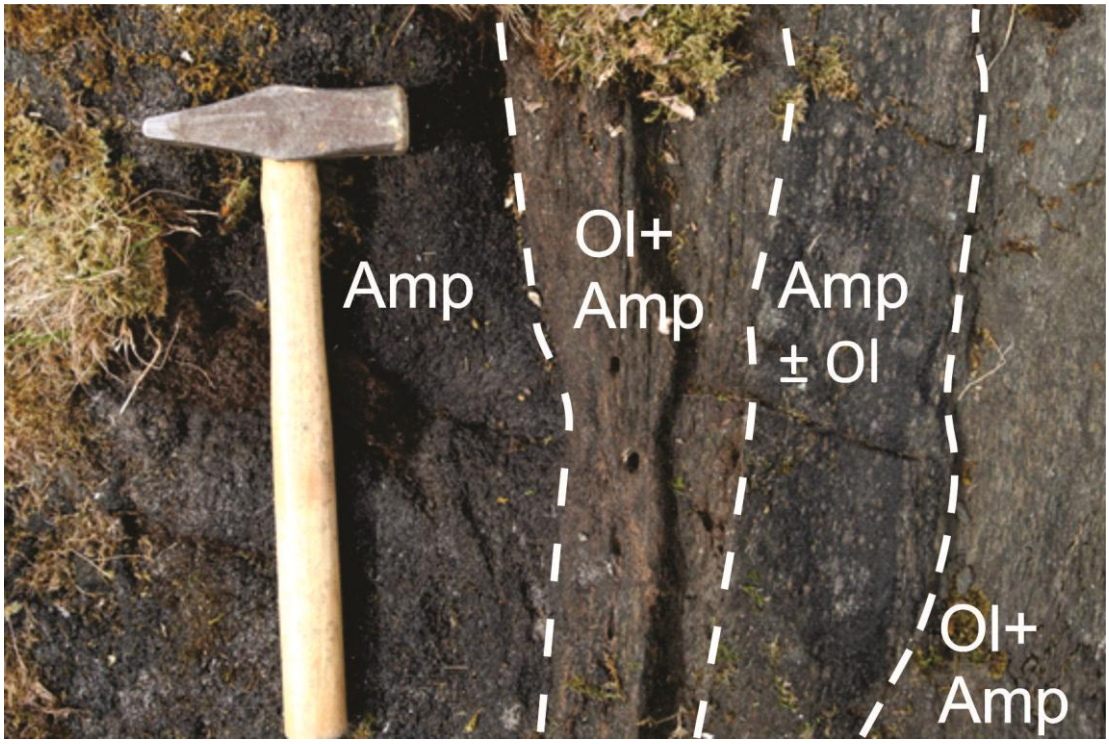

Fig.2.2.6. Discordant phase contact between layers within a mafic-ultramafic body (locality 585). Abbreviations for mineral names are the same as in Fig.2.2.1.

2.3. Intrusive relationship and relative age

As it was mentioned before, the contacts between the ultramafic lenses and the host rock are commonly tectonically modified. However, at Nøringen (locality 634) an intrusive contact between the amphibolite and an olivine pyroxene-hornblendite has been observed. The contact is marked by a 20-30 cm thick zone of almost pure hornblendite composition, which looks like a chilled margin (Fig.2.3.1). The presence of an apophyse along this contact makes it clearly different from the interlayering of mafic and ultramafic rocks within the intrusive body described in section 2.2 (e.g. Fig.2.2.3).

The dark greenish spotted ultramafic rock at the contact between the black hornblende-rich zone and the mafic amphibolite is characterized by texturally graded layering. With increased distance from the contact, the size of the brown-colored orthopyroxene patches becomes gradually larger without any compositional change of the rock (Fig.2.3.2).

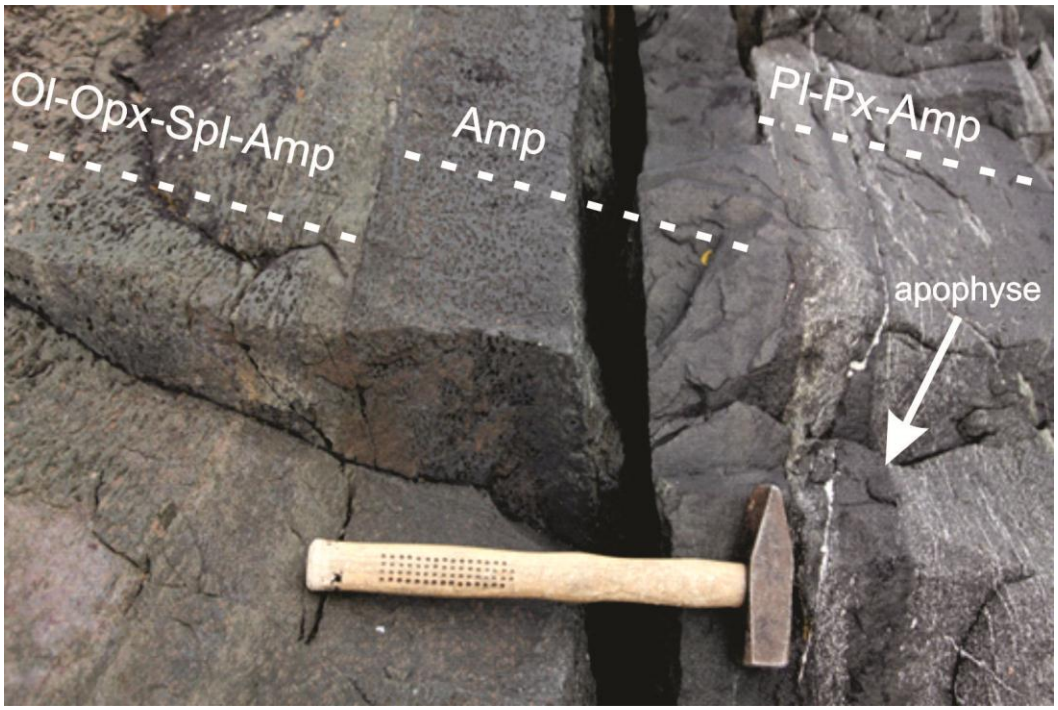

Fig.2.3.1. Intrusive contact between mafic amphibolite and olivine-pyroxene-amphibole rock (locality 634).

Fig.2.3.2. Texturally graded layering in ultramafic spinel-bearing olivine-pyroxene-amphibole rock beside its contact to a mafic amphibolite (locality 634).

A 0.5 m thick black dyke cutting across igneous layering textures preserved in olivine-amphibole rock was observed on the western shore of Baltsfjord (Fig.2.3.3). The rock making up the dyke is entirely composed of phlogopite and hornblende. Within the dyke, one about 20 cm big angular xenolith of a gabbroic rock was observed, approving an intrusive origin of the body.

The relative age of the studied layered mafic-ultramafic rock association of NW Senja can be roughly assumed based on xenolith findings. The only xenolith found in the studied ultramafic rock is represented by a foliated calc-silicate rock (Fig.2.3.4), which most likely has a genetic affinity to metasedimentary calc-silicate sequences documented on the eastern shore of Baltsfjord (Pedersen, 1997). One xenolith of strongly altered ultramafic rock was observed in a late granite pegmatite (Fig.2.3.5) similar to those dated at 1.6-1.63 Ma. These observations indicate that the emplacement of the ultramafic rock took place after formation of metasedimentary units, but before the emplacement of Svecofennian/post-Svecofennian granite pegmatites.

Fig.2.3.3. A phlogopite-hornblende dyke cutting across the olivine hornblendite (locality 580).

Fig.2.3.4. Xenolith of a calc-silicate rock within ultramafic rock (locality 535).

Fig.2.3.5. Xenolith of altered ultramafic rock within granite pegmatite (locality 630).

Chapter 3. Petrography

3.1. High P-T assemblage

As it was mentioned in chapter 2, the mafic-ultramafic rock association makes up both homogenous and layered bodies. The most abundant type commonly constitutes massive homogenous lenses, and in hand specimen scale it is characterized by a specific patched texture or banding (Fig.3.1.1a), with alternation of brownish and dark-greenish domains. Mostly, the alternation occurs as a planar textural feature and is generally parallel to the orientation of the entire lens and the concordant metamorphic fabric of the country rock units. Brownish domains frequently form up to 10-15 cm big patches. Typically the brownish patches constitute 20-40 modal % of the rock and are 1-3 cm thick.

Microscope studies of the patched variety (Fig.3.1.1, 3.1.2) reveal that these textures have igneous cumulate origin. The brown-weathering patches are formed by large oikocrysts of orthopyroxene (Fig.3.1.1b, e, Fig.3.1.2e), enclosing euhedral grains of olivine and amphibole, which are 0.1-0.7 mm in diameter. The largest brownish patches enclose up to 30 modal % olivine, which represents the early cumulus phase incorporated into 2-5 cm long orthopyroxene oikocrysts. The dark greenish "matrix" filling in the space between brownish bands or patches (Fig.3.1.1a) is composed of olivine, amphibole, smaller poikilitic ortopyroxene and green spinel, having equilibrium relationships (Fig.3.1.1c, d; Fig.3.1.2b, c) Amphibole (magnesiohornblende) is the predominant modal component of the matrix. It forms light-greenish to almost colorless euhedral 0.1-0.5 mm long crystals characterized by typical amphibole cleavage. Olivine also constitutes a significant part of the greenish matrix; its content varies from 5 modal % to 40 modal % between different samples. For some of them, olivine occurs as large (up to 1 cm) isometric or irregular fractured aggregates, which incorporate both spinel and amphibole grains (Fig.3.1.1c). In another sample (Fig.3.1.2), olivine forms subhedral or euhedral grains, 0.2-0.5 mm in diameter (Fig.3.1.2c). Rare findings of amphibole inclusions within olivine grains (Fig.3.1.2d) and abundance of olivine inclusions within amphibole grains (Fig.3.1.2b) suggest that most of the olivine grains crystallized prior to amphibole, but some of them later than the amphibole. Spinel is a minor constituent of the rock, but its content of 10-20 modal % in the matrix often exceeds the content of olivine. Spinel often occurs in aggregates of small brown greenish to bright greenish subhedral grains coating amphibole grains (Fig.3.1.1d). In sample 593 spinel forms conformably aligned xenomorphic aggregates and therefore can be considered as an intercumulus phase (Fig.3.1.2b)

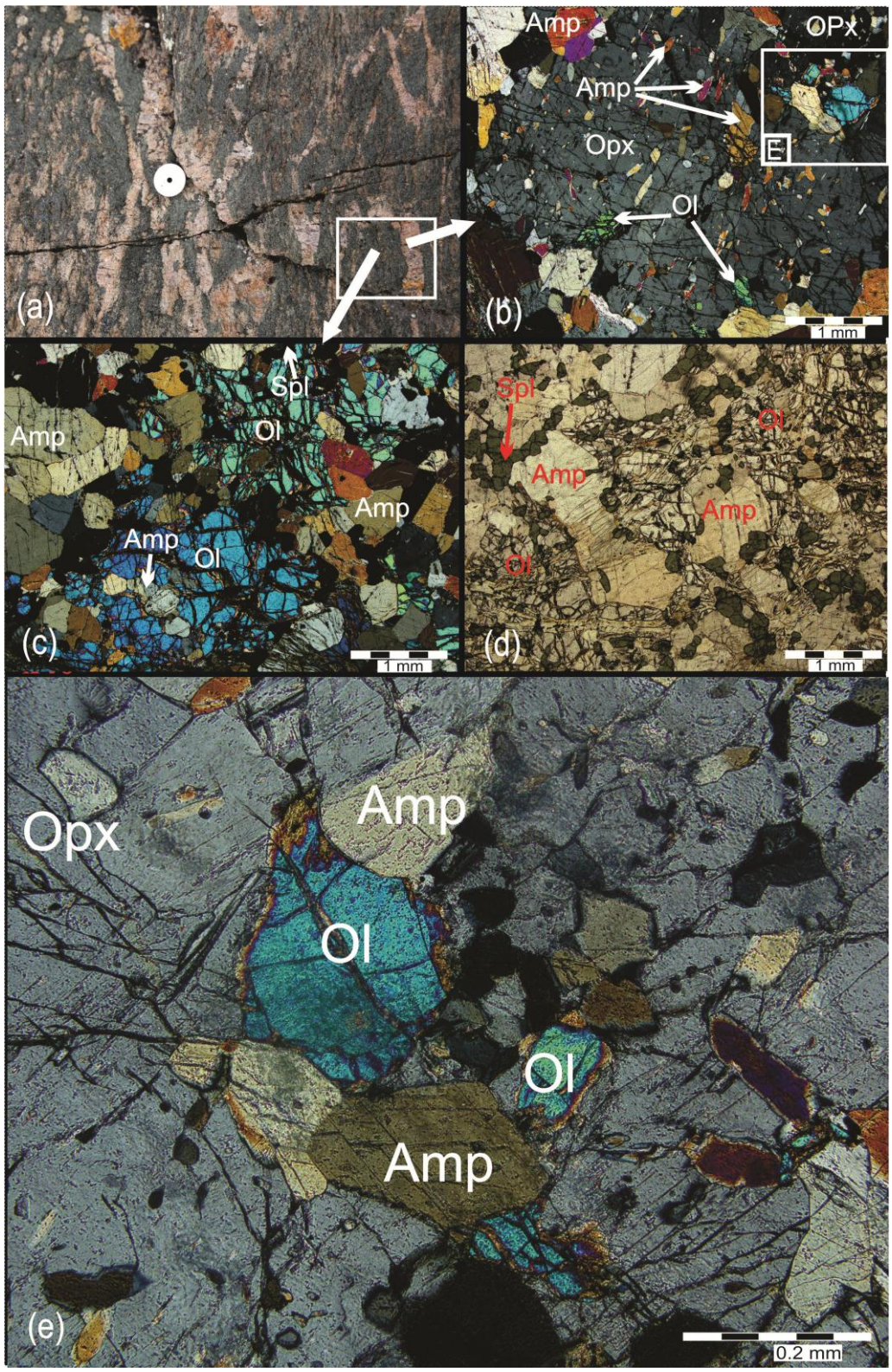

Fig.3.1.1. Field (a) and microphotographs (b-e) showing texture and composition of the patched variety of ultramafic rock, sample 529. (b, c, e) - in polarized light, (e) – in parallel light. Abbreviations of mineral names after Whitney and Evans, (2010). (a) Macroscopic view of the patched texture. (b) Oikocryst of orthopyroxene. (c) Relationship between minerals comprising fine-grained matrix of the rock. Olivine forms isometric patches enclosing amphibole and spinel. (d) Green spinel forms aggregates coating amphibole grains. (e) Orthopyroxene enclosing euhedral grains of olivine and amphibole.

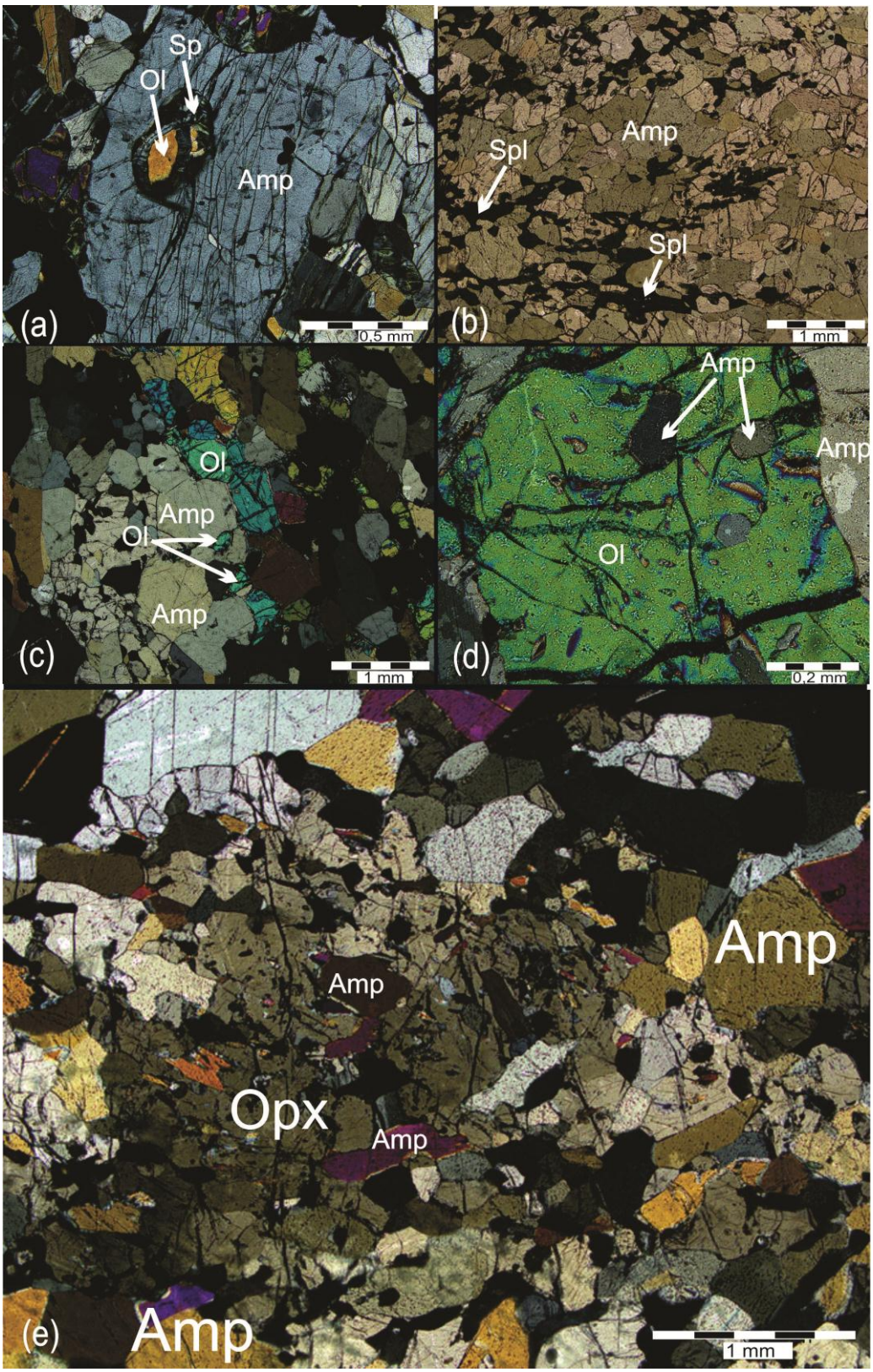

Fig.3.1.2. Microphotographs showing texture and composition of the patched variety of ultramafic rock, sample 593. (a, c-e) - in polarized light, (b) - in parallel light. Abbreviations of mineral names after Whitney and Evans (2010). (a) Inclusion of serpentinized olivine within an amphibole grain. (b) Elongated xenomorphic spinel filling intercumulus space. (c) Relationship between olivine and amphibole. (d) Olivine enclosing tiny amphibole grains. (e) Poikilocryst of orthopyroxene enclosing amphibole grains.

Another petrographic variety belonging to the studied mafic-ultramafic rock association is represented by a laminated olivine-amphibole rock showing a panidiomorphic texture, characterized by grain boundary triple point junctions, indicating equilibrium (Fig.3.1.3b, c). Phase lamination occurs through alternation of olivine and magniohornblende/tremolite content in a scale of 0.5 – 1 cm (Fig.3.1.3b). There were distinguished 3 different types of laminas. The first type contains 95 modal % of strongly serpentinezed olivine and 0-5 modal % amphibole. The second type in average contains 50 modal % of olivine and 50 modal % of amphibole, while the laminas of third type are composed of amphibole only. Findings of enclosed euhedral olivine grains in amphibole-rich laminas (Fig.3.1.3a) give an evidence for earlier crystallization of olivine in the rock. Figure 3.1.3c shows however, that for the olivine-amphibole laminas, the grains of olivine tend to have anhedral shape and fill in the interstitial space between amphibole grains. Notable is that the size of amphibole grains in amphibolitic laminas is 3-4 times larger compared to those in olivine-amphibole laminas (Fig.3.1. 3b, c), where they do not exceed 0.5 mm.

A meta-gabbronorite rock, which occurs as interlayers within the olivine-bearing ultramafic rocks and hornblendite is characterized by granoblastic texture and is composed of 40 modal % plagioclase, 40 modal % Fe-rich brownish hornblende and approximately 20 modal % of pyroxene. Among the latter the majority is represented by orthopyroxene (Fig.3.1.4c). Clinopyroxene has been found as rare relics partly altered to hornblende (Fig.3.1.4. a, b).

Interlayers of black hornblende-rich rock within mafic-ultramafic layered bodies are entirely composed of greenish grains of magnesiohornblende, 1 – 3 mm in diameter, and display panidiomorphic texture (Fig.3.1.5).

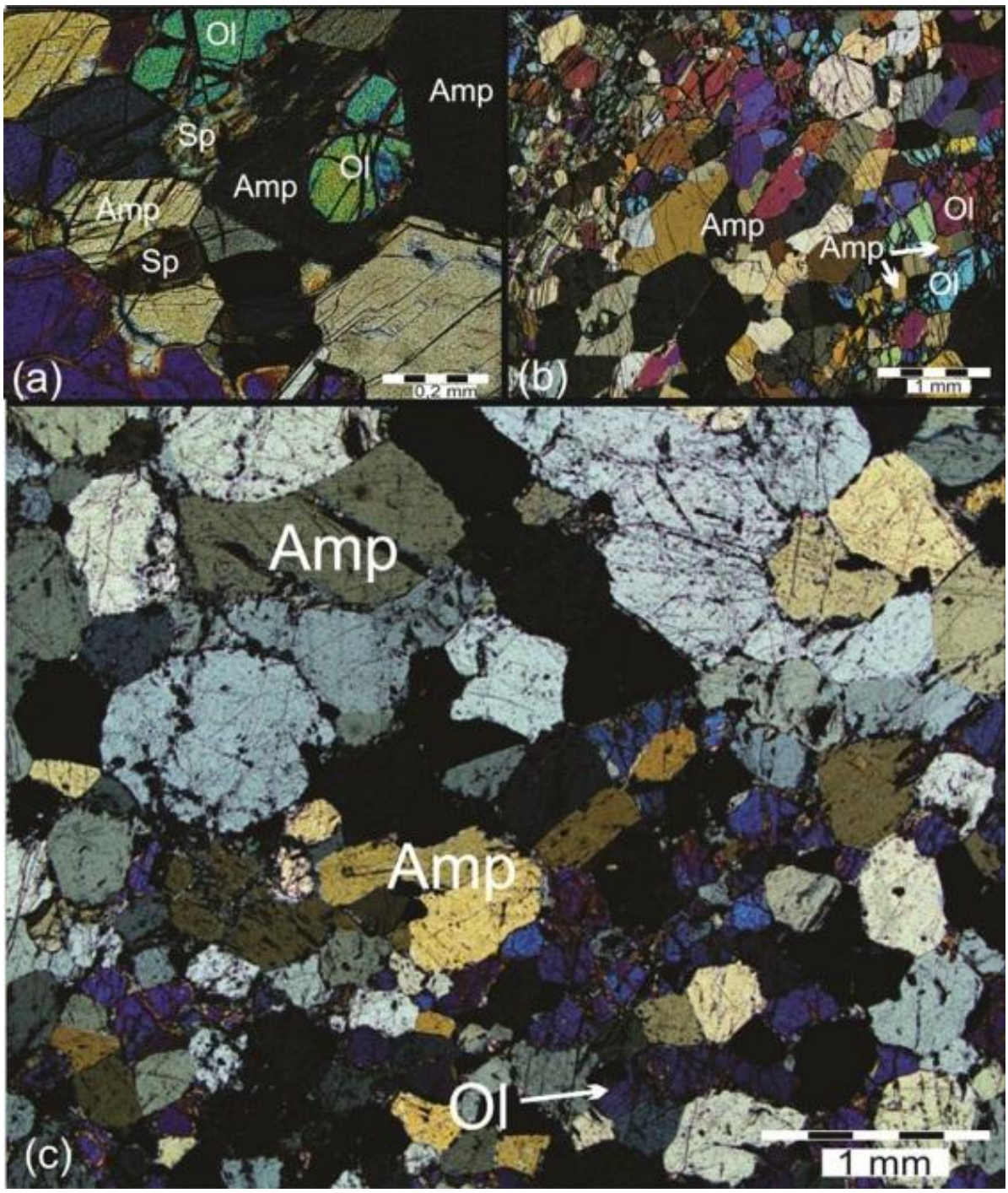

Fig.3.1.3. Microphotographs in polarized light showing texture and composition of the thin laminated variety of olivine-amphibole ultramafic rock, samples 530 (b,c) and 564/1 (a). Abbreviations of mineral names after Whitney (2010). (a) Euhedral grains of serpentinized olivine enclosed in amphibole. (b) Phase lamination in ultramafic rock. (c) Textural relationship between two different laminas and their components.

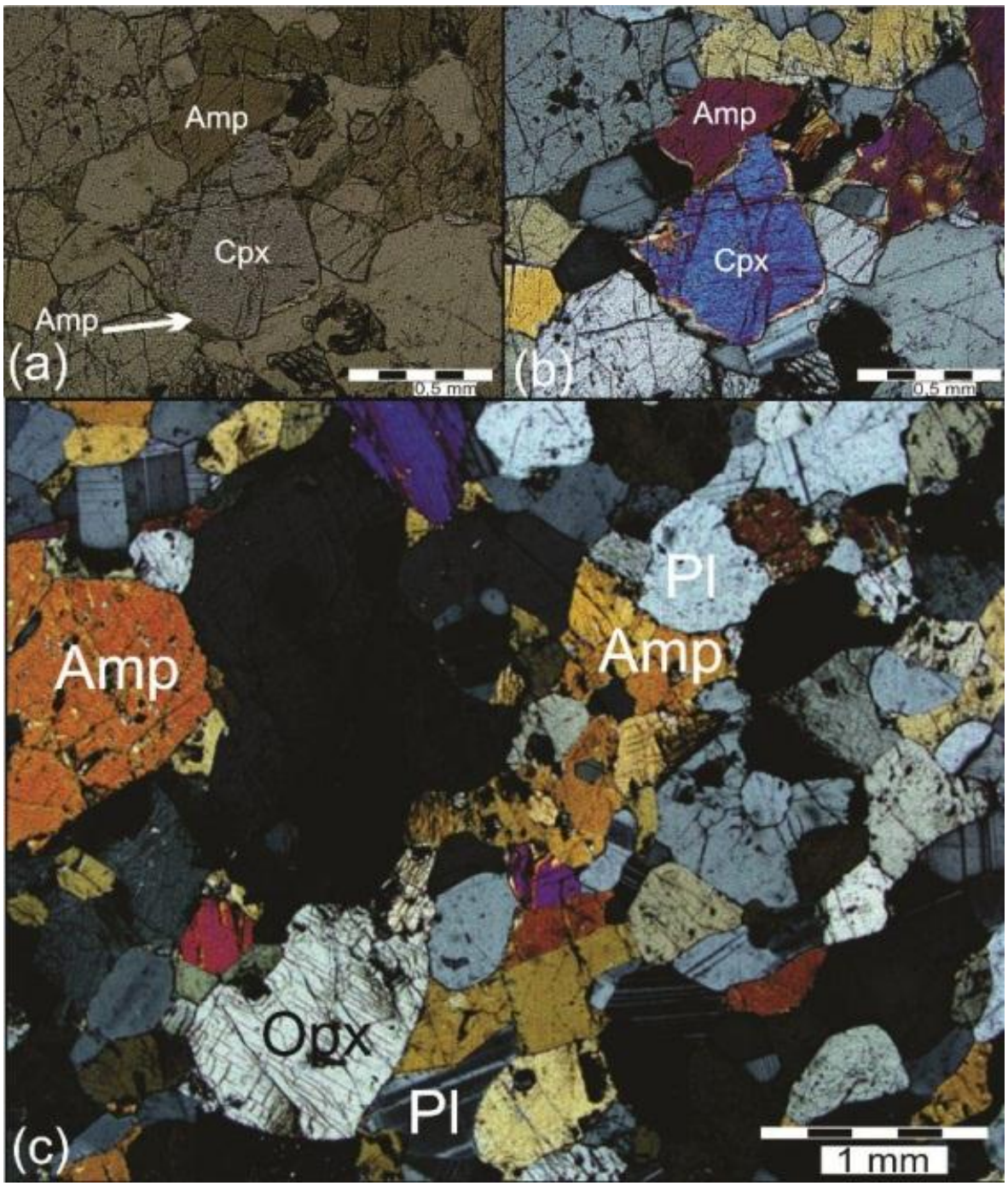

Fig.3.1.4. Microphotographs showing texture and composition of metagabbroic rock, sample 585-2. (a) - in parallel light, (b,c) – in polarized light. Abbreviations of mineral names after Whitney and Evans (2010). (a,b) Replacement of clinopyroxene by hornblende. (c) Granoblastic texture and modal composition of metagabbroic rock.

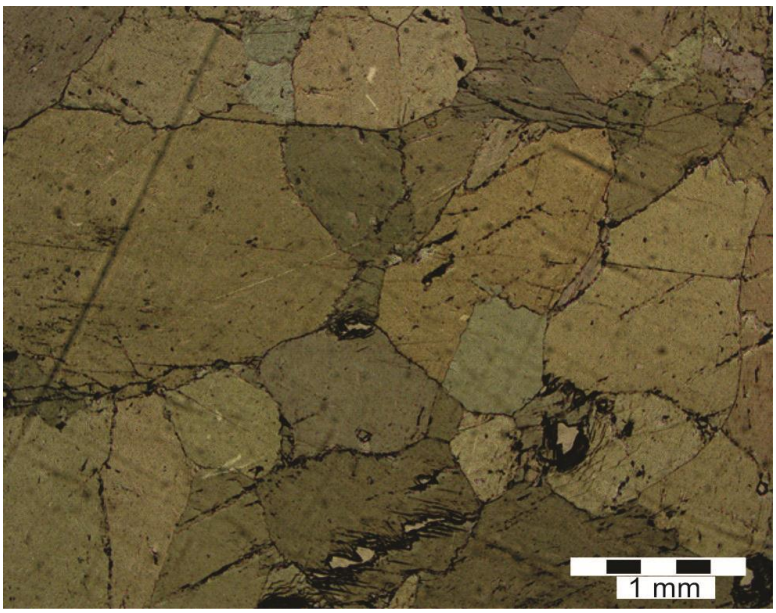

Fig.3.1.5. Microphotograph showing texture of the rock entirely composed of hornblende, sample 585.

3.2. Low P-T assemblage

Some of the samples contain also a low P-T metamorphic assemblage including serpentine, magnetite, phlogopite and chlorite, which clearly overprint the textures described in the previous section.

Serpentine replaces olivine along margins and fractures commonly forming typical mesh texture (Fig. 3. 2.1c). In a few cases, total replacement of olivine has been observed. As the degree of serpentinization increases, the content of magnetite increases correspondingly, as a result of olivine hydration reaction.

Chlorite and phlogopite occur as euhedral, 0.5 – 2 mm long grains, often showing the same orientation (Fig.3.2.1 a, b). Phlogopite has been documented in strongly serpentinized amphibole-olivine-orthopyroxene-spinel rock (Fig.3.2.1c), where its content approaches 20 modal %. It is also observed in hornblende-rich rock (Fig.3.2.1b). In both cases, phlogopite clearly overprints igneous mineral textures.

Chlorite has been found in several samples, and its highest content of approximately 30 modal % has been documented in a sample from a lense occurring within metasedimentary rocks. As in the case of phlogopite, chlorite clearly overprints the igneous assemblage (Fig.3.2.1a).

As a result of fluid infiltration along cracks, some of the rocks show extensive carbonatization. The zones of carbonatization (Fig. 3.2.2) crosscut the igneous texture and are therefore also inferred to be result of late metamorphic processes.

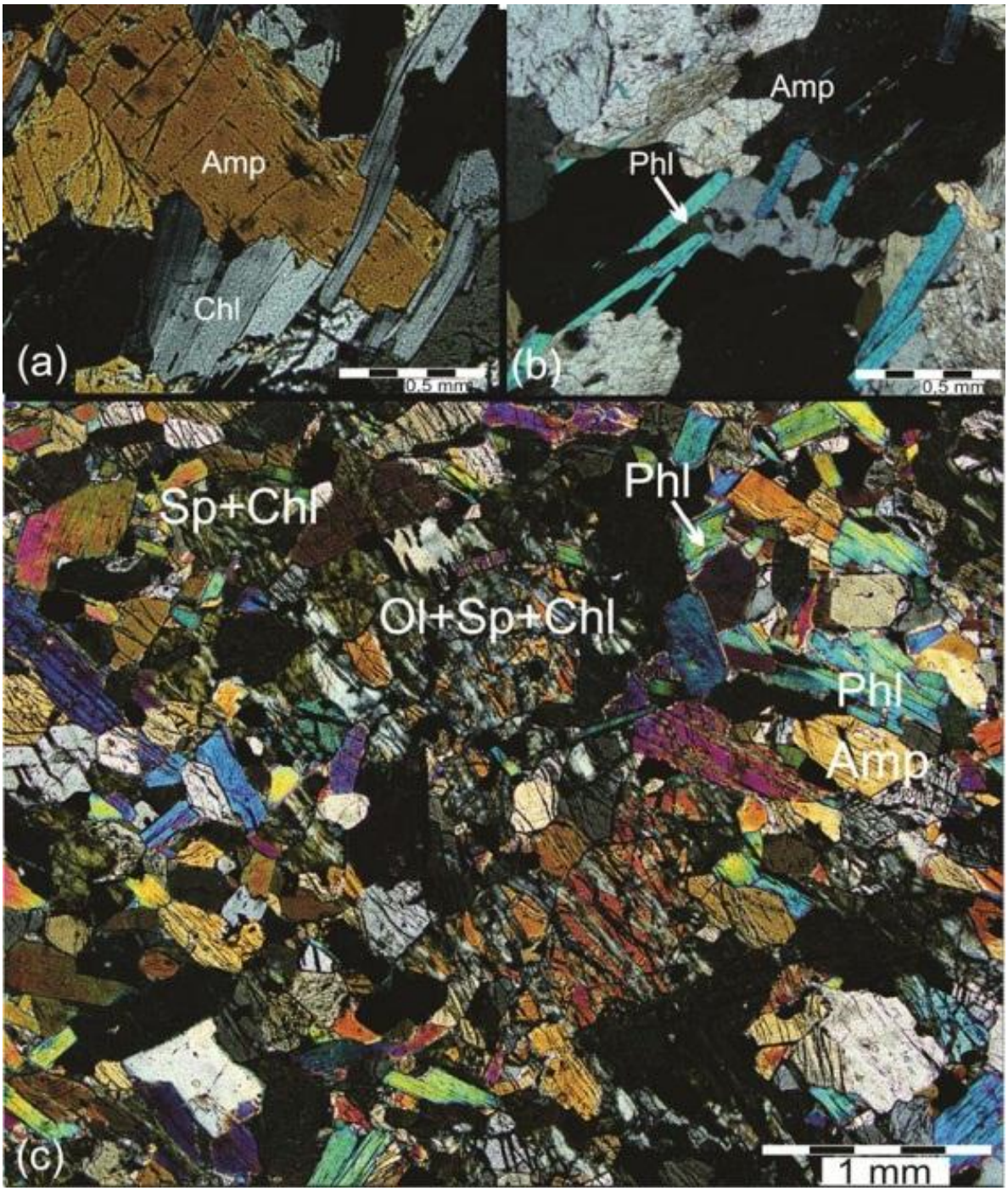

Fig.3.2.1. Microphotographs showing texture and composition of altered olivine-pyroxene-amphibole rock, samples 613 (a), 605 (b), 527-2 (c), in polarized light. Abbreviations of mineral names after Whitney and Evans (2010). (a) Chlorite flakes overgrowing an amphibole grain. (b) Aligned set of phlogopite overgrowing an amphibole grain. (c) Serpentinization and intense development of phlogopite flakes covering the igneous texture of an ultramafic rock.

Fig.3.2.2. A zone of carbonatization within olivine-amphibole rock.

3.3. Modal classification

As the microscope studies reveal that the rock-forming mineral phases of high P-T assemblage display equilibrium relationships with features typical for cumulates, the triangular diagram after Streckeisen (1974) rocks can be used for modal classification of the ultramafic amphibole-bearing rocks from NW Senja. According to this scheme, the ultramafic varieties of mafic-ultramafic layered association are represented by (1) hornblendite, (2) olivine hornblendite and (3) hornblende peridotite (both laminated rocks of olivine-amphibole paragenesis), (4) olivine pyroxene hornblendite (rocks of spinel-pyroxene-olivine-amphibole paragenesis).

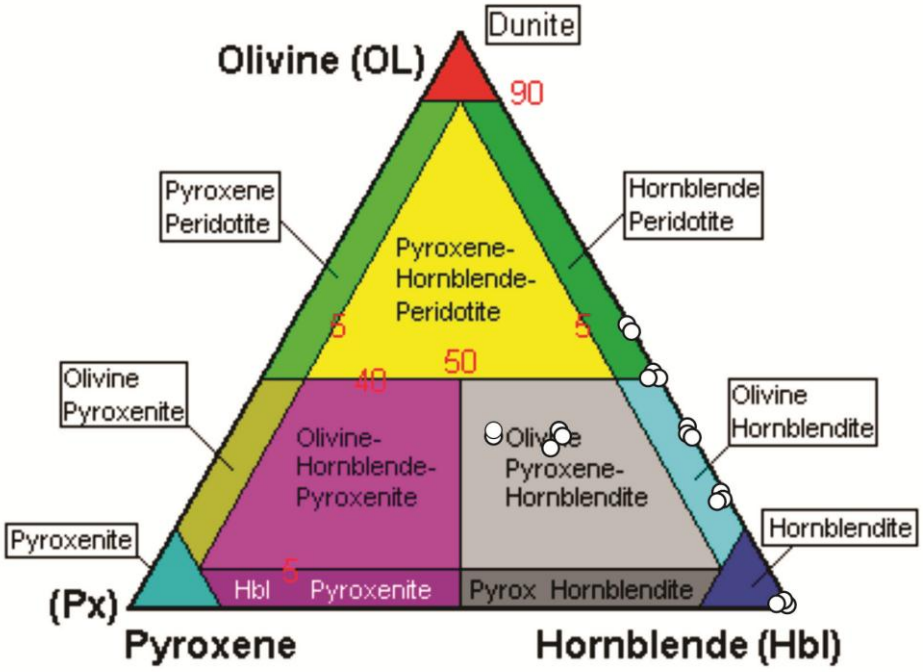

Fig.3.3.1. Compositions of ultramafic rocks from NW Senja in the modal classification diagram for amphibole-bearing ultramafic rocks after Streckeisen (1974).

Chapter 4. Geochemistry

4.1. Analytical procedure

The major part (see Appendix 2) of the collected samples was analyzed at the University of Huelva, Spain. For the ICP-MS analysis of trace elements the analytical procedure at the University of Huelva is reported as following: 100 mg of rock were digested for 24 hours with 8 ml of HF and 3 ml of concentrated HNO_3 in SAVILLEX ® PTFE at 90 °C on a hotplate. Samples were dried on a hotplate and then digested again with 3 ml of concentrated HNO_3 on a hotplate for 24 h. Then, the samples were taken again to dryness and dissolved with 3 ml of HCl and placed on a hotplate. After 24 hours samples were taken to dryness and dissolved in 100 ml of 2% HNO_3. All acids were of the mark MERCK Suprapur®. Trace metal analysis was performed on an ICP-MS system Agilent 7700x. He collision cell mode was used. Tuning of the ICP-MS was performed with a 1:10 dilution of a solution containing 10 ppb of Ce, Co, Li, Mg, Tl, and Y, and were monitored ^{59}Co, ^{89}Y, ^{205}Tl obtaining a standard deviation of less than 5 %.

To quantify metals, external calibration was performed. The drift and other effects arising from the use of the collision cell were corrected with the use of an internal standard, Rh, which was monitored by analyzing a 10 ppb standard monitor solution for every 10 unknown rock sample in each test sequence. The calculated measurement accuracy based on the repetition of 10% of the sample analysis was for all elements in the range 5-10%.

The accuracy of the method was determined by replicate analysis of digestion and reference material SARM1 (granite) and SARM4 (norite) of the South Africa Geological Institute, and is around 5-10%. Similarly the accuracy of the method was determined performing digestion duplicates of some of the samples (10% of total samples) to be within the range 5-10%. The quantification limit of the method is 0.005 ppm in digestion for most elements.

The XRF analyses for major oxide contents of the same samples were performed at the University of Huelva, Spain. However, the details of analytical procedure remain uncertain, since the requests for it have not been replied.

The major oxide and some of the trace element contents in several samples (see Appendix 2) have been analyzed by the author at the Department of Geology, University of Tomsø, Norway, using the Bruker S8 Tiger XRF. For analysis of major elements in each sample, the rock powder was mixed together with Li-tetraborate ($Li_2B_4O_7$) in the ratio of 1:7 (0.6 g of rock powder and 4.2 g of Li-tetraborate). Then the mixture was being molten during approximately 6 minutes in small

platinum pot at temperatures around 1200 ^{o}C. Finally, the hot melt was cooled down in platinum molds. For trace element analysis the first stage of analytical procedure was weighing up 9.0 g of rock powder and mixing it with 9 wax pills (POLYSIUS PORLAB® Mahlhilfe) in a mortar. After the mixing, the final step was to place the sample material in a cylindrical shaped container and pressed with a piston into pill.

4.2. Major oxide contents

The major oxide compositions of all analyzed samples are given in Appendix 2. The major oxide contents (recalculated to volatile-free basis) show that all samples of spinel-bearing olivine pyroxene-hornblendite, hornblende peridotite and olivine hornblendite belong to the high-magnesian (MgO = 20-36 wt %) ultrabasic and basic rock class. The contents of SiO_2, CaO and Al_2O_3 show considerable variations: SiO_2 = 40-48 wt %; Al_2O_3 = 5-13 wt %; CaO = 3.5-10 wt % and are negatively correlated to the content of MgO (Appendix 2; Fig.4.2.1). The total content of iron oxide is relatively constant in the range of 10-14 wt %. The Na_2O and TiO_2 contents vary in the range 0.1-1.5 wt % and 0.1-0.6 wt % respectively, and decrease as the content of MgO increases (Fig.2.4.1). The contents of K_2O, MnO and P_2O_5 in olivine-bearing samples are generally negligible. Enhanced concentrations of K_2O (up to 1.7 wt %) characterize some of the retrogressed samples containing phlogopite.

The analyzed samples of hornblendite which is interlayered with olivine-bearing rocks show constant composition reflecting the composition of amphibole: MgO = 11.5-16 wt %, Fe_2O_3=12-13 wt %; Al_2O_3=12-13%; CaO= 10-11 wt %; Na_2O=2-3 wt %. The contents of other major oxides are insignificant.

Amphibolite associated with olivine-bearing rocks and hornblendite is characterized by relatively constant chemical compositions. The SiO_2 content varies in the range 43-51 wt %; Fe_2O_3=8.5-15 wt %; MgO=6-13 wt %; CaO=7.5-10.5 wt %; Al_2O_3=11-15 wt %; Na_2O=2-4 wt %. The contents of other oxides are low or insignificant: TiO_2<1.5 wt %, K_2O<0.9 wt %; P_2O_5<0.2 wt % (Appendix 2; Fig.4.2.1).

In Fig.4.2.1 it can be observed that all samples belonging to the layered mafic-ultramafic rock association display negative correlations between MgO and SiO_2, Al_2O_3, CaO, Na_2O and Y. Moreover, the compositional data form continuous trends implying that all samples belong to the same magmatic suite and represent products of different degrees of fractionation.

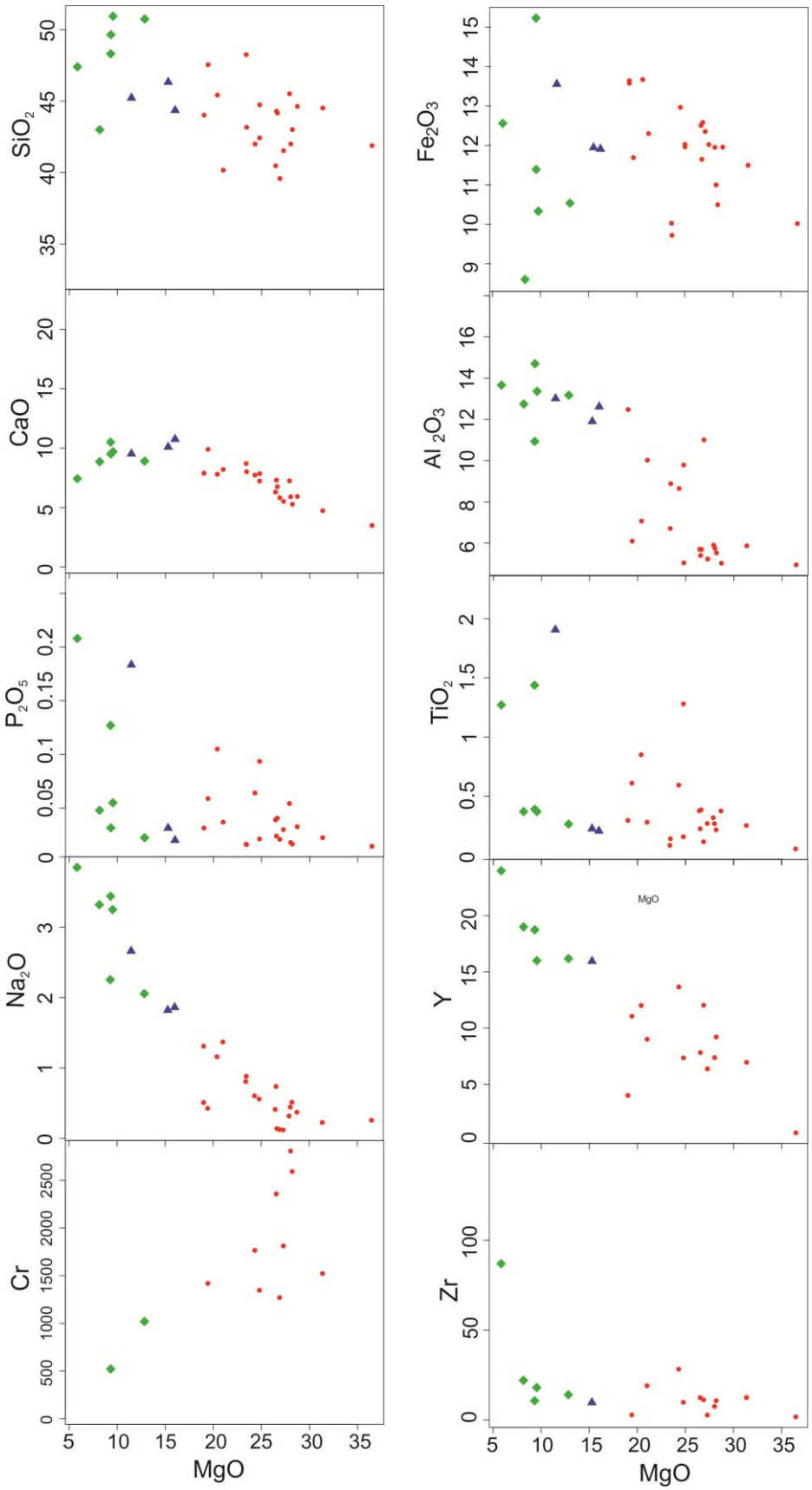

Fig.4.2.1. Element vs. MgO bivariate plots for the layered mafic-ultramafic rock association from Senja (major elements in wt.%; trace elements in ppm). Red circles – olivine-bearing rocks (olivine hornblendite, hornblende peridotite, spinel-bearing olivine pyroxene hornblendite); blue triangles – hornblendite; green rhombs – amphibolite.

On the bivariate diagrams of element vs. MgO (Fig.4.2.2), samples of massive and volcanoclastic amphibolite (black circles on Fig. 4.2.2) collected within various parts of the Astridal supracrustal belt show some weak positive correlations between MgO and Fe_2O_3, TiO_2, P_2O_5 and Zr. The compositional data of amphibolite belonging to mafic-ultramafic rock association (open triangles in Fig.4.2.2) do not fit to these trends and are scattered on the diagrams element vs. MgO, implying that the amphibolite found in the layered association and the massive/volcanoclastic amphibolite from the supracrustal zones are most likely not cogenetic, and therefore belong to different magmatic suites. On the contrary, the two data points of the dyke-like amphibolite enclaves within tonalitic gneiss (Fig. 4.2.2; see section ???) show compositions more similar to the volcanoclastic/massive amphibolite.

The TAS diagram for plutonic rocks (Cox et al., 1979, Fig.4.2.3) shows that the samples of mafic-ultramafic layered association belong to the basic and ultrabasic chemical class. All olivine-bearing varieties plot outside the defined fields, while hornblendite and amphibolite samples plot within the gabbroic field. On the SiO_2-Zr/TiO_2 diagram (Winchester and Floyd, 1977; Fig.4.2.4) the majority of the olivine-bearing rocks also plot outside the fields, while the samples of hornblendite and amphibolite from the layered mafic-ultramafic association plot within field of subalkaline basalt. This implies that the contents of alkalies have not been significantly changed by any secondary processes. The diagram SiO_2 vs. FeO^t/FeO^t+MgO (Fig. 4.2.5a) is used to discriminate between ultramafic and mafic cumulates (Coleman, 1977). The majority of the analyzed samples of the studied layered association plot in the mafic cumulate field, except from four samples, which plot close to the field of mafic cumulate and one which plots at the edge of ultramafic cumulate field (Fig.4.2.5a). Coleman (1977) also provided the ternary discrimination diagram Al_2O_3–CaO–MgO (Fig. 4.2.5b). All the analyzed samples of olivine-bearing ultramafic varieties clearly plot whithin the field of ultramafic cumulate while the compositions of hornblendite and amphibolite fall into the field of mafic cumulate (Fig.4.2.5b). Compared to the composition of metamorphic peridotite (originated in orogenic belts) the studied olivine-bearing varieties show higher concentrations of Al_2O_3 and CaO, which are, however, lower than those defining the compositional field of komatiite (Colemann, 1977).

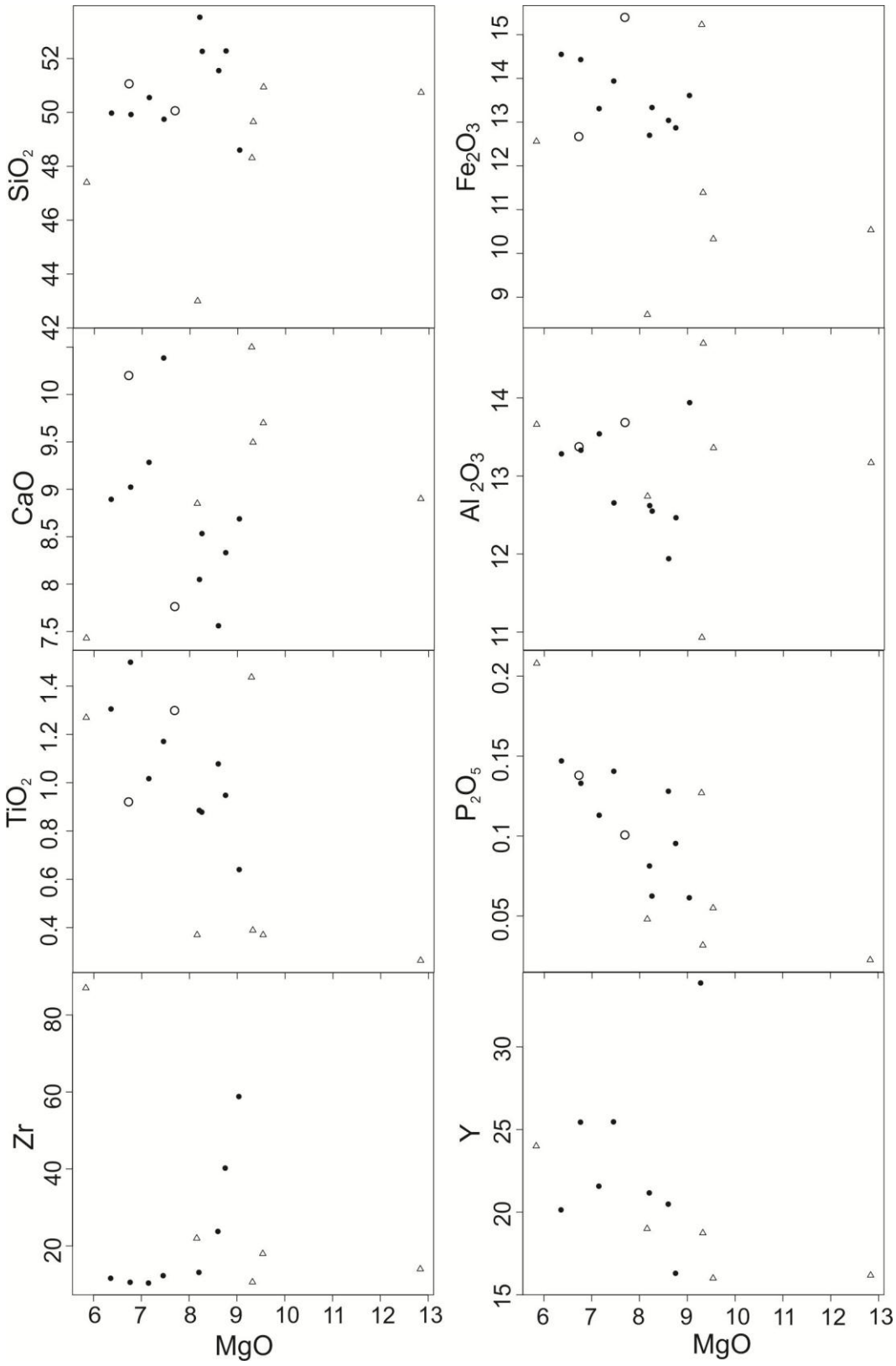

Fig.4.2.2. Element vs. MgO bivariate plots for various amphibolites from the Astridal supracrustal belt (major elements in wt. %; trace elements in ppm). Black circles – massive and volcanoclastic amphibolite from Astridal supracrustal zone; open circles – massive amphibolite from dyke-like enclaves within tonalitic gneisses; open triangles – amphibolite from the layered mafic-ultramafic rock association.

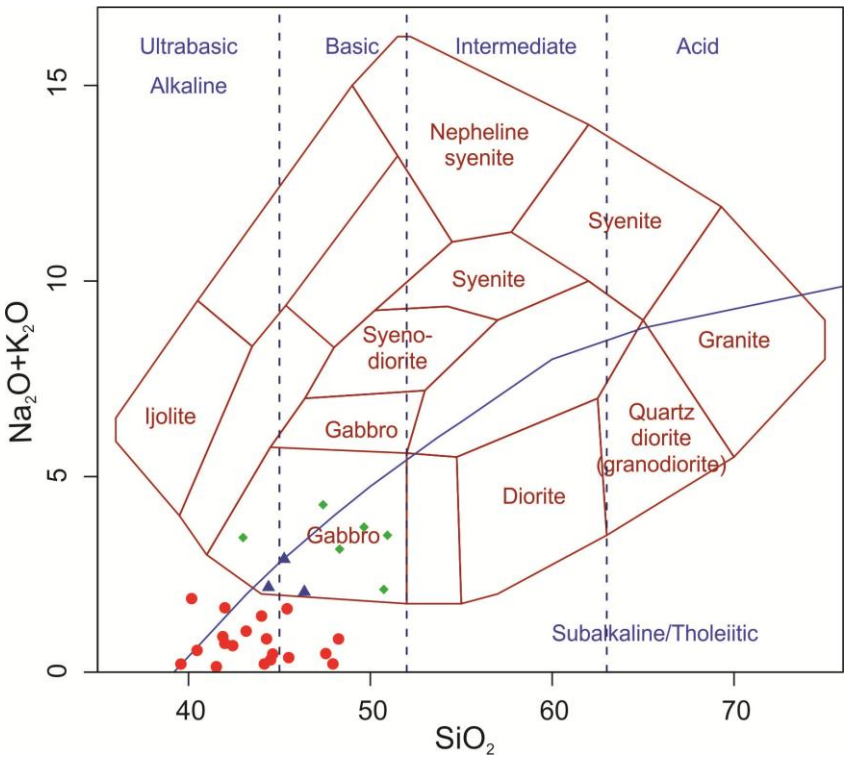

Fig.4.2.3. Compositional data of samples from the mafic-ultramafic rock association in the TAS diagram for plutonic rocks after (Cox et al., 1979). Symbols are the same as in Fig.2.4.1.

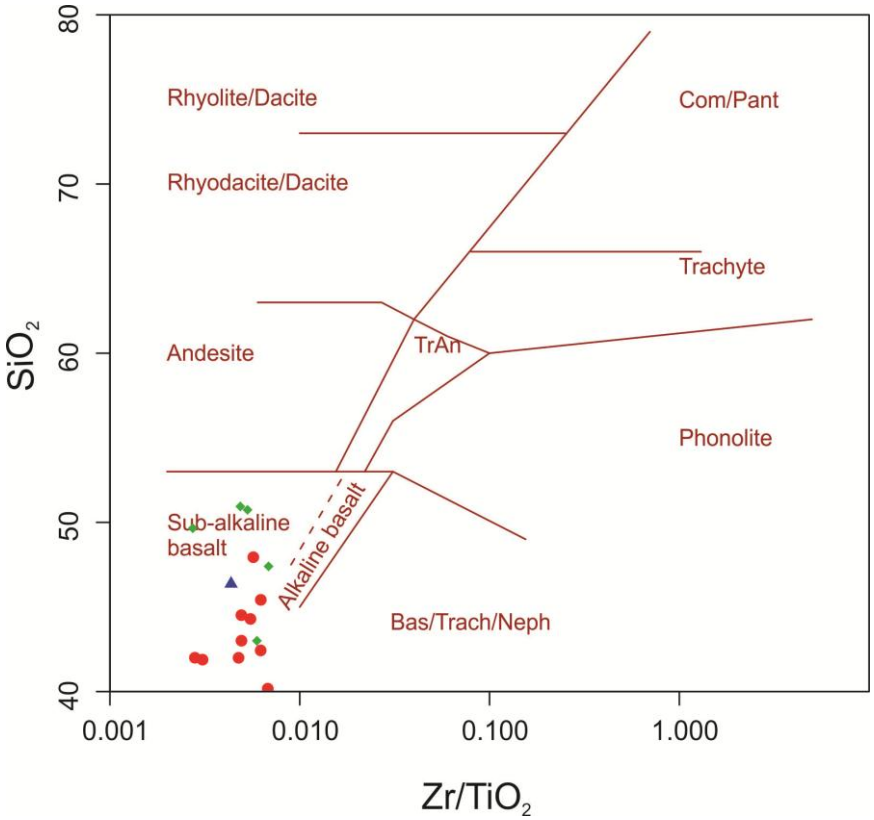

Fig.4.2.4. Compositional data of samples from the mafic-ultramafic rock association in the classification diagram with immobile elements after Winchester and Floyd (1977). Symbols are the same as in Fig.2.4.1.

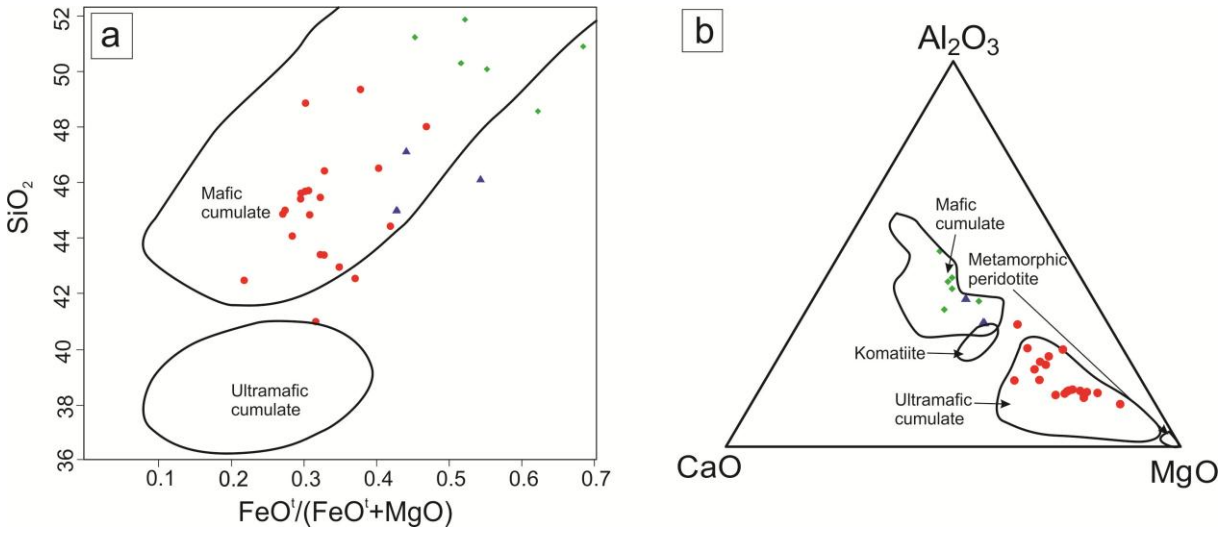

Fig.4.2.5. Compositional data of samples from the mafic-ultramafic rock association in the discrimination diagrams SiO_2 vs.$FeO^t/(FeO^t+MgO)$ (a) and CaO-Al_2O_3-MgO (b) after Coleman (1977). Symbols are the same as in Fig.2.4.1.

The compositions of the two amphibolite types, one belonging to the layered mafic-ultramafic association and one represented by the massive/volcanoclastic amphibolite collected from the supracrustal suites have been plotted on the AFM diagram (Fig. 4.2.6; Irvine and Baragar, 1971). The compositions of both types of amphibolite lie just above the line separating calc-alcaline and tholeitic series. Compared to the volcanoclasic/massive amphibolite, the compositions of the amphibolite from the layered association show wider range in MgO (generally higher, see also Fig.4.2.2).

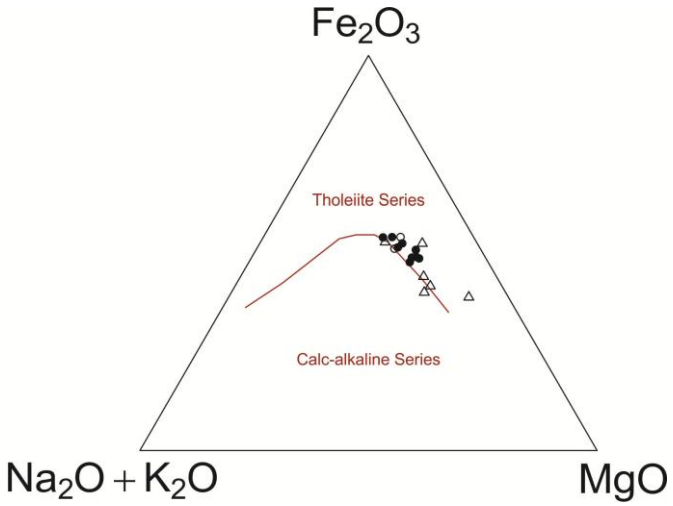

Fig.4.2.6. Compositional data of amphibolites in the AFM diagram after Irvine and Baragar (1971). Symbols are the same as in Fig.4.2.2.

4.3. Trace element contents

Trace element and REE compositions of the studied rocks are given in Appendix 2. The analyzed ultramafic varieties, both olivine-bearing (hornblende peridotite, olivine hornblendite, spinel-bearing olivine pyroxene-hornblendite) and hornblendite show the following compositional variation: Zr=2-50 ppm, Nb = 0.2-4.1, ppm, Cr=655-2592 ppm, Ba=0.7-41.3 ppm, Sr=5-50 ppm, Cs=0.03-13.7 ppm, Y=0.7-16 ppm. The analyzed contents of U, Th and Pb generally are below the detection limit (<0.01 ppm). Total REE content varies in range 8-36.8 ppm, with Ce/Yb ratios varying from 0.5 to 7.1. The content of Rb varies over wide range, from 0.2 to 227 ppm. The concentrations of Co and Ni vary from <0.01 to 203 ppm and from 1629 to 4500 ppm respectively (in some of the samples the analyzed Ni content was below detection limit). Such anomalously high contents of Ni and Co indicate that these elements may be partly incorporated in ore minerals.

Two samples of the amphibolite of the layered mafic-ultramafic layered rock association show the following trace and REE element contents: Zr =10.6-87 ppm, Nb = 0.4-13 ppm, Cr = 519-1038 ppm, Ni=216-268 ppm, Co= 49-65 ppm, Ba=24-36 ppm, Sr=77.6-87.6 ppm, Y=16.2-24 ppm. The contents of Cs, Rb, U, Th and Pb are very low and do not exceed 5 ppm. The total content of REE for the two samples is 14.6 and 18.3 ppm, with Ce/Yb ratios of 0.86 and 1.2.

The trace element patterns are generally relatively similar for all the olivine-bearing varieties (Fig.4.2.7a, b, c). In general, the samples show compositions close to primitive mantle, in particular the spinel-bearing variety (Fig.4.2.7c). The samples of hornblende peridotite and olivine hornblendite (Fig.4.2.7a) are slightly more enriched in incompatible elements compared to primitive mantle and the samples from the olivine-orthopyroxene-amphibole-green spinel paragenesis (Fig.4.2.7c). For all varieties, Ta-Ti-Nb anomalies are absent, suggesting no significant crustal contamination. The dramatic positive anomalies of K, Rb and Cs characterize altered (retrogressed) samples (Fig.4.2.7b) and are most likely related to the presence of phlogopite. These samples do not show any enrichment in other incompatible elements giving evidence for a non-magmatic origin of phlogopite. The origin of the pronounced U-Th-Pb negative anomalies is uncertain, but may be related to analytical problems.

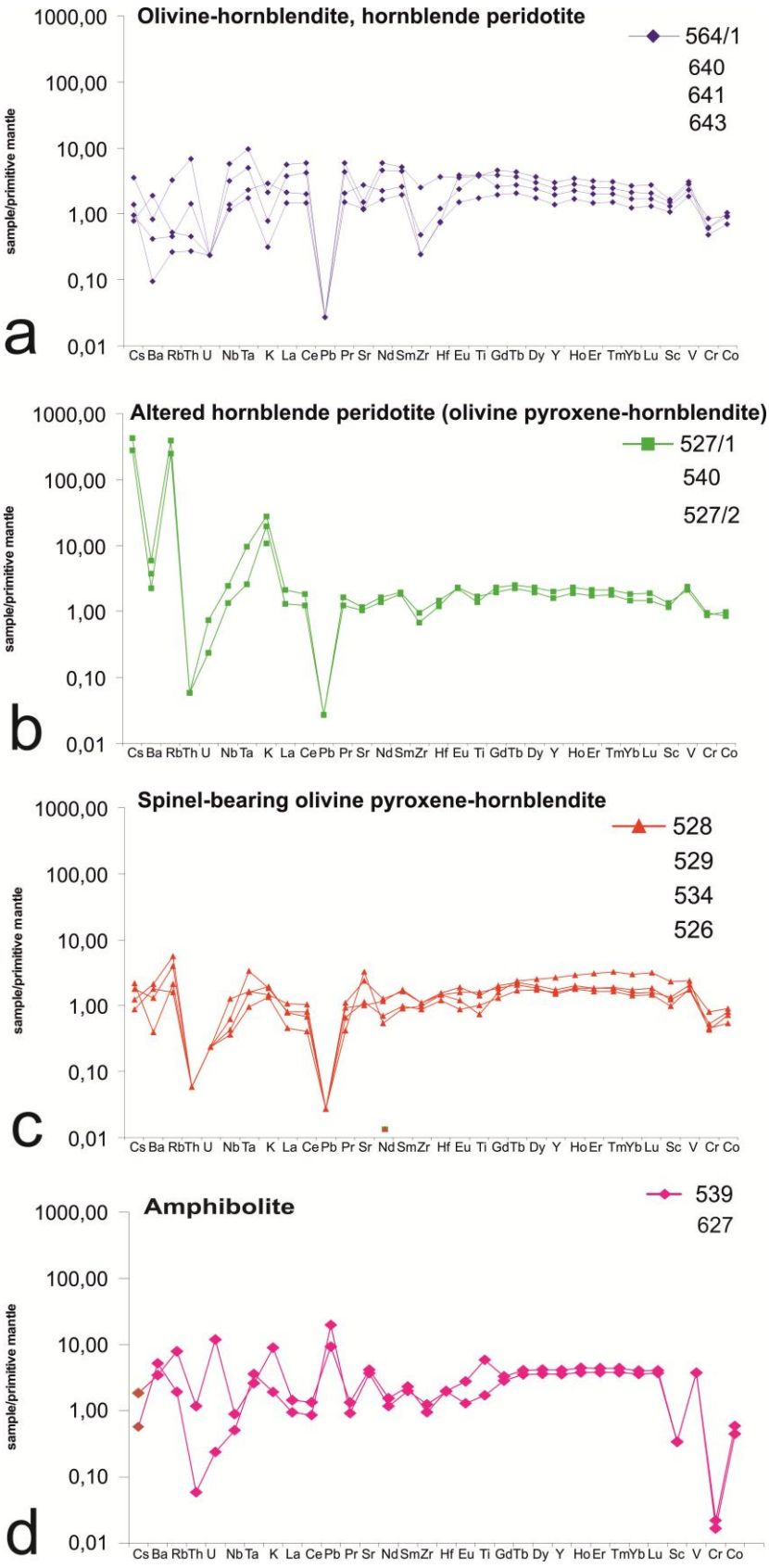

Fig.4.2.7. Spider plots for different varieties of the mafic-ultramafic rock association from Senja, normalized to primitive mantle after Sun and McDonough (1989).

Compared to the unaltered olivine-bearing varieties, the amphibolite samples from the layered mafic-ultramafic association show enhanced concentrations of K, Rb, Cs (Fig.4.2.8), a positive Pb anomaly and negative Sc-V anomalies.

The REE patterns (Fig. 4.2.8) are MORB-like, non-fractionated for samples containing the olivine-amphibole paragenesis and slightly fractionated with depletion in LREE compared to MREE and HREE for samples containing green spinel. This correlates with generally higher #Mg (indicating lower degree of fractionation) in spinel-bearing olivine pyroxene-hornblendite. This indicates that the differences in chemistry and composition between the spinel-bearing rock and the olivine-amphibole rock are due to primary magmatic features and not any secondary alteration processes.

The amphibolite associated with olivine-bearing rocks is characterized by slightly LREE-depleted patterns (Fig.4.2.9). In contrast, the massive/volcanoclastic amphibolite, which not is associated with the ultramafics, shows conformal LREE-enriched patterns with Ce/Yb =2-15 (Fig.4.2.9).

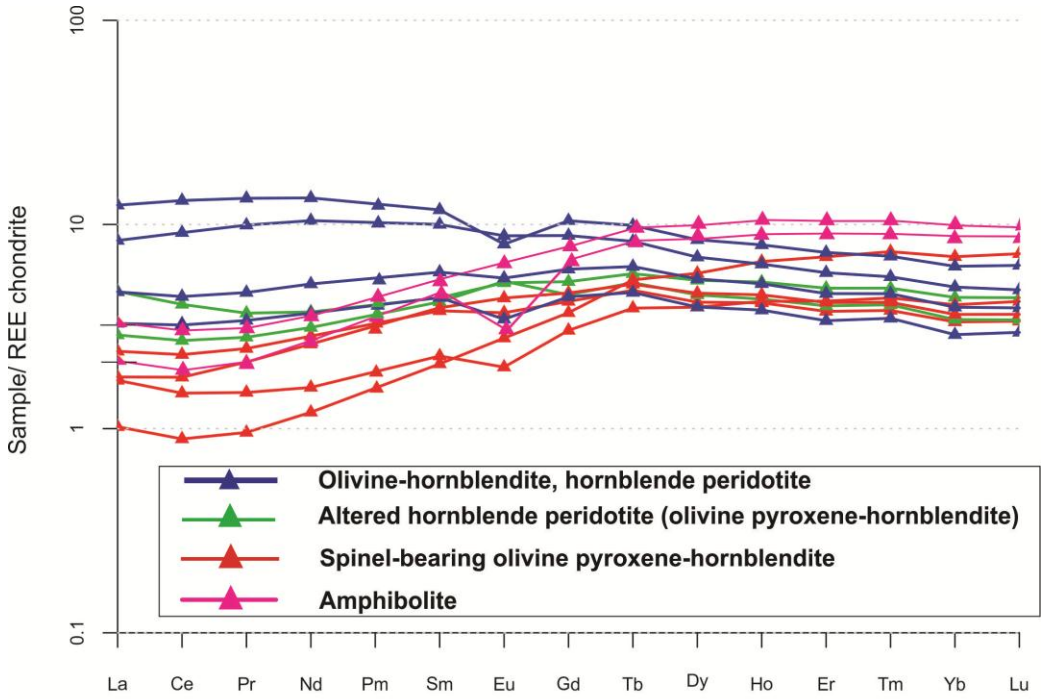

Fig.4.2.8. REE patterns of different rock varieties comprising mafic-ultramafic rock association from Senja, normalized to chondrite after Boynton (1984).

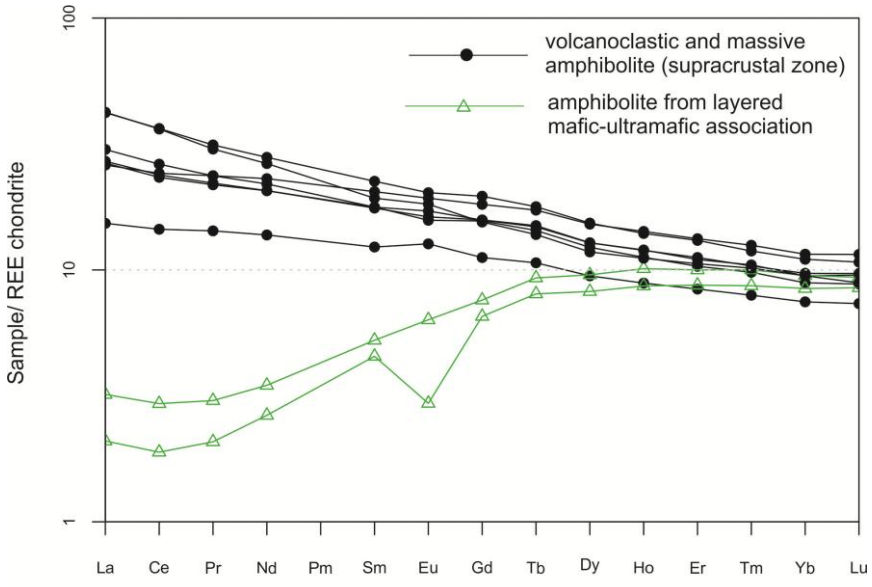

Fig.4.2.9. REE patterns of different amphibolites from Senja, normalized to chondrite after Boynton (1984).

Chapter 5. Mineral chemistry

5.1. Analytical procedure

Mineral compositions were determined by a JXA8530F JEOL HYPERPROBE Field Emission Electron Probe Microanalyser (FE-EPMA), at the Centre for Experimental Mineralogy, Petrology and Geochemistry (CEMPEG), Uppsala University. Operating conditions during the analyses were as follows: a 10 nA beam current with 15 kV accelerating voltage and counting times of 10 seconds for peak and 5 seconds for ±background. Mineral standards: Si, Ca - wollastonite, Na - albite, K - orthoclase, Mn, Ti – pyrophanite ($MnTiO_3$), and pure element oxides: Al_2O_3, MgO, Fe_2O_3, Cr_2O_3 were used for calibration. All elements were analysed by Kα spectral lines. Raw counts were corrected using the PAP routine. The analyses of mineral compositions are given in Appendix 3.

5.2. Results

Amphibole occurs as a rock-forming mineral for all varieties of the Senja ultramafic rocks. It is represented by euhedral colorless or light greenish grains and occurs both in the matrix of the rocks and as small inclusions in olivine grains and oikocrysts of orthopyroxene (Fig.5.2.1b). In some of the most amphibole-rich samples (olivine hornblendite and hornblendite), zonation of amphibole grains has been documented (Fig.5.2.1a).

Amphibole analyses (36 spots from 11 samples) are given in Appendix 3. All of the analyzed amphibole grains are represented by calcic varieties (1.61 -1.96 atoms of Ca per formula unit), and they are rich in iron (0.4-1.33 atoms per formula unit) and magnesium (3-4.35 atoms per formula unit). According to the classification scheme after (Leake et al., 1997) the compositions continuously range from tchermakitic to high-Mg actinolitic. Compositions in the actinolite field plot close the boundary between actinolite and tremolite, Fig.5.2.2). The majority of the analyzed amphibole grains show compositions similar to magnesiohornblende. Any clear correlative relationship between rock modal composition and amphibole composition has not been revealed (Fig.5.2.2). There is also no significant compositional difference between the matrix amphibole and the small amphibole inclusions enclosed in orthopyroxene or olivine (Fig.5.2.2). The analyses performed for several zoned grains indicate however that the rims are represented by high-Mg actinolite while the cores correspond to the composition of magnesiohornblende.

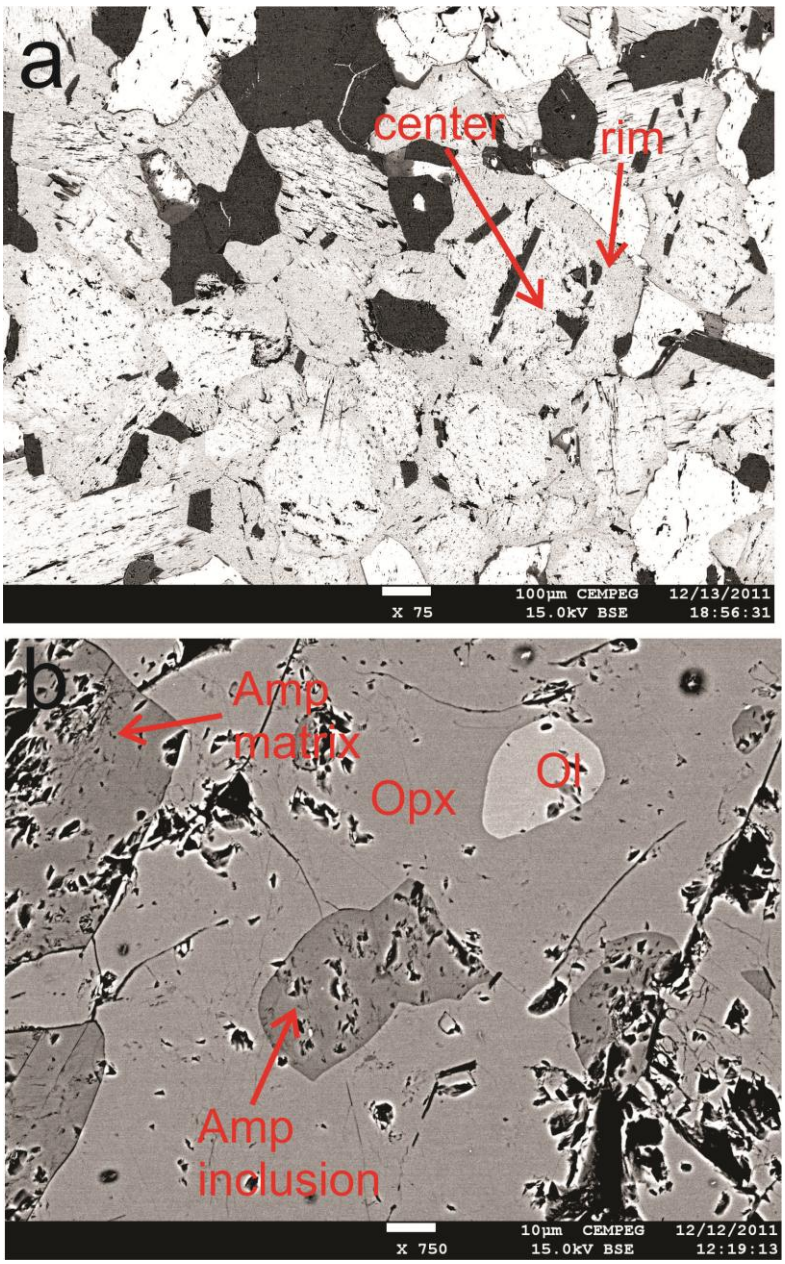

Fig.5.2.1.Back-scatter images of zoned amphibole grains in sample 613 (a) and textural relationship between amphibole and other mineral phases in sample 529 (b).

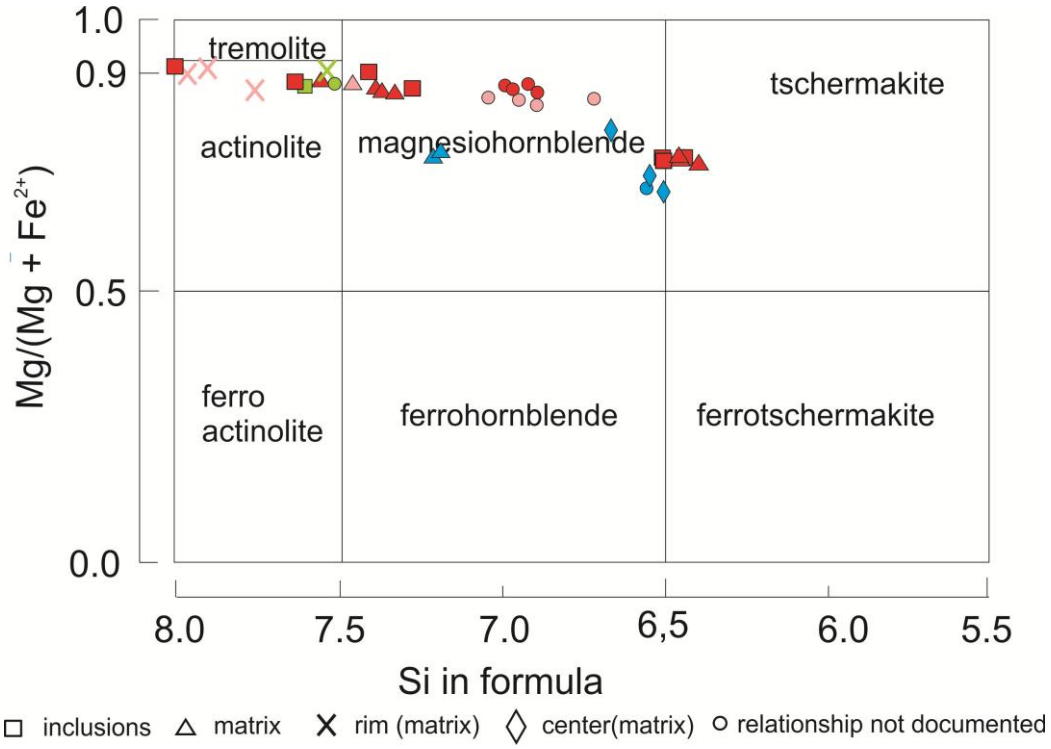

Fig.5.2.2. Compositional variations of amphiboles from the Senja ultramafic rocks in the classification diagram after Leake et al. (1997). Red color shows analyses from spinel-bearing olivine-pyroxene hornblendite; pink color from hornblendite peridotite and olivine hornblendite; blue color from hornblendite; green color from retrogressed olivine-pyroxene hornblendite and olivine hornblendite.

Olivine occurs as a rock-forming mineral in the majority of the ultramafic rocks belonging to mafic-ultramafic layered association of NW Senja. It makes up the matrix of the rocks and is also preserved as inclusions in oikocrysts of orthopyroxene. Olivine analyses (19 spots in 6 samples) are given in Appendix 3. Olivine is characterized by a significant range in forsterite content from Fo_{65} to Fo_{85}, which is much lower than the values Fo_{84}-Fo_{95} reported for mantle olivine (Arai et al., 2001; Takahashi, 1986). The content of Mn varies over the range 0.003-0.01 atoms per formula unit (MnO=0.15-0.46 wt %), while Ni varies over the range 0.003-0.01 atoms per formula unit (NiO=0.13-0.51 wt %). It has not been revealed any correlative relationship between NiO and forsterite content. However, the trend of forsterite content of olivine is consistent with Mg# of orthopyroxene and whole rock Mg# trends (Fig.5.2.3).

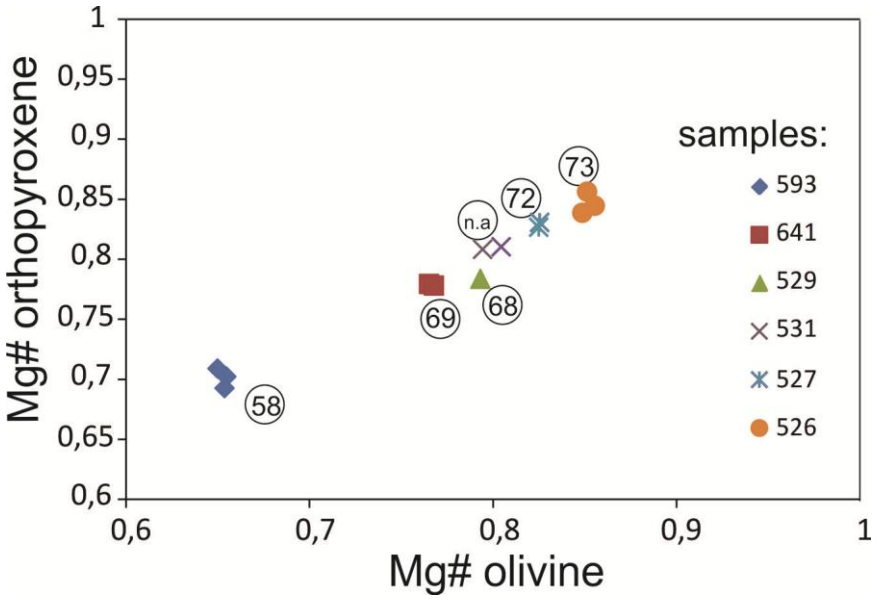

Fig.5.2.3. Mg# of olivine vs. Mg# of coexisting orthopyroxene for 6 samples of the Senja ultramafic rocks. The numbers in circles indicate whole rock 100Mg/(Mg+Fe). n.a=not analyzed.

Orthopyroxene occurs in an equilibrium paragenesis together with olivine, amphibole and green spinel. It forms up to 2-3 cm long oikocrysts, which commonly enclose large amounts of olivine and amphibole grains. Orthopyroxene analyses (18 spots in 6 samples, Appendix 3) show that the compositions correspond to the solid solution series between enstatite and ferrosilite with the enstatite component ranging from En_{64} to En_{85} (Fig.5.2.3). Orthopyroxene is poor in calcium (CaO<0.15 wt %,) and alumina (Al_2O_3=0.51-2.34 wt %, 0-0.05 atoms of Al per formula unit). The contents of other oxides are negligible. The analyses performed on different parts of a single grain of orthopyroxene indicate that the oikocrysts are largely homogenous and not characterized by any compositional zonation.

Spinel occurs in equilibrium paragenesis together with olivine, orthopyroxene and amphibole as an intercumulus phase. In thin-section, spinel shows colors varying from bright dark green to light brownish green. In some of the retrogressed samples, partial replacement of spinel by magnetite has been observed. Fourteen analyses performed from 4 samples (Appendix 3) indicate that spinel is characterized by relatively constant composition. It is Mg-rich (0.45-0.65 atoms per formula unit), extremely Al-rich and Cr-poor (Fig.5.2.4) as Cr/Cr+Al does not exceed 0.1. Ferric iron ranges from 0.03-0.09 atoms per formula unit, while Fe^{2+} is 0.33-0.54 atoms per formula unit. Based on its composition spinel can be referred to as pleonast (Al-rich variety).

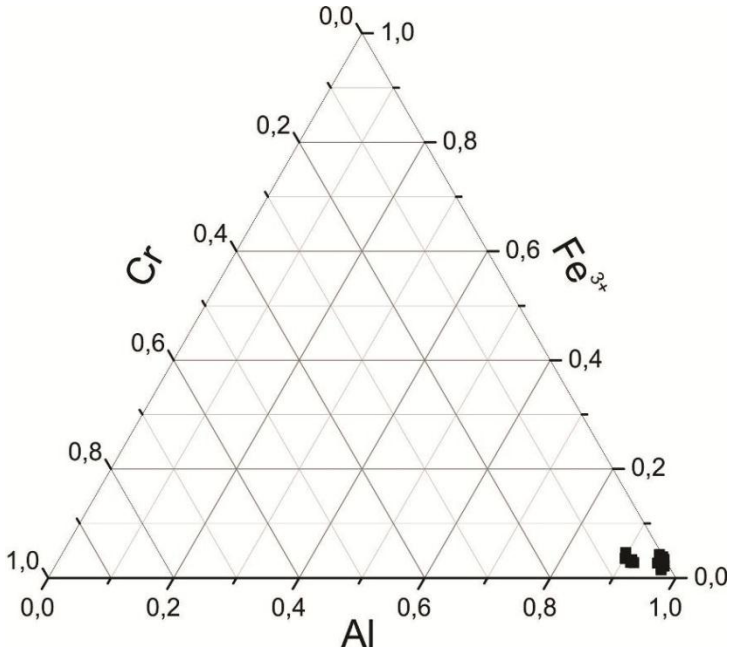

Fig.5.2.4. Triangular Cr-Fe^{3+}-Al plot showing compositions of green spinels from Senja ultramafic rocks.

The only opaque mineral phase is represented by magnetite. It occurs in most of the ultramafic rock varieties belonging to layered association (except hornblendite). In some of the spinel-bearing samples, clear replacement textures of spinel by magnetite are visible. Analyses of magnetite (4 spots in 4 different samples, Appendix 3) show relatively high content of chromium (Cr_2O_3=3.3-4.9 %) indicating that in addition to spinel also magnetite accommodates a significant portion of chromium in the rock. The content of TiO_2 is 0.8-1.3 wt % while the role of other oxides is negligible.

The presence of secondary low P-T mineral assemblages including serpentine, chlorite and phlogopite were identified during microprobe work.

Chapter 6. U-Pb ID-TIMS zircon dating

6.1. Sample preparation and analytical procedure

For zircon separation, sample 65/2 (sample location see in Appendix 1; chemical composition is given in Appendix 3) of an amphibolitized gabbroic rock spatially associated with hornblendite and olivine hornblendite was chosen, because it was the most Zr-rich (Zr=87 ppm) of the studied samples. The rock shows a massive coarse-grained texture (Fig.6.1.1). The first stage of the sample preparation procedure was to crush and mill the rock. Zircon was concentrated in several stages by means of water separation, sieving at 0.2 mm, magnetic separation and separation by the use of heavy liquid.

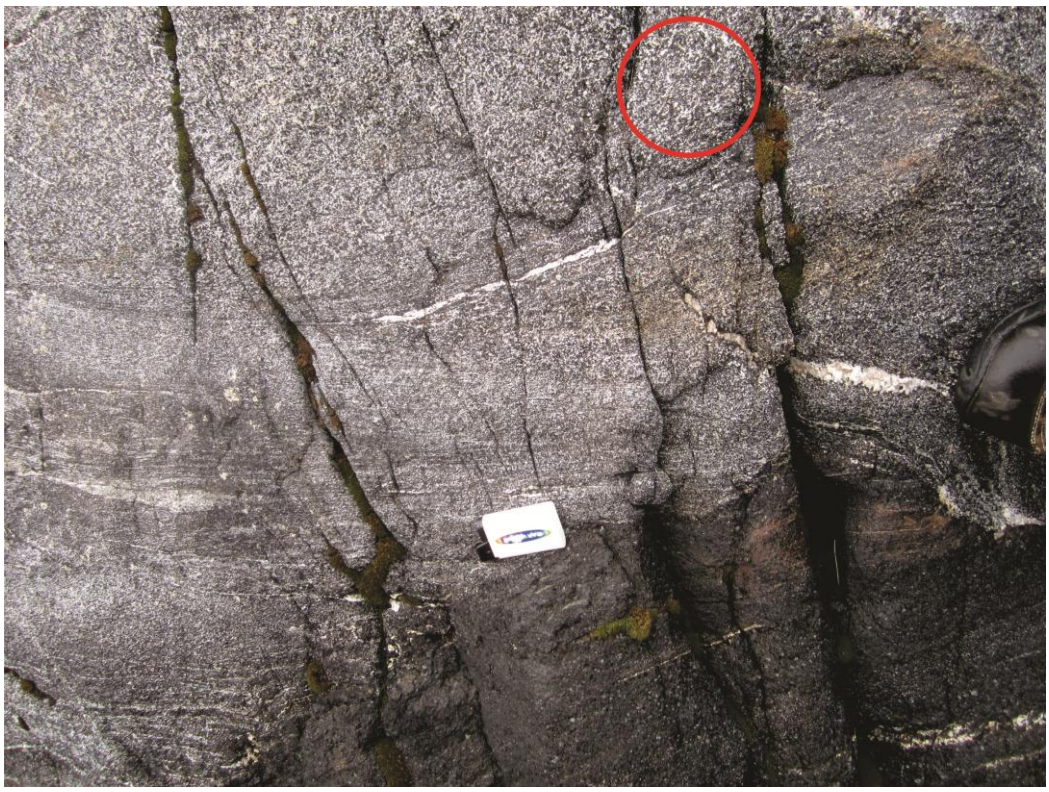

Fig.6.1.1. Field photograph showing the metagabbroic rock collected for U-Pb dating. Red circle indicates location of sample 65/2.

Only five zircon grains were found in the heavy non-magnetic fraction after separation processing. Four of them were small grains (less than 0.1 mm in diameter), while the fifth one was represented by a tiny (~0.01 mm in diameter) inclusion in a rounded apatite grain (Fig. 6.2.2). All of the grains were homogenous and characterized by a subhedral rounded shape which is common for metamorphic zircons (e.g. Corfu et al., 2006). Zircon analyses were carried out by the isotope dilution method at the University of Oslo, Norway. The selected samples were

subsequently washed using HNO_3, H_2O and acetone, weighed on a microbalance, and spiked with a mixed $^{205}Pb/^{235}U$ tracer. Dissolution of zircon was carried out with HF (+HNO_3) in Teflon bombs (Krogh, 1973) at 184˚C. Then the solution was transformed to the columns with fresh resin and multiply washed using HCl and H_2O. After evaporation two of the samples, which successfully went through the procedures, were loaded on zone-refined Re filaments with Si-gel and H_3PO_4. Then, the samples were measured on a MAT 262 mass spectrometer on Faraday cups in static mode/ by peak-jumping in an ion-counting secondary electron multiplier and for $^{207}Pb/^{204}Pb$ ratios by peak-jumping in an ion-counting secondary electron multiplier following the standard procedure. The data were corrected and recalculated using methodology described in detail by Corfu (2003). The initial common Pb in zircon was corrected using the Pb isotope composition predicted by the model of Stacey and Kramers (1975) for the age of the sample as 1980 Ma for sample 63-2-357/27 and 1700 Ma for sample 63-2-357/28. The data plotting and age calculations were performed using the program ISOPLOT of Ludwig (1999).

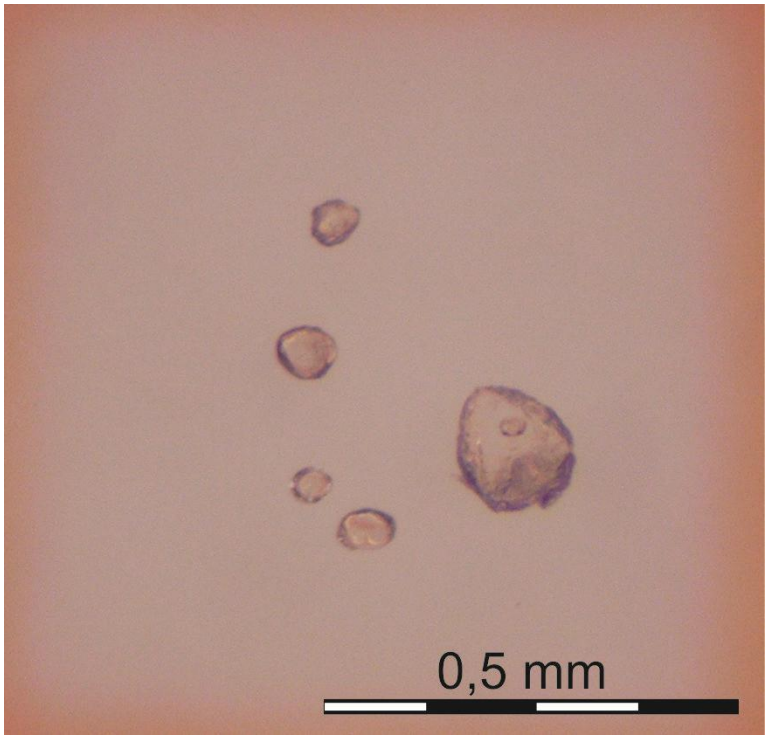

Fig. 6.2.2. Optical image of four zircon grains and one zircon inclusion in apatite separated from sample 65/2 for isotope dating.

6.2. Results

The analytical results for two dated samples are given in Appendix 4. The two analyzed samples show U contents of 141 and 69 ppm, and low inferred Th/U of 0.17 and 0.21.

Thorium and U contents are often helpful for interpretation of zircon genesis. In igneous zircon from mafic intrusive rocks the typically reported contents of U content vary in the range from ~10 ppm to 700 ppm (Belousova et al., 2002), with a median value of 270 ppm (Wang et al., 2011). Th/U ratios vary in the range 0.4-2.4 (Heaman et al., 1990), with a median ratio of Th/U=0.81 has recently been reported (Wang et al., 2011). Lowering of the Th/U ratios together with resetting of the U-Pb isotope system occur through solid-state recrystallization of zircon during metamorphism (Hoskin and Black, 2000). Th/U ratio reaches extremely low values in zircons that are newly grown during anatexis (<0.07, Rubatto, 2002). The zircons analyzed in this study show inferred Th and U contents that closely resemble the compositions of metamorphic zircon, rather than igneous zircons from gabbroic rocks. A metamorphic origin is also supported by the rounded shape of the investigated zircons.

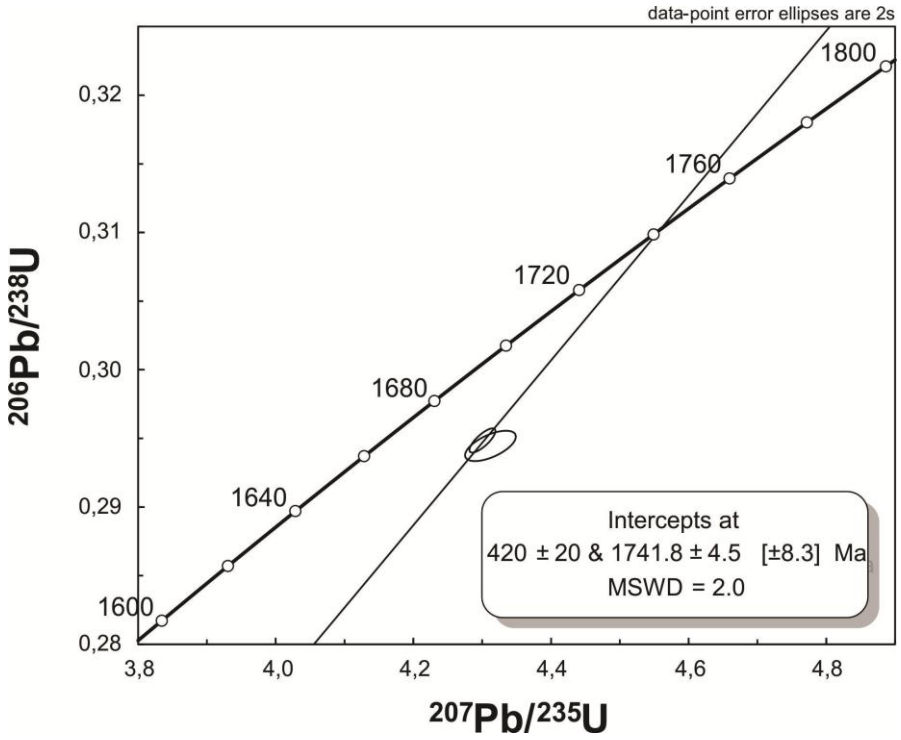

Fig.6.2.1. Isotope compositions of two analyzed zircon grains shown in the discordia diagram.

The data obtained for two zircon grains is shown in the discordia diagram in Fig.6.2.1. The discordia was plotted by assumption of the lower intercept at 420 ± 20 Ma. This lower intercept age was chosen on basis of previous U-Pb isotope dating in the West Troms Basement Complex, which shows that Paleoproterozic zircons are substantially affected by Caledonian metamorphic overprint (e.g. Corfu et al., 2003). The upper intercept yields an age of 1741.8 ± 4.5 Ma with MSWD=2 and can be considered as the age of zircon crystallization.

Chapter 7. Discussion

7.1. Petrogenesis

As the studied layered mafic-ultramafic rock association of NW Senja occurs within amphibolite-facies metamorphic rocks, it might be possible that the mineral parageneses making up the studied ultramafic rocks are metamorphic. Indeed, rocks with similar rock-forming mineral assemblages have been reported from several occurrences around the world (e.g. Peltonen, 1995; Frost, 1975; Desmarais, 1981; Trommsdorff and Evans, 1974; Vance and Dungan, 1977). In the Vammala Nickel Belt in Finland, a rock composed of green spinel, olivine, orthopyroxene and amphibole has been inferred to represent picrite metamorphosed at upper amphibolite facies (Peltonen, 1995). Such a paragenesis has been described by Evans (1977) as typical for metaperidotite and has been inferred to result from chlorite dehydration reactions, e.g: clinochlore = forsterite + 2 enstatite + spinel + 4 H_20, which takes place at 750-775°C and 3.5-4 kbar (Fawcett and Yoder, 1966). Peltonen (1995), however, does not discuss in detail the textures approving a metamorphic origin of the studied rocks, what makes it complicated to compare the ultramafics from NW Senja with the rock from the Vammala Nickel Belt. Mineral assemblages identical to these described from NW Senja have been reported from Ruby Range, Montana, USA (Desmarais, 1981). A metamorphic origin of the mineral assemblages was approved by abundant deformation fabrics in orthopyroxene, indicating that the formation of megacrysts occurred at an early stage of metamorphism. In the rocks from Ruby Range, relics of original serpentinite textures, such as included S-surfaces of opaque oxides in both matrix and megacryst phases have been documented. Furthermore, orthopyroxene, which occurs both in matrix and as megacrysts in the ultramafics from Ruby Range is characterized by different Al_2O_3 and CaO contents implying that orthopyroxene in matrix crystallized at an igneous stage, while the megacrysts were formed at lower temperature during metamorphism. Thus, based on a number of evidences, Desmarais (1981) proposed that the protolith for the metamorphic rocks from Ruby Range was olivine websterite, which underwent serpentinization and progressive metamorphism under upper amphibolite facies conditions involving a number of dehydratation reactions.

Obviously, the studied ultramafic rocks form NW Senja seem to be very similar to those described from Ruby Range. Among the main common features are 1) field occurrence as podiform bodies (boudins) within amphibolite facies metamorphic suites, 2) rock-forming mineral assemblage and whole-rock composition, 3) textural similarities (e.g. megacrysts of orthopyroxene

enclosing olivine and amphibole). However, textural features approving syn-metamorphic growth of orthopyroxene as well as relics of serpentinite fabric have not been documented from the ultramafics from NW Senja. Furthermore, some of the features, such as aligned anhedral spinel filling in the interstitial space, clearly support cumulate origin of the texture.

The composition of olivine can be also used to constrain its petrogenesis. The studies of meta-ultramafic rocks formed by de-serpentinization (e.g. Vance and Dungan, 1977; Trommsdorff and Evans, 1972; Pluemper et al., 2012) show that "primary" high-temperature olivine can be distinguished from the "secondary" one (formed during metamorphic de-serpentinization reactions) based on the NiO and MnO contents. Plots of NiO and MnO versus the forsterite content of high-temperature olivine generally define narrow linear trends (Fig.7.1.1). In contrast, secondary olivines analyzed by Vance and Dungan (1977) show no systematic relationship between their NiO, MnO content and forsterite content. In addition, secondary olivine often has extremely low NiO (0.10 wt %), even at highly magnesian compositions. Hence, the incipient olivine incorporates most of the Mn in the rock; its content in the olivines formed by dehydratation reactions is higher by approximately an order of magnitude than that of the olivine with similar forsterite content in high-temperature peridotites (Fig. 7.1.1b).

Olivine from the ultramafic suite of NW Senja shows no correlation between forsterite and NiO content (Fig. 7.1.1a), but generally the concentration of NiO with respect to the forsterite content is slightly higher than typical for primary olivine in ophiolite cumulates. It is less variable than observed in secondary olivine from amphibolite facies metamorphic rocks, and significantly higher compared to the NiO content in low-temperature metamorphic olivine (Fig.7.1.1). The studied olivines also differ from secondary olivines by their MnO contents. In the MnO vs. forsterite content diagram, olivine forms a trend, which is generally consistent with the trend of primary olivine typical for ophiolite cumulates (Fig.7.1.1b). In contrast, secondary olivines are characterized by more variable and sometimes anomalously high concentrations of MnO(Fig.7.1.1b).

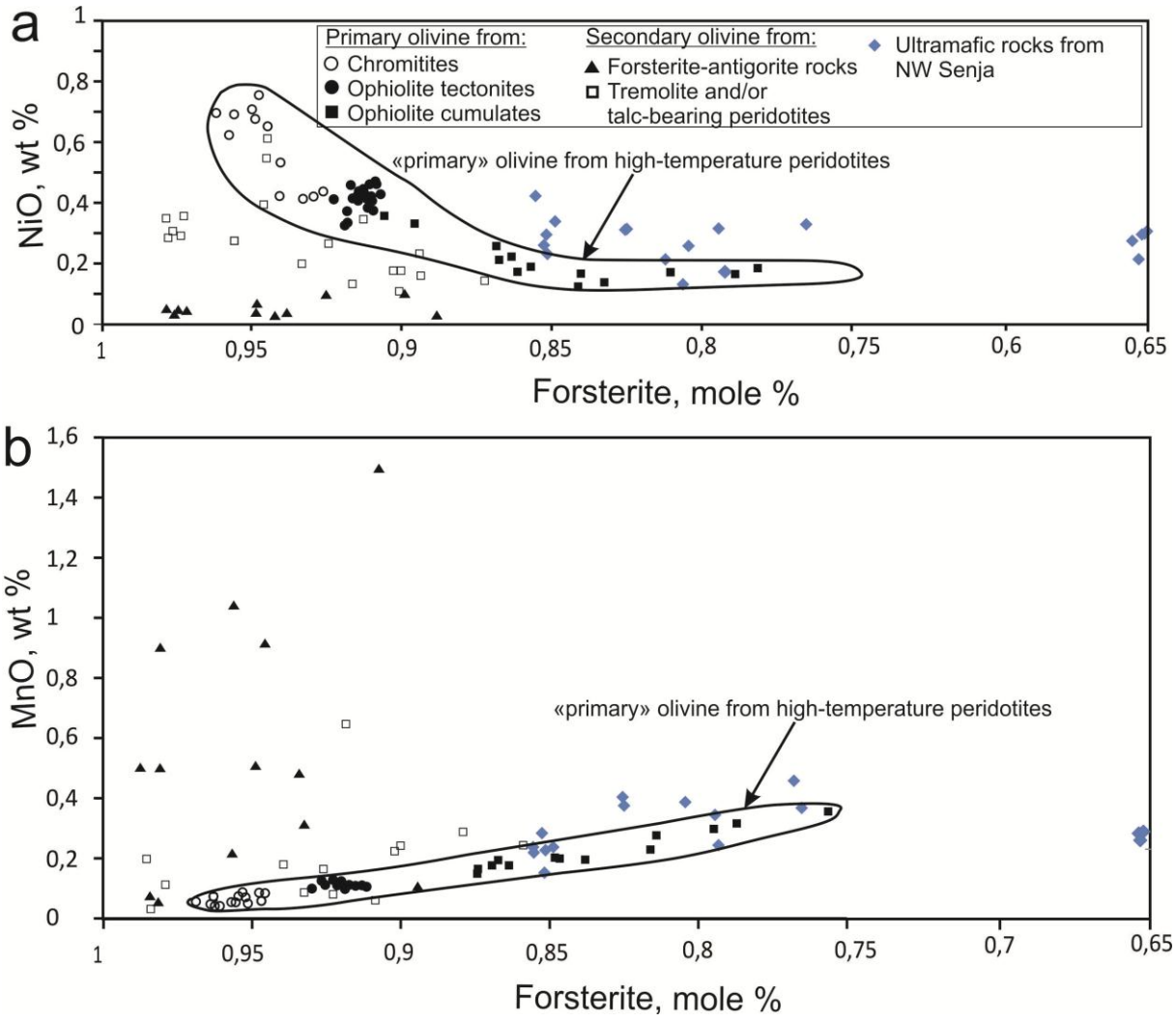

Fig.7.1.1. Plots of NiO (a) and MnO (b) versus the forsterite content for olivine from the mafic-ultramafic suite of NW Senja. Data for primary and secondary olivines are from (Vance and Dungan, 1977).

Thus, there are no clear evidences in favor of metamorphic formation of olivine and orthopyroxene in the studied layered ultramafic suite. The origin of amphibole in the rock, however, is more complicated to identify. Ca-amphibole typically replaces clinopyroxene in amphibolite facies meramorphic rocks, and clinopyroxene-rich ultramafic cumulates are far more abundant than those rich in igneous amphibole. Fleet (1978) suggested that the distribution of aluminium between tetrahedral and octahedral sites (i.e. Al^{IV} and Al^{VI}) of the structure of amphibole indicates the conditions during amphibole crystallization. On the diagram Al^{IV} vs. Al^{VI} (Fig.7.1.2) the compositions of the analyzed amphiboles plot within fields of igneous amphibole, low-pressure metamorphic amphibole and high-pressure metamorphic amphibole independent on whether the analyzed grain occurs in matrix of the rock or represents an inclusion in orthopyroxene oikocrysts. The zoned grains analyzed in sample 613 and 585 show, however, that the rims are characterized by lower Al^{IV}/Al^{VI} compared to the cores, which have Al^{IV}/Al^{VI} closer to

ratio characteristic for igneous amphibole. These observations suggest that the originally igneous amphibole may have been partly or completely altered in response to metamorphism. Furthermore, it has not been observed any clinopyroxene relics in the rock, what also is in favor of an igneous origin of amphibole.

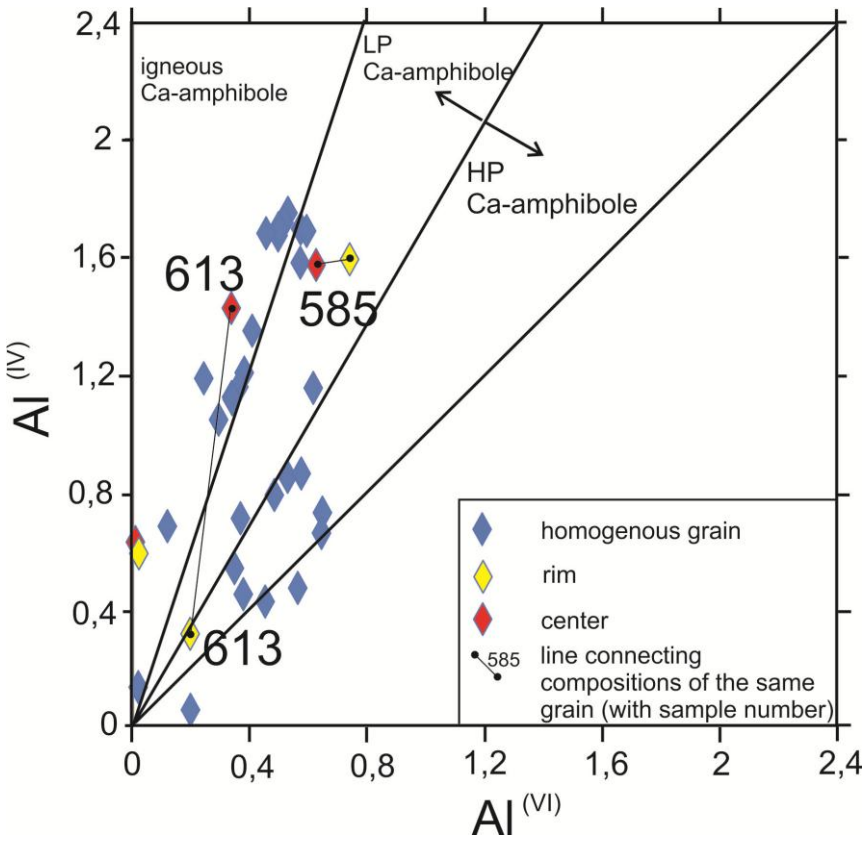

Fig.7.1.2. Al^{IV} vs. Al^{VI} diagram from Eyubolglu et al. (2011) for amphibole from the studied ultramafic rocks. Fields are modified after Fleet (1978).

Based on the evidences discussed above it can be concluded that the entire rock-forming mineral assemblages of the studied ultramafic rocks represent magmatic mineral assemblages. The igneous textures preserved indicate that the ultramafic varieties are olivine-amphibole cumulates. Textural relationships imply post cumulus growth of orthopyroxene and spinel in most of the observed cases, as (1) orthopyroxene oikocrysts enclose olivine and amphibole grains and (2) spinel mostly forms anhedral aligned grains occupying interstitial space between olivine and amphibole grains (see chapter 3). Following the classical terminology of Wager (1960) the studied cumulate can be classified as a type resembling adcumulate (olivine-amphibole varieties) and heteradcumulate (orthopyroxene-bearing varieties). In contrast to adcumulate, heteradcumulate is texturally similar to orthocumulate,which also contains a significant amount of an intercumulus phase compared to cumulus material. However, in contrast to orthocumulate, hederadcumulate is

characterized by homogenous composition of post-cumulus poikilocrysts (e.g. the analyzed poikilocrysts of orthopyroxene from the studied ultramafic rocks, see Fig.5.2.3, chapter 5). Homogenous composition of such poikilitic crystals from heteradcumulate is explained to be a result of crystallization resembling the equilibrium crystallization model. It occurs through continued growth of both cumulus and poikilitic crystals at constant temperature until little or no pore liquid remains (Wager, 1960). In contrast to the former, orthocumulate formation is assumed to occur through a process resembling fractional crystallization model.

A cumulate origin of the rocks is also supported by whole rock geochemical data. Clear correlative relationships between MgO and SiO_2, CaO and Al_2O_3 indicate that the rocks were formed during various degree of fractionation (Fig. 4.2.1, chapter 4). The high MgO content (up to 36 wt.%) is consistent with accumulation of olivine and orthopyroxene, and the increase in SiO_2 and Al_2O_3 with decreasing MgO, suggests fractionation of olivine and orthopyroxene. Al_2O_3 and CaO show negative correlations with MgO, suggesting accumulation of amphibole, which is the dominant mineral in the rocks, and also spinel. Most likely, the hornblendite and metagabbroic rock (amphibolite), which are associated with the ultramafics, crystallized from highly fractionated portions of the melt. A strong degree of fractionation is also expressed by the composition of olivine, which is far less forsteritic than that reported for mantle array. Finally, the documented intrusive relationship and macroscopic textures typical for layered intrusive suites clearly exclude the possibility that the studied rocks represent tectonically emplaced mantle.

It is clearly evident from the field observations that the studied layered mafic-ultramafic rock association has been deformed and therefore also metamorphosed together with its host rock. The rocks may be also have been metasomatized by fluids released from later granite intrusions (see Chapter 2). The influence of high-grade metamorphism on the mineral and whole rock chemical compositions should be considered prior to any discussion on the tectonic setting of the studied suite.

Indeed, an important compositional feature of the rocks from Senja, which characterize high-grade metamorphic complexes, is that they contain high-Al green spinel (Fig.7.1.3). High-Al, but low-Cr spinel has been reported from meta-troctolites (Tenthorey et al., 1996; Berger et al., 2010), metasedimentary rocks and high P-T Alpine complexes (Barnes and Roeder, 2001). In metamorphosed Archean chromitite-anorthosite associations from Greenland and metamorphosed layered ultramafic-mafic-anorthositic rocks from the Guelb el Azib layered complex, Mauritania (Berger et al., 2012), such spinel compositions have been considered to result

from high-grade metamorphism, which has led to leaching of Cr from spinel. This interpretation was based on a compositional trend for the initially Cr-rich spinel undergoing progressive metamorphism. By introducing the trend, Evans and Frost (1977) showed that through progressive metamorphism, the Fe^{3+} and Cr contents in spinel continuously decrease while Mg and Al contents increase. In some of the studies (e.g. Rollinson et al., 2002) the same compositional shift is interpreted as a replacement trend which results from late magmatic interaction between high-Cr spinels and an evolved interstitial melt. Anyhow, as (1) the studied spinels may have been partially equilibrated during high-grade metamorphism and (2) significant portion of Cr is accommodated in magnetite, which replaces spinel (see chapter 5), any assumptions of parental magma compositions based on the composition of spinel should be limited. Indeed, spinel composition plots outside the defined fields on most of discrimination diagrams (Fig.7.1.4).

For the metagabbroic rock (amphibolite) associated with ultramafic rocks, the metamorphic overprint clearly resulted in replacement of clinopyroxene by hornblende. It is documented by replacement relationship shown in Fig.3.1.4 (a, b), chapter 3.

The more pronounced influence of metamorphism on the ultramafic varieties is low-temperature alteration, such as replacement of spinel by magnetite, serpentinization and development of phlogopite. This alteration, however, has not significantly modified the contents of major and trace elements, except from enrichment in K, Rb and Cs of altered rocks. These elements are typically concentrated in phlogopite.

Summarizing the discussion above, in comparison to other metamorphosed layered ultramafic-mafic suites, by their petrogenesis the rocks from NW Senja mostly resemble the rocks reported from the Guelb el Azib layered complex, Mauritania (Berger et al., 2012), which are characterized by abundant igneous olivine-amphibole cumulates, hornblendite and metagabbroic rocks that have been modified during high-grade metamorphism.

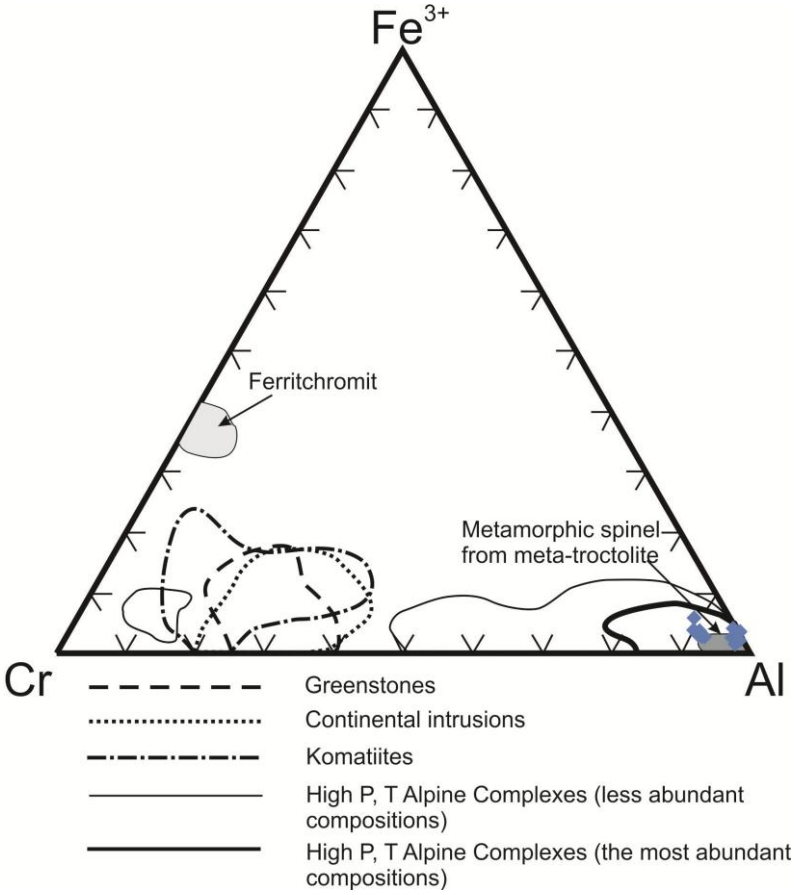

Fig.7.1.3. Fe^{3+}-Al-Cr plot for spinel from the ultramafics of NW Senja compared to spinel and chromite from various igneous and metamorphic complexes. Comparison fields are from Barnes and Roeder (2001).

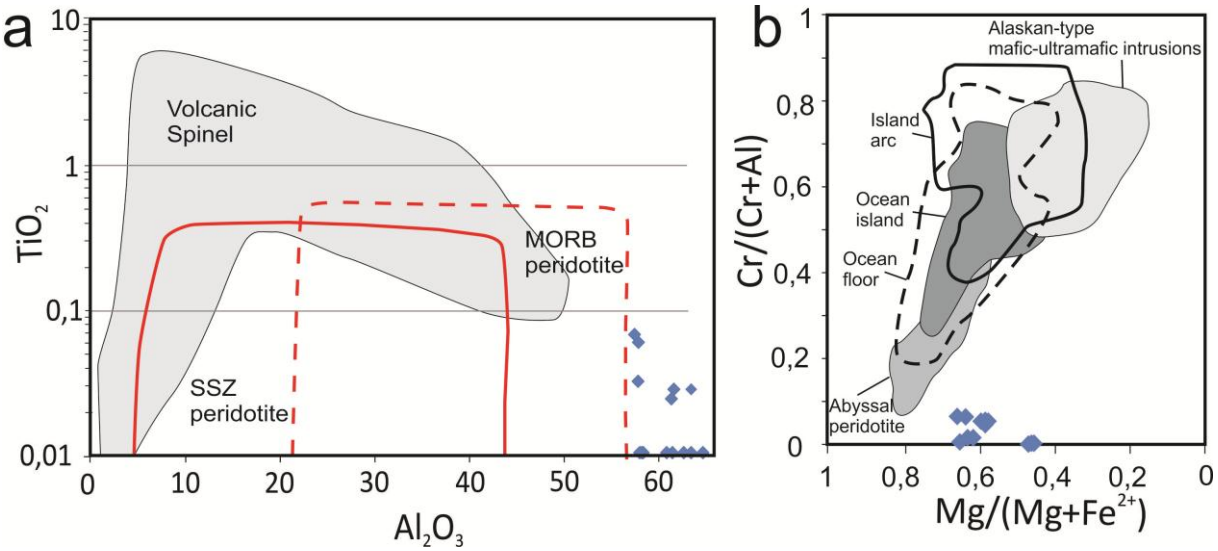

Fig.7.1.4. TiO_2 vs. Al_2O_3 (a) and Cr/(Cr+Al) vs. $Mg/(Mg+Fe^{2+})$ (b) plot for spinel from the ultramafics of NW Senja. Compositional fields for spinel from various tectonic settings are from Barnes and Roeder (2001) for (a) and Kamenetsky et al. (2001) for (b).

7.2. Tectonic setting

Whole rock compositional data for the studied cumulate rocks from NW Senja may be used to constraint the tectonic setting of the rocks. On the AFM diagram (Fig.7.2.1) the compositional points of mafic-ultramafic layered rock association fall into the fields of ultramafic and mafic cumulates. The olivine-bearing varieties clearly differ from metamorphic peridotites by their lower magnesium content, and from komatiites by lower iron content. After Beard (1986), hornblendites, amphibolites and olivine-bearing rocks belong to arc-related mafic and ultramafic cumulates. Furthermore, the olivine-bearing rocks plot within the fields of ultramafic and mafic ophiolite cumulate fields based on the classification introduced by Coleman (1977).

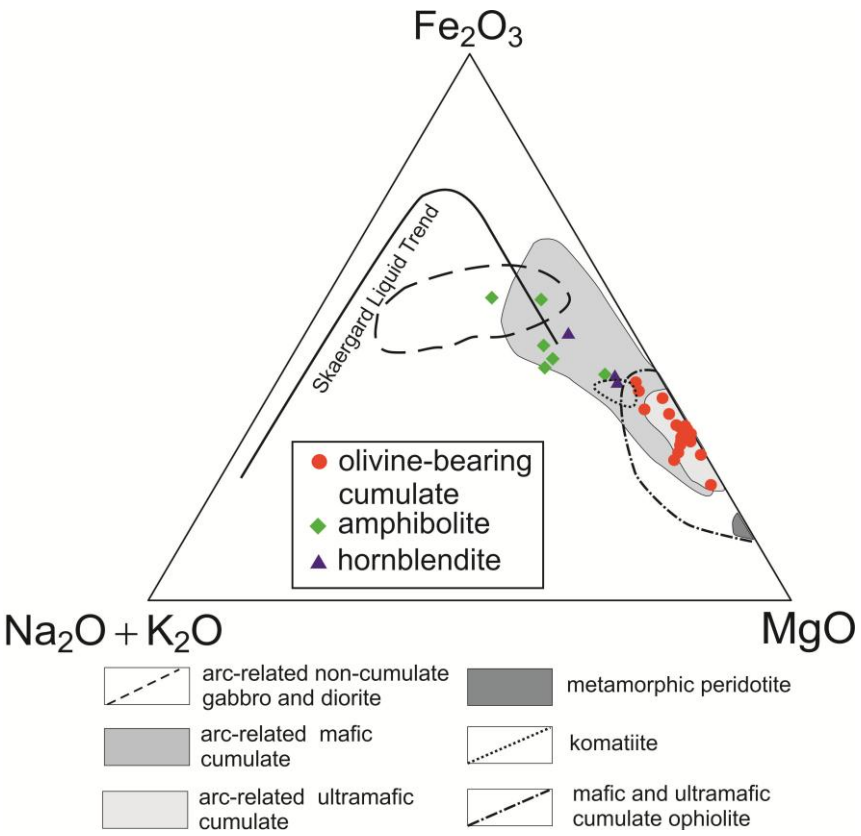

Fig.7.2.1. AFM compositions of the cumulate rocks from layered mafic-ultramafic rock association from NW Senja. Fields of arc-related rocks, komatiite and metamorphic peridotite are from Beard (1986), field of mafic and ultramafic cumulate ophiloite from Colemann (1977).

Trace and REE element compositions of the studied mafic-ultramafic rock association indicate that the rocks have been derived from a source resembling primitive mantle and have not been contaminated by crustal material. This is supported by the absence of negative Ta, Ti and Nb

anomalies (Fig.4.2.7), which are typical for rocks from volcanic arc and within-plate continental settings that have been contaminated by crustal material. The REE patterns are non-fractionated (Fig.4.2.8) and closely resemble the patterns of E- and N-MORB basalts. As the parental melt for similar cumulates commonly is considered to be hydrous high-alumina tholeitic (e.g. Berger et al, 2013; Weaver et al., 1981; Polat et al., 2012), the rocks may represent the early cumulates of basalts formed in the oceanic lithosphere. However, such hydrous melts leading to the formation of amphibole-bearing cumulates are more common for supra-subduction settings, which seems to be inconsistent with the geochemical affinity of the studied rocks. In order to solve this problem and make more detailed constraints for the possible tectonic setting for the rocks, a number of discrimination diagrams have been applied below.

Pearce et al. (1984) postulated a diagram to discriminate between the supra-subduction zone ophiolites (SSZ) and mid-ocean ridge basalt ophiolites (MORB) on the basis of their Cr and TiO_2 contents. All of the analyzed samples (both mafic and ultramafic) from NW Senja plot within the field of MORB ophiolites and associated cumulates, i.e. most likely they formed in an extensional setting rather than during the initial stages of subduction, as most of the SSZ ophiolite cumulates.

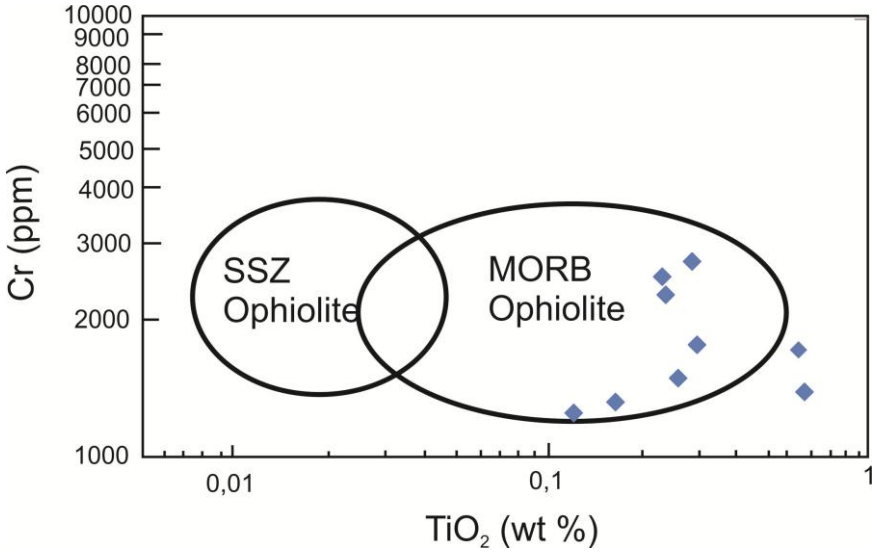

*Fig.7.2.2. Compositional points of the layered mafic-ultramafic suite from NW Senja in the Cr vs. TiO_2 discrimination diagram after Pearce et al. (*1984*).*

In the Nb/Yb versus Th/Yb diagram (Pearce, 2008), the analyzed mafic and ultramafic samples, which have appropriately high Th/Yb ratios, plot within the MORB array (Fig.7.2.3). The data from the samples showing Th content below the detection limit (<0.01 ppm) were also plotted on the diagram, by assuming a Th content corresponding to the half of the detection limit.

However, these data plot notably lower than the defined MORB-OIB array. Strictly speaking, such compositions seem to be unrealistic, and as previously mentioned, the negative U, Pb and Th anomalies observed for some of the samples (Fig.4.2.7.) may be related to analytical problems. For comparison, the diagram also shows the compositional fields of mantle and crustal igneous rocks of the oceanic lithosphere from subduction-unrelated (continental margin, mid-ocean-ridge and plume) settings, and subduction-related (suprasubduction-zone and volcanic arc) settings (Dilek and Furnes, 2011). In contrast to the subduction-unrelated suites, which generally fit the MORB array, the compositions of the subduction-related ophiolitic suites show a compositional shift towards the arc array defined by Condie and Kröner (2011).

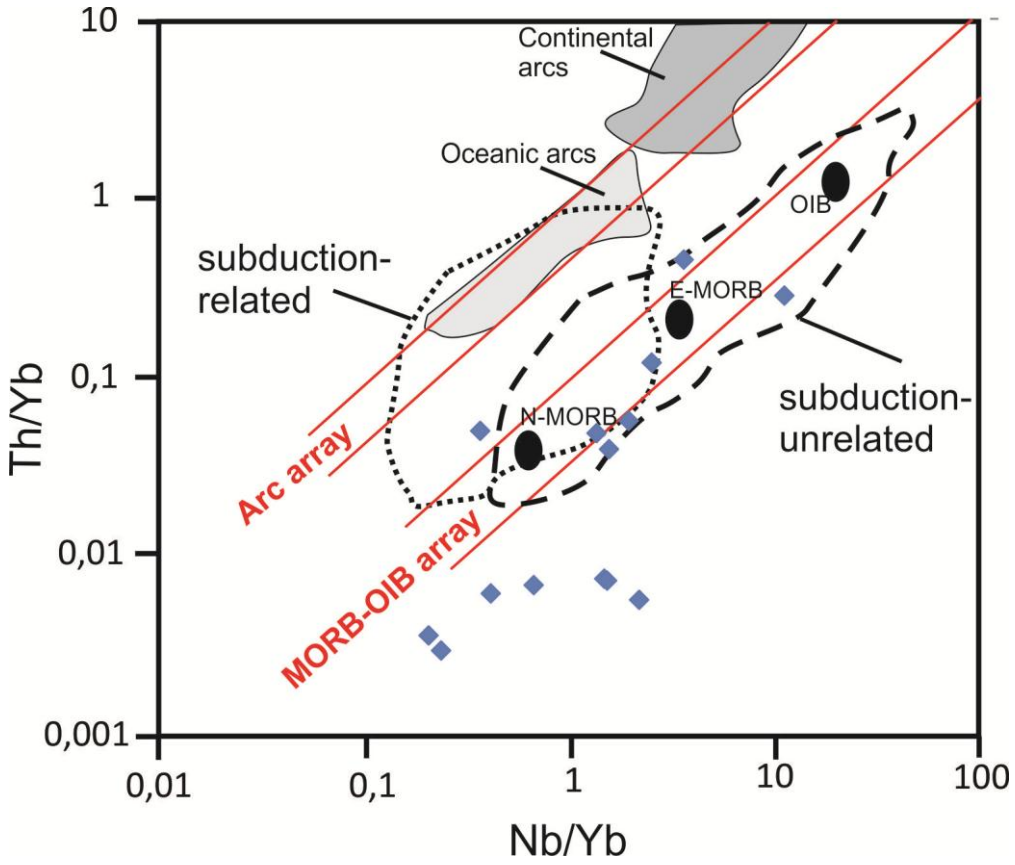

Fig.7.2.3. Compositional variations of the layered mafic-ultramafic suite of NW Senja shown in the in Nb/Yb-Th/Yb discrimination diagram (Pearce, 2008). Fields of subduction-unrelated and subduction-related ophiolite types plotted based on data from Dilek and Furnes (2011) and references therein. Fields of rocks from oceanic and continental arcs after Condie and Kröner (2011).

The compositions of rock-forming mineral phases in mafic and ultramafic cumulates are also often used as indicators of tectonic setting. Unfortunately, in case of the studied rock association from NW Senja, such opportunities are limited because of (1) complete absence of clinopyroxene, which is most commonly used, and (2) the possibly strong influence of metamorphism on spinel composition. Figure 7.2.4a shows the Mg numbers (expressed as 100*Mg/(Mg+Fe)) of coexisting

olivine and orthopyroxene from the studied cumulate in comparison to the olivine and orthopyroxene compositions of ultramafic and gabbroic rocks of the oceanic lithosphere. Olivine and orthopyroxene from the studied samples show compositions that are comparable to those from oceanic mafic and ultramafic rocks. The compositions of the studied samples plot outside the field of HP-mantle xenoliths as defined by Frey and Prinz (1978), implying that the rocks represent fractionated products that crystallized at pressures lower than during formation of mantle peridotites.

The contents of CaO and Al_2O_3 in orthopyroxene are also used as indicators of the crystallization environment, because Al and Ca more likely enter the structure of pyroxene under high pressures (Herzberg, 1978; Gasparik, 1984). The Al_2O_3 content of the orthopyroxene is plotted against the Mg number for the mafic cumulates in Figure 7.2.4b. All of the data plot outside the high-pressure environment, but close to the compositional field of the mafic cumulate from the Pozanti-Kazanti ophiolite (Antalya), which has been inferred to represent low-pressure (2–2.5 kbar) crystallization products (Bagci et al., 2006). In addition, the studied orthopyroxene approaches the compositional trend of orthopyroxene from the Skaergaard intrusion, suggesting possibly similar conditions during crystallization at relatively high crustal levels (roofing at approximately 2 km, Nielsen, 2004).

As shown in chapter 5 (Fig.5.2.2), amphibole from the analyzed ultramafic rock is mainly Ca-amphibole, (tschermakite, magnesiohornblende and actinolite) according to Leake et al. (1997). Although it cannot be ruled out that amphibole is metamorphic (section 7.1), the compositional variations of the analyzed amphibole are consistent with those of amphibole from plutonic rocks in the oceanic lithosphere (Fig 7.2.5). Even though many compositional points fall out of the oceanic lithosphere field, none of the samples show compositions similar to those reported from arc-related settings.

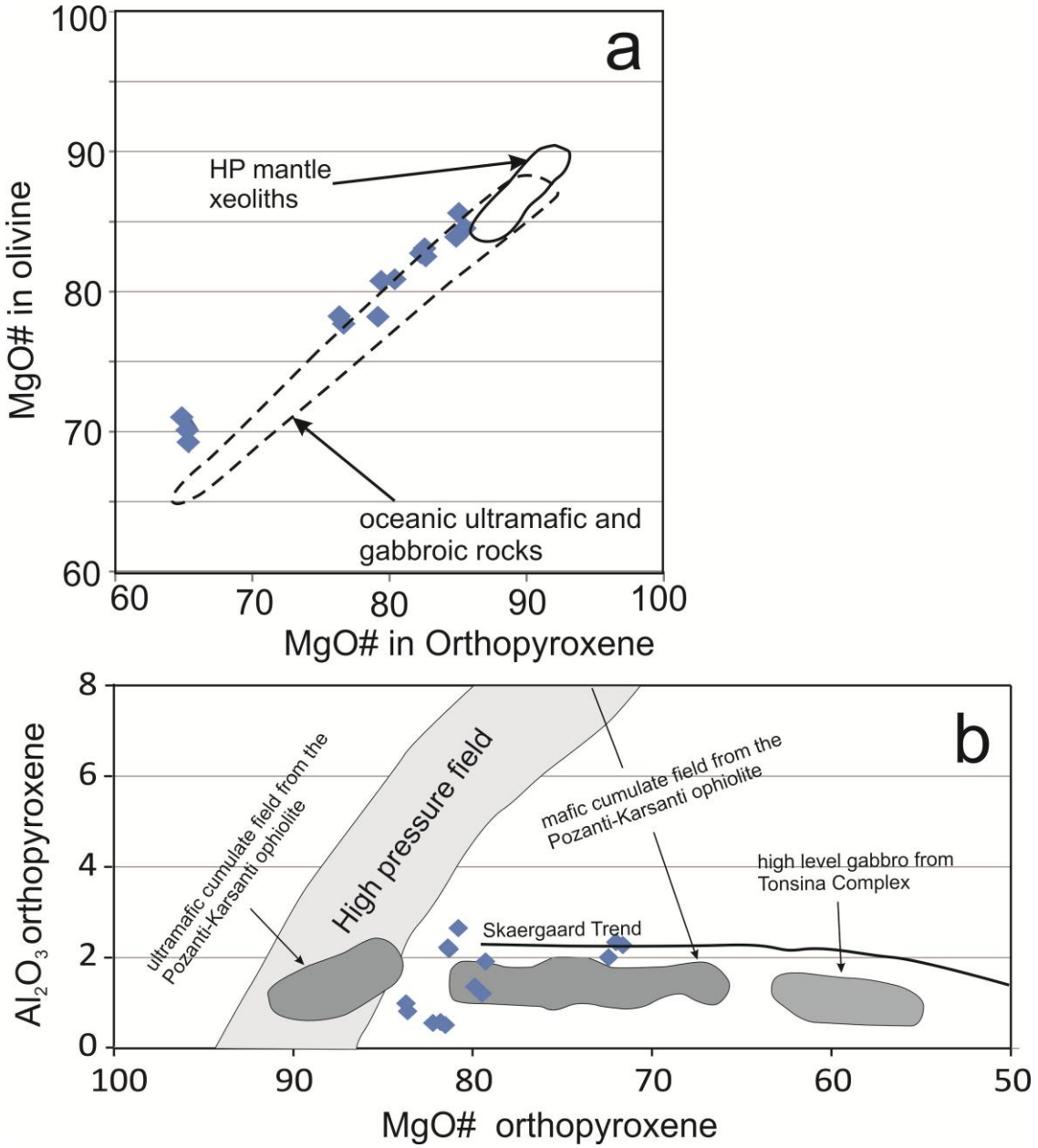

*Fig.7.2.4. (a) - Mg numbers [100*Mg/(Mg+Fe)] of coexisting olivine vs. orthopyroxene from the studied mafic-ultramafic suite. The field of high-pressure mantle xenoliths is from Frey and Prinz (1978). The field of oceanic cumulates is from Tiezzi and Scott (1980) and Hodges and Papike (1976); (b) - Plot of Al_2O_3 versus Mg numbers in orthopyroxene from the studied mafic-ultramafic suite. The field of high-pressure peridotite is after Medaris (1972). The data from Pozanti-Karsanti (Parlak et al. 2000, 2002), Skaergaard and Tonsina complex (DeBari and Coleman 1989) are for comparison.*

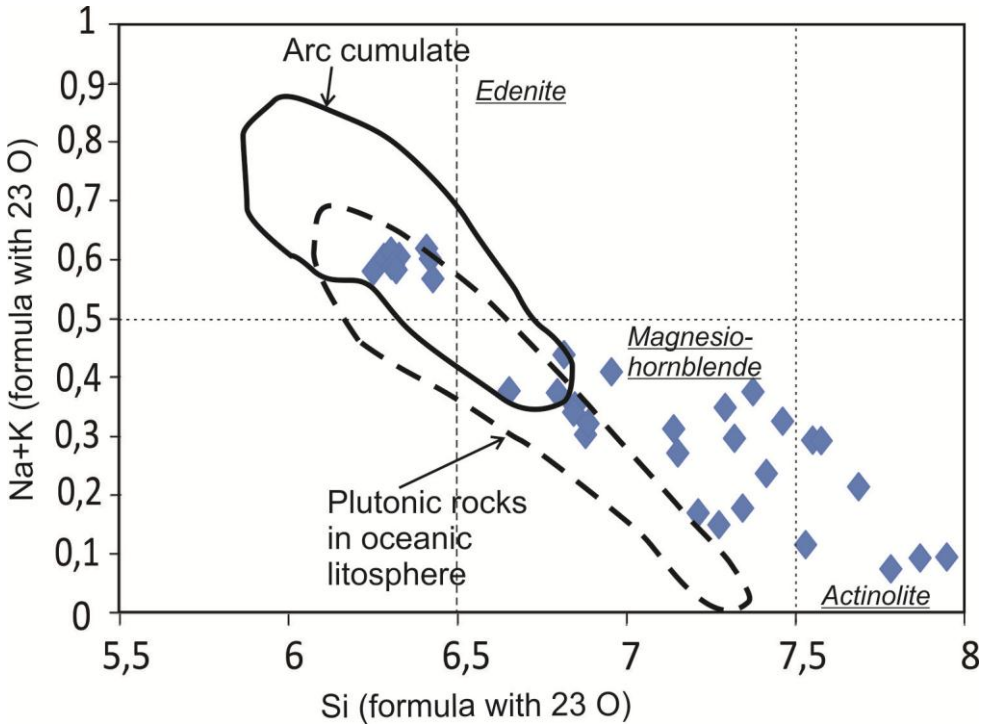

Fig.7.2.5. Composition of amphibole from the ultramafic rocks in the classification diagram of Leake et al. (1997). The arc-cumulate field (including intermediate to ultramafic rocks) is from Beard and Barker (1989). The field for plutonic rocks in oceanic lithosphere is defined from the data of Constantin et al. (1995).

From the discussion above, it is evident that the studied ultramafic-mafic layered association shows a pronounced geochemical signature that characterizes ophiolite cumulates crystallized within the oceanic crust in a MORB-like tectonic setting. In general, such a setting is very common for the occurrences of large volumes of ultramafic and mafic cumulates. The best known example is perhaps the Eocene Skaerggard intrusion, Greenland, which shares geochemical features with the studied rocks. It has been inferred that the Skaergaard intrusion formed at a rifted continental margin during an oceanic stage (Nielsen, 2004; Von Gruenewaldt, Harmer, 1992).

7.3. Regional implication

As the present study partly aimed to improve the understanding of the tectonic setting of the Astridal shear belt, the U-Pb zircon dating of the metagabbroic rock from the layered mafic-ultramafic suite initially aimed to obtain an igneous age of the suite. However, as discussed in chapter 6, the two analyzed zircon grains show morphology and Th-U contents more typical for zircons of metamorphic genesis. Furthermore, the obtained age of 1741.8 ± 4.5 Ma coincides well with zircon and titanite ages (1740-1760 Ma) from the granitic rocks occurring both on the

western and the eastern shores of Baltsfjord, which were deformed during the F1 stage (Fernando Corfu and Steffen Bergh, personal communication 2012). The most reasonable conclusion from the isotope data is that the dated zircons formed contemporaneously with the main Svecofennian tectono-thermal event responsible for the amphibolite facies metamorphism, major deformation and granitic magmatism that can be recognized over the entire WTBC (Corfu et al., 2003).

It is evident from the present study that the layered mafic-ultramafic suite formed in an oceanic rift setting, which is in good agreement with the associated lithologies like sulphide-rich quartz-mica schist, carbonate-rich metasedimentary rocks and mafic metavolcanic and intrusive rocks as reported by Bergh et al. (2011) and from this study.

The intrusive ages of the studied oceanic cumulate rocks remains uncertain. However, it is clear that the suite emplaced earlier than 1740 Ma, which is supported by its metamorphic age, and also field relationships to the granitic rocks. Further, a number of indirect field evidences suggest that the emplacement of the studied cumulate suite might have been temporally associated with the formation of the Astridal supracrustal suites. These evidences include: (1) close spatial and structural association of the layered mafic-ultramafic suite with the supracrustal rocks of the Astridal belt, (2) intrusive contacts to amphibolites belonging to the supracrustal zone, (3) the finding of a xenolith possibly representing a calc-silicate rock similar to the calc-silicate rock reported from the supracrustal suite (Pedersen, 1997; Bergh et al., 2010). Unfortunately, the supracrustals of Astridal have never been dated and in the strict sense they can be of any age prior to inferred metamorphic (1740-1760 Ma), including Archean. However, based on many common architectural and lithological characteristics with the Mjelde-Skorelvatn and Torsnes belts, Bergh et al. (2011) proposed that the supracrustal suite of the neighboring Astridal belt might be a correlative of the supracrustals from the Mjelde-Skorelvatn and Torsnes. The Mjelde-Skorelvatn and Torsnes belts have been inferred to have an age of 1990 - 1970 Ma (Myhre et al., 2011). If the supracrustal sequences of the Astridal belt and the studied layered mafic-ultramafic rock association are of about 1.98 Ga old, they may represent crustal remnants of the Svecofennian ocean, and therefore be genetically related to the ophiolites documented in Finland. These ophiolite complexes represented by mantle peridotites and associated MORB suites include the 1.95 Ga Jormua (Huhma, 1986; Kontinen, 1987; Peltonen and Kontinen, 2004) and the 1.97 Ga Outokumpu (Park, 1988) and Nuttio (Hanski et al., 1997). In addition, Presvecofennian possibly ophiolite-related MORB mafic suites have been reported further southeast from the Finnish ophiolites along the northeastern shore of the Ladoga Lake (e.g. Ivanikov et al., 1988). Finally, the

studied cumulates show a geochemical affinity and consequently a tectonic setting that are different from cumulate rocks comprising the ~1.89-1.87 Ga arc-related intrusions from Finland (e.g. in Kotalahti, Vammala, Tampere, Pirkanmaa Belts, Peltonen, 1995; Peltonen, 2005 and references therein). Most of these intrusions occur within the Svecofennian domain (primitive and evolved arc complexes) of the Fennoscandian shield and not whithin the Archean basement as the studied rocks.

Even though the Archean continental crust is present towards SW of the study area within the Lofoten and Vesterålen Islands, it cannot be excluded that the suture of the Svecofennian Ocean may be found within the Senja Shear Belt, as evidenced by the abundance of ocean floor formations. More isotopes studies of igneous suites and supracrustal rocks from the Astridal belt and petrological studies of the mafic and ultramafic suites may help to better understand the tectonic setting of the Senja Shear Belt and its Precambrian evolution.

References

1. Arai, S., Abe, N., Hirai, H., Shimizu, Y., 2001. Geological, petrographical and petrological characteristics of ultramafic-mafic xenoliths in Kurose and Takashima, northern Kyushu, southwestern Japan. Sci. Report, Kanazawa Univ., 46, 9-38.
2. Bağcı, U., Parlak, O., Hock, V., 2008. Geochemistry and tectonic environment of diverse magma generations forming the crustal units of the Kızıldağ (Hatay) ophiolite southern Turkey. Turkish Journal of Earth Sciences 17, 43–71.
3. Barnes, S. J., and Roeder, P. L., 2001. The range of spinel compositions in terrestrial mafic and ultramafic rocks. Journal of Petrology 42, 2279-2302.
4. Beard, J.S., 1986. Characteristic mineralogy of arc-related cumulate gabbros: implications for the tectonic setting of gabbroic plutons and for andesite genesis. Geology 14, 848–851.
5. Beard, J.S., Barker, F., 1989. Petrology and tectonic significance of gabbros, tonalites, shoshonites, and anorthosites in a late Paleozoic arc-root complex in the Wrangellia Terrane, southern Alaska. Journal of Geology 97, 667–683.
6. Belousova, E.A., Walters, S., Griffin, W.L., O'Reilly, S.Y., Fisher, N.I., 2002. Zircon trace-element compositions as indicators of source rock type. Contributions to Mineralogy and Petrology 143, 602-622.
7. Berger, J., Diot, H., Lo, K., Ohnenstetter, D., Féménias, O., Demaiffe, D., Bernard, A.B., 2012. Petrogenesis of Archean PGM-bearing chromitites and associated ultramafic–mafic–anorthositic rocks from the Guelb el Azib layered complex (West African craton, Mauritania). Precambrian Research 224, 612–628.
8. Berger, J., Féménias, O., Ohnenstetter, D., Plissart, G., Mercier, J.C.C., 2010. Origin and tectonic significance of corundum–kyanite–sapphirine amphibolites from the Variscan French Massif Central. Journal of Metamorphic Geology 28, 341–360.
9. Bergh, S.G., Kullerud, K., Armitage, P.E.B., Zwaan, K.B., Corfu, F., Ravna, E.J.K. & Myhre, P.I., 2010. Neoarchaean to Svecofennian tectono-magmatic evolution of the West Troms Basement Complex, North Norway. Norwegian Journal of Geology 90, 21-48. Trondheim 2010.
10. Boynton, W.V. 1984. Geochemistry of the rare earth elements: meteorite studies, in: Henderson, P. (Ed.), Rare Earth Element Geochemistry, Elsevier, pp. 63-114.
11. Coleman, R. G., 1971. Plate tectonic emplacement of upper mantle peridotite along continental edges. Journal of Geophysical Research 76, 1212-22.
12. Coleman, R.G., 1977. Ophiolites. Springer-Verlag, New York, 229 p.
13. Condie, K.C., Kröner, A., 2011. The building blocks of continental crust: evidence for a major change in the tectonic setting of continental growth at the end of the Archean. Gondwana Research 23, 394–402.
14. Constantin, M., Hékinian, R., Ackermand, D., Stoffers, P., 1995. Mafic and ultramafic intrusions into upper mantle peridotites from fast-spreading centers of the Easter microplate (south east Pacific), in: Vissers, R.L.M., Nicolas, A. (Eds.), Mantle and Lower Crust Exposed in Oceanic Ridges and in Ophiolites. Kluwer, Dordrecht, Netherlands, pp. 71–120.
15. Corfu, F., Armitage, P.E.B., Kullerud, K., Bergh, S.G., 2003. Preliminary U-Pb geochronology in the West Troms Basement Complex, North Norway: Archaean and Palaeoproterozoic events and younger overprints. Geol. Soc. Norway Bulletin 441, 61-72.
16. Corfu, F., Hanchar, J.M., Hoskin, P.W.O., Kinny, P., 2006. Atlas of zircon textures, in: Hanchar, J.M., Hoskin, P.W.O (Eds.), Zircon. Mineralogical Society of America, Reviews in Mineralogy and Geochemistry 53, 468-500.
17. Corfu, F., 2004. U-Pb age, setting and tectonic significance of the anorthosite-mangerite-charnockite-granite suite, Lofoten-Vesteralen, Norway. Journal of Petrology 45, 1799-1819.
18. Cox, K.G., Bell, J.D., Pankhurst, R.J. 1979. The Interpretation of Igneous Rocks. George, Allen and Unwin, London.

19. DeBari, S.M., Coleman, R.G., 1989. Examination of the deep levels of an island arc: evidence from the Tonsina ultramafic-mafic assemblage, Tonsina, Alaska. Journal of Geophysical Research 94, 4373–4391.
20. Desmarais, N.R., 1981. Metamorphosed Precambrian ultramafi c rocks in the Ruby Range, Montana. Precambrian Research 16, 67–101.
21. Dilek, Y., Furnes, H., 2011. Ophiolite genesis and global tectonics: Geochemical and tectonic fingerprinting of ancient oceanic lithosphere. Geological society of America Bulletin 123, 387-411.
22. Evans, B.W., 1977. Metamorphism of Alpine peridotite and serpentine. Ann. Rev. Earth and Planetary Science Letters 5, 397-447.
23. Evans, B.W., Frost, B.R., 1975. Chrome-spinel in progressive metamorphism - a preliminary analysis. Geochimica et Cosmochimica Acta, 39, 959-972.
24. Eyuboglu, Y., Santosh, M., Bektaş, O., Chung, S.L., 2011. Late Triassic subduction-related ultramafic–mafic magmatism in the Amasya region (eastern Pontides, N. Turkey): ımplications for the ophiolite conundrum in Eastern Mediterranean, In: Chetty, T.R.K., Santosh, M., Tsunagae, T. (Eds.), Suture zones and geodynamic processes. Journal of Asian Earth Sciences 42 (3), 234–257.
25. Fareth, E. 1983. Mefjordbotn, berggrunnskart 1433 IV, 1:50 000, forelopig utgave. Norges geologiske undersokelse.
26. Fawcett, J.J. and Yoder, H.S., 1966. Phase relationship of chlorites in the system MgO-Al_20_3-$Si0_2$-H_2O. American Mineralogist 51, 353-380.
27. Fleet, M.E., Barnett, R.L., 1978. Al(IV)/Al (VI) partitioning in calciferous amphiboles from the mine, Sudbury, Ontario. Canadian Mineralogist 16, 527–532.
28. Frey, F.A., Prinz, M., 1978. Ultramafic inclusions from San Carlos, Arizona: petrologic and geochemical data bearing on their petrogenesis. Earth and Planetary Science Letters 38, 129–176.
29. Frost, B.R., 1975. Contact metamorphism of serpentinite, chloritic blackwall and rodingite at Paddy-Go-Easy Pass, central Cascades, Washington. Journal of Petrology 16, 272–313.
30. Gaàl, G., Gorbatschev, R., 1987. An outline of the Precambrianevolution of the Baltic Shield. Precambrian Research 35, 15–52.
31. Gasparik, T., 1984. Two pyroxene thermometry with new experimental data in the system CaO-MgO-Al_2O_3-SiO_2. Contributions to Mineralogy and Petrology 87, 87–89.
32. Hanski, E.J. 1997. The Nuttio serpentinite belt, central Lapland: an example of Palaeoproterozoic ophiolitic mantle rocks in Finland. Ofioliti 22, 35-46.
33. Heaman, L.M., Bowins, R., Crocket, J., 1990. The chemical composition of igneous zircon suites: Implications for geochemical tracer studies. Geochimica et Cosmochemica Acta 54, 1597-1607.
34. Herzberg, C.T., 1978. Pyroxene geothermometry and geobarometry: experimental and thermodynamic evaluation of some subsolidus phase relations involving pyroxenes in the system CaO-MgO-Al_2O_3-SiO_2. Geochimica et Cosmochimica Acta 42, 945–957.
35. Hodges, F.N., Papike, J.J., 1976. DSDP site 334: magmatic cumulates from oceanic layer 3. Journal of Geophysical Research 81, 4135–4151.
36. Hoskin, P.W.O., Black, L.P., 2000. Metamorphic zircon formation by solid-state recrystallization of protolith igneous zircon. Jornal of Metamorphic Geology 18, 423-439.
37. Huhma, H. 1986. Sm-Nd, U-Pb and Pb-Pb isotopic evidence for the origin of the Early Proterozoic Svecokarelian crust in Finland. Geological Survey of Finland, Bulletin 337. 48 p.
38. Irvine, T.N. and Baragar, W.R.A., 1971. A guide to the chemical classification of the common volcanic rocks. Canadian Journal of Earth Sciences, 8: 523-548.
39. Ivanikov, V.V., Philippov, N.B., Bogachev, Muradymov, G.S. Mineralogical and geochemical evidence for ophiolitic association in Ladoga area, in Proc. of the International Conf. “Rifting, magmatism and metallogeny of the Precambrian. Correlation of geological suited in Fennoscandia”. Petrozavodsk, KARSC RAS, pp.53-55.
40. Kamenetsky, V.S., Crawford, A.J., Meffre, S., 2001. Factors controlling chemistry of magmatic spinel: an empirical study of associated olivine, Cr-spinel and melt inclusions from primitive rocks. Journal of Petrology 42, 655–671.

41. Khedr, M.Z., Arai, S. Petrology and geochemistry of prograde deserpentinized peridotites from Happo-O'ne, Japan: Evidence of element mobility during deserpentinization. Journal of Asian Earth Sciences 43, 150–163.
42. Koistinen, T., Stephens, M.B., Bogatchev, V., Nordgulen, Ø.,Wennerström, M., Korhonen, J., 2001. Geological map of the Fennoscandian Shield, scale 1:2 000 000. Geological Surveys of Finland, Norway and Sweden and the North-West Department of Natural Resources of Russia.
43. Kontinen, A.T., 1987. An Early Proterozoic ophiolite – The Jormua ophiolite mafic-ultramafic complex. Precambrian Research 35, 313–341.
44. Krogh, T. E., 1973. A low contamination method for hydrothermal decomposition of zircon and extraction of U and Pb for isotopic age determinations. Geochimica et Cosmochimica Acta 37, 485–494.
45. Kullerud, K., Corfu, F., Bergh, S.G., Davidsen, B. & Ravna, E. K. 2006.U-Pb constraints on the Archaean and Early Proterozoic evolution of the West Troms Basement Complex, North Norway (Abstract).Bulletin of the Geological Society of Finland Special Issue I, p. 79.
46. Lahtinen, R., Korja, A. and Nironen, M., 2005. Palaeoproterozoic tectonic evolution, in: Lehtinen, M, Nurmi, P. and Rämö, O.T. (Eds.), Precambrian Geology of Finland—Key to the evolution of the Fennoscandian Shield. Developments in Precambrian Geology 14, Elsevier B.V., Amsterdam.
47. Leake, B.E., Woolley, A.R., Arps, C.E.S., Birch, W.D., Gilbert, M.C., Grice, J.D., Hawthorne, F.C., Kato, A., Kisch, H.J., Krivovichev, V.G., Linthout, K., Laird, J., Mandarino, J.A., Maresch, W.V., Nickel, E.H., Rock, N.M.S., Schumacher, J.C., Smith, D.C., Stephenson, N.C.N., Ungaretti, L., Whittaker, E.J.W., and Touzhi, G., 1997. Nomenclature of amphiboles: Report of the Subcommittee on Amphiboles of the International Mineralogical Association, Commission on New Minerals and Mineral Names. American Mineralogist 82, 1019-1037.
48. Ludwig, K. R., 1999. Isoplot/Ex Version 2.03. A Geochronological Toolkit for Microsoft Excel. Berkeley Geochronology Center Special Publication 1, 43 p.
49. Medaris, L.G., 1972. High-pressure peridotites in South-Western Oregon. Geological Society of America Bulletin 83, 41–58.
50. Moores, E. M., 1973. Geotectonic significance of ultramafic rocks. Earth Science Review 9, 241-58.
51. Moores*, E. M.,* Raymond*, L. A.,* 1972. On the origin of ultramafic rocks*:* Discussion*.* Geol. Soc. America Bulletin 83, 3157-3160.
52. Myhre, P. I., Corfu, F., Bergh, S.G., 2011. Palaeoproterozoic (2.0-1.95 Ga) pre-orogenic supracrustal sequences in the West Troms Basement Complex, North Norway. Precambrian Research 186, 89-100.
53. Nielsen, T.F.D., 2004. The shape and volume of the Skaergaard intrusion, Greenland: implications for mass balance and bulk composition. Jornal of Petrology 45, 507–530.
54. Paktunc, A. D. (1984). Petrogenesis of ultramafic and mafic rocks of the Thompson Nickel Belt, Manitoba. Contrib. Mineral. Petrol., 88 (1984), pp. 348–353
55. Park, A F., 1988. Nature of the early Proterozoic Outokumpu assemblage, eastern Finland. Precambrian Research 38, 131—146.
56. Parlak, O., Hoeck, V., Delaloye, M., 2000. Suprasubduction zone origin of the Pozanti-Karsanti ophiolite (southern Turkey) deduced from whole rock and mineral chemistry of the gabbroic cumulates, in: Bozkurt, E., Winchester, J.A., Piper, J.D.A. (Eds.), Tectonics and Magmatism in Turkey and the Surrounding Area. Special Publication 173. Geological Society, London, pp. 219–234.
57. Parlak, O., Hoeck, V., Delaloye, M., 2002. The suprasubduction zone Pozanti-Karsanti ophiolite, southern Turkey: evidence for high-pressure crystal fractionation of ultramafic cumulates. Lithos 65, 205–224.
58. Pearce, J.A., 2008. Geochemical fingerprinting of oceanic basalts with applications to ophiolite classification and the search for Archean oceanic crust. Lithos 100, 14–48.
59. Pearce, J.A., Lippard, S.J., Roberts, S., 1984. Characteristic and tectonic significance of supra-subduction zone ophiolites, in: Kokeldar, B.F., Howells, M.F (Eds.), Marginal Basin Geology. Geol. Soc. Spec. Publ. 16, 77–94.

60. Pedersen, B.R.S., 1997. Strukturell analyse av en prekambrisk, duktiltdeformert metasuprakrustalsone (Astridal-skjarsonen?) pa NO-Senja, Troms. Unpublished Cand. scient. thesis, University of Tromso, 166 p.
61. Peltonen, P., 1995. Petrogenesis of ultramafic rocks in the Vammala Nickel Belt: implications for crustal evolution of the early Proterozoic Svecofennian arc terrane. Lithos 34, 253-274.
62. Peltonen, P., Kontinen, A., 2004. The Jormua Ophiolite: a maficultramafic complex from an ancient ocean-continent transition zone, in: Kusky, T.M., (Ed.) Precambrian ophiolites and related rocks. Developments in Precambrian geology 13, 35–71.
63. Peltonen, P., 2005. Mafic-Ultramafic intrusionsof the Svecofennian Orogen, In: Lehtinen, M., Nurmi, P.A, Rämö, O.T. (Eds.), Precambrian of Finland – a Key to the Evolution of the Fennoscandian Shield. Amsterdam: Elsevier, p. 413 – 447.
64. Plümper, O., Piazolo, S., Austrheim, H., 2012. Olivine pseudomorphs after serpentinized orthopyroxene record transient oceanic upper mantle dehydration (Leka Ophiolite Complex, Norway). Journal of Petrology 53(9), 1943-1968.
65. Polat, A., Fryer, B.J., Samson, I.M., Weisener, C., Appel, P.W.U., Frei, R., Windley, B.F., 2012. Geochemistry of ultramafic rocks and hornblendite veins in the Fiskenæsset layered anorthosite complex, SW Greenland: evidence for hydrous upper mantle in the Archean. Precambrian Research 214–215, 124–153.
66. Rollinson, H.R., Appel, P.W.U., Frei, R., 2002. A metamorphosed, early Archaean chromitite from west Greenland: implications for the genesis of Archaean anorthositic chromitites. Journal of Petrology 43, 2143–2170.
67. Rubatto, D., 2002. Zircon trace element geochemistry: partitioning with garnet and the link between U-Pb ages and metamorphism. Chemical Geology 184, 123-138.
68. Stacey, J. S., Kramers, J. D., 1975. Approximation of terrestrial lead isotope evolution by a two-stage model. Earth and Planetary Science Letters 34, 207–226.
69. Streckeisen, A. L., 1974. Classification and Nomenclature of Plutonic Rocks. Recommendations of the IUGS Subcommission on the Systematics of Igneous Rocks. Geologische Rundschau 63, 773-785.
70. Sun, S.S., McDonough, W.F., 1989. Chemical and isotopic systematics of oceanic basalts; implications for mantle composition and processes, in: Saunders, A.D. and Norry, M.J. (Eds.), Magmatism in the ocean basins. Geological Society of London, London, pp. 313-345.
71. Takahashi, E., 1986. Origin of basaltic magmas: Implication from peridotite melting experiments and an olivine fractionation model (in Japanese with English abstract), Bull. Volcanol. Soc. Japan, 30, 17– S40.
72. Tenthorey, E.A., Ryan, J.G., Snow, E.A., 1996. Petrogenesis of sapphirine-bearing metatroctolites from the Buck Creek ultramafic body, southern Appalachians. Journal of Metamorphic Geology 14, 103–114.
73. Tiezzi, L.J., Scott, R.B., 1980. Crystal fractionation in a cumulate gabbro, Mid-Atlantic Ridge, 26_N. Journal of Geophysical Research 85, 5438–5454.
74. Tracey, R.J., Robinson, P., Wolff, R.A., 1984. Metamorphosed ultramafic rocks in the Bronson Hill Anticlinorium, central Massachusetts. American Journal of Science 284, 530-558.
75. Trommsdorff, V., Evans, B. W. (1972). Progressive metamorphism of antigorite schist in Bergell Tonalite Aureole (Italy). American Journal of Science 272, 423-437.
76. Vance, J. A., Dungan, M. A., 1977. Formation of peridotites by deserpentinization in Darrington and Sultan Areas, Cascade Mountains, Washington. Geol. Soc. America Bulletin 88, 1497-1508.
77. Von Gruenewaldt, G., Harmer, R.G., 1992. Tectonic setting of Proterozoic layered intrusions with special reference to the Bushveld Complex, in Condie, K.C. (Ed.), Proterozoic Crustal Evolution. Elsevier, Amsterdam, pp. 181-213.
78. Wager, L.R., Brown, G.M., Wadsworth, W.J., 1960. Types of igneous cumulates. Journal of Petrology 1, 73–85.
79. Wang, X., Griffin, W.L., Chen, J., Huang, P., Li, X., 2011 U and Th Contents and Th/U Ratios of Zircon in Felsic and Mafic Magmatic Rocks: Improved Zircon-Melt Distribution Coefficients. Acta Geologica Sinica 85, 164-174.

80. Weaver, B.L., Tarney, J., Windley, B., 1981. Geochemistry and petrogenesis of the Fiskenaesset anorthosite complex, southern West Greenland: nature of the parent magma. Geochimica Et Cosmochimica Acta 45, 711–725.
81. Whitney, D.L., Evans, B.W., 2010. Abbreviations for names of rock-forming minerals". American Mineralogist 94, 185-187.
82. Winchester, J.A., Floyd, P.A., 1977. Geochemical discrimination of different magma series and their differentiation products using immobile elements. Chemical Geology 20, 325-343.
83. Wyllie, P.J., 1967. Ultramafic and ultrabasic rocks, in: Wyllie, P.J. (Ed.), Ultramafic and related rocks: New York and London, John Wiley & Sons, p. 1–7.

Appendixes

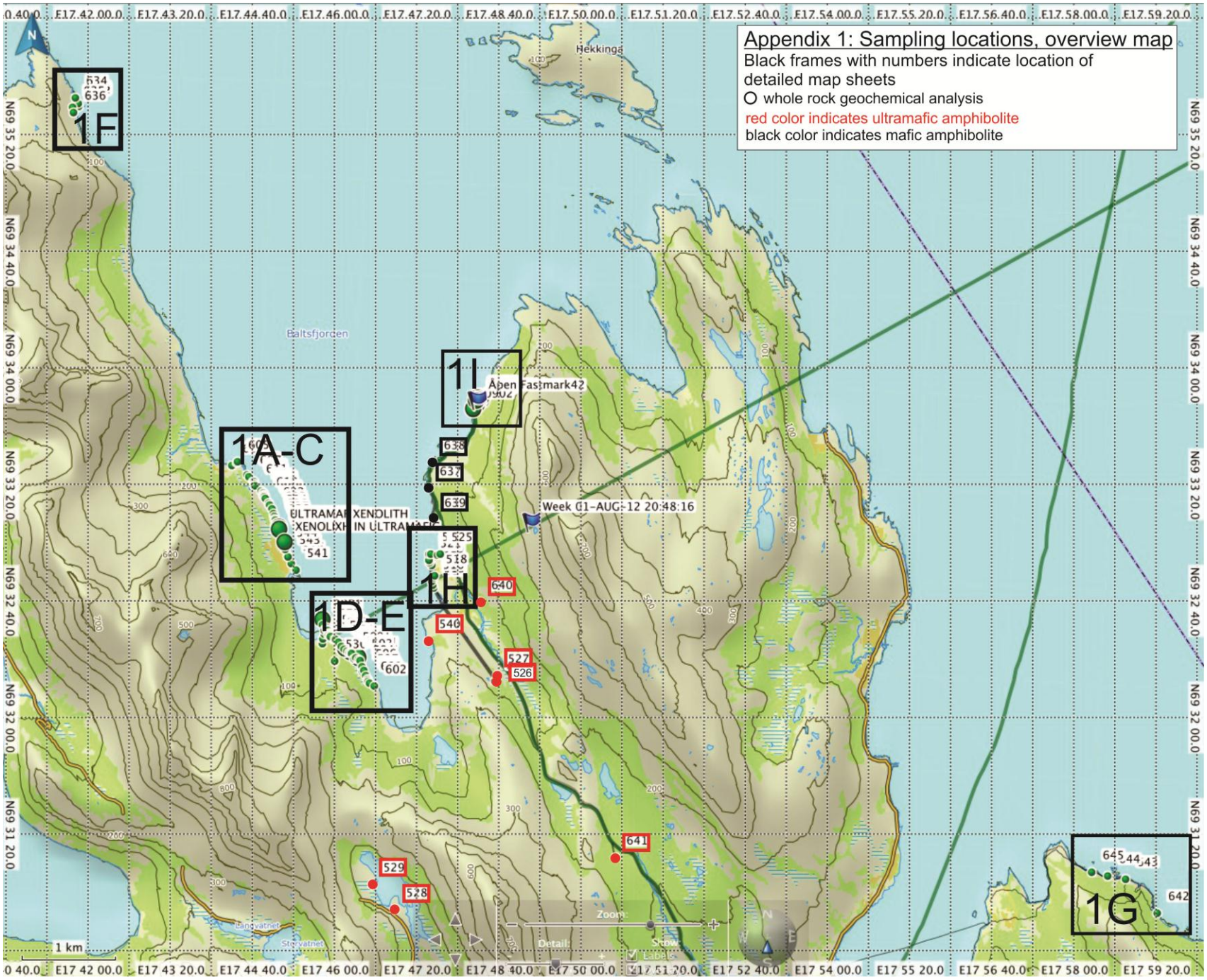
Appendix 1: Sampling locations, overview map
Black frames with numbers indicate location of detailed map sheets
O whole rock geochemical analysis
red color indicates ultramafic amphibolite
black color indicates mafic amphibolite
1F
1A-C
1D-E
1H
1I
1G
Hekkinga
Åben Fastmark42
Week 01-AUG-12 20:48:16
1 km

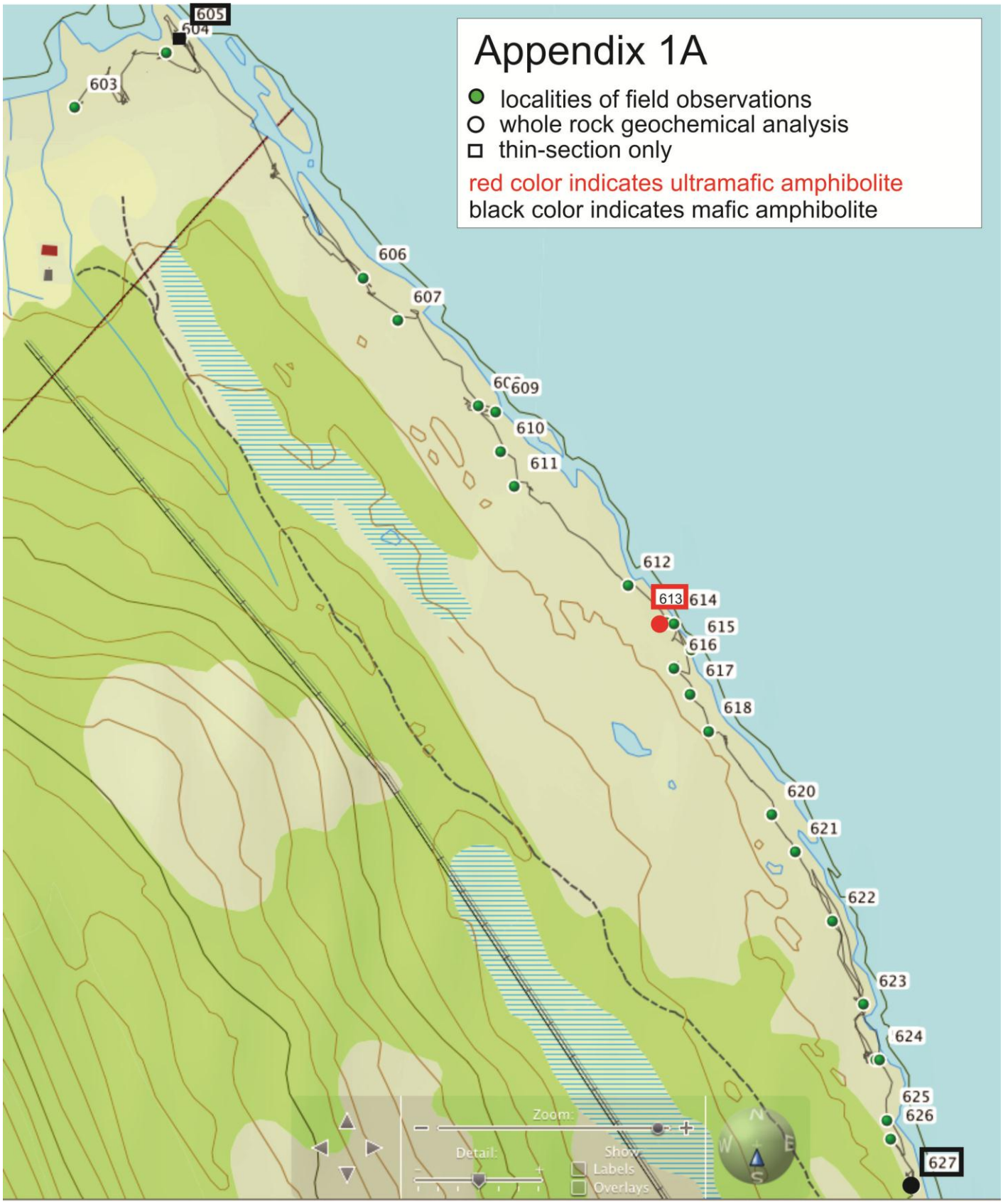
Appendix 1A
localities of field observations
whole rock geochemical analysis
thin-section only
red color indicates ultramafic amphibolite
black color indicates mafic amphibolite
605
604
603
606
607
609
610
611
612
613
614
615
616
617
618
620
621
622
623
624
625
626
627
Zoom:
Detail:
Show
Labels
Overlays
N
W
E
S

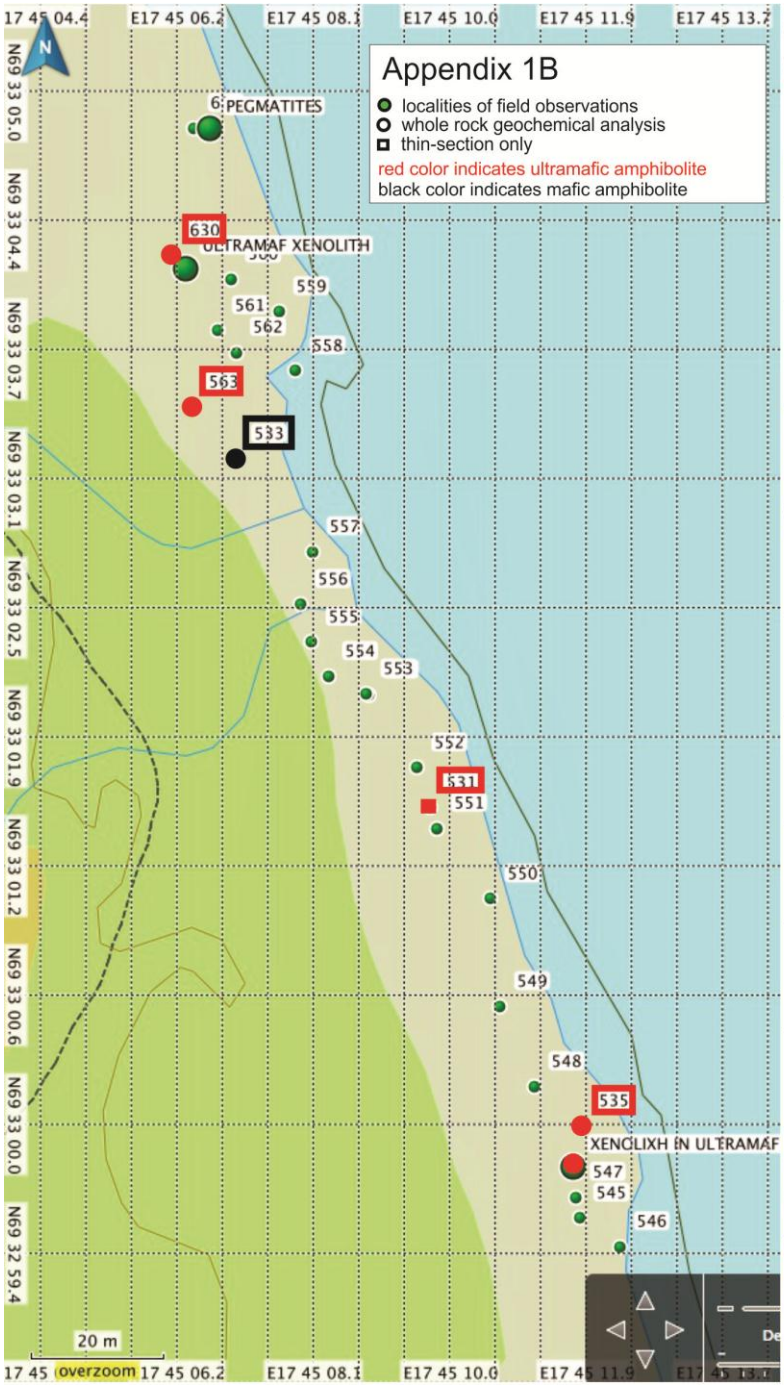
Appendix 1B
localities of field observations
whole rock geochemical analysis
thin-section only
red color indicates ultramafic amphibolite
black color indicates mafic amphibolite
PEGMATITES
630
ULTRAMAF XENOLITH
559
561
562
558
563
533
557
556
555
554
553
552
531
551
550
549
548
535
XENOLIXH IN ULTRAMAF
547
545
546
20 m
overzoom

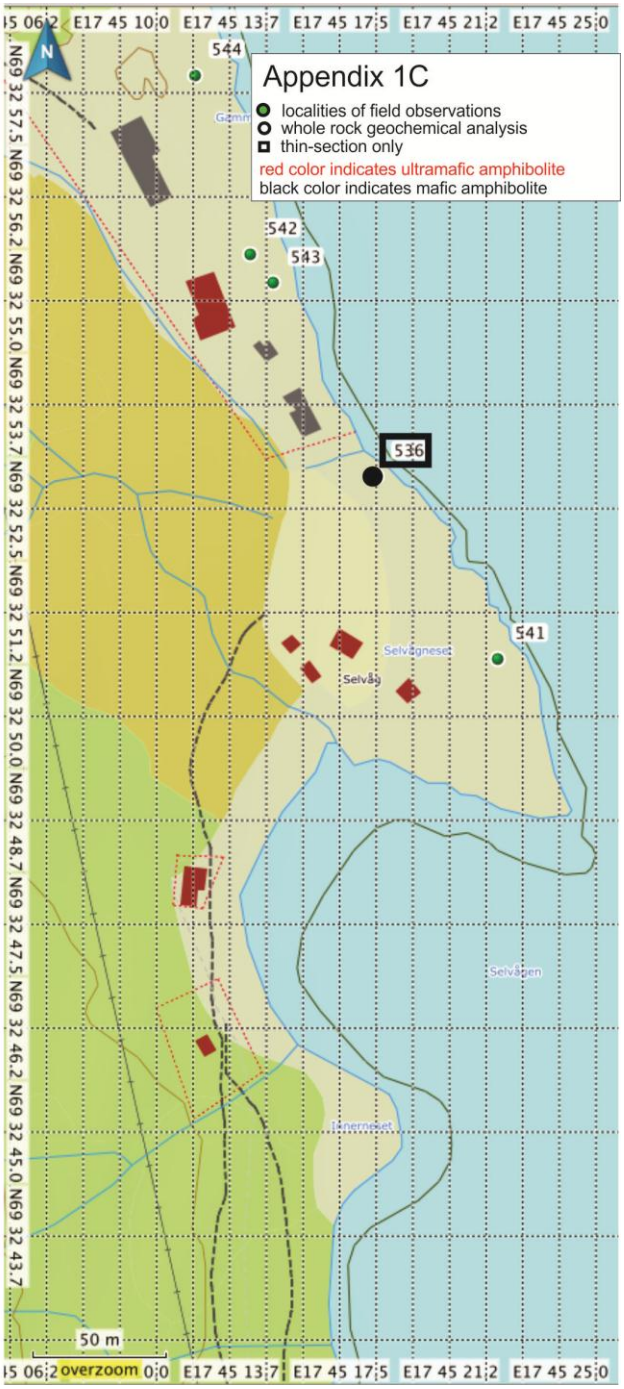
Appendix 1C
localities of field observations
whole rock geochemical analysis
thin-section only
red color indicates ultramafic amphibolite
black color indicates mafic amphibolite
544
542
543
536
541
Selvågneset
Selvåg
Selvågen
50 m
overzoom

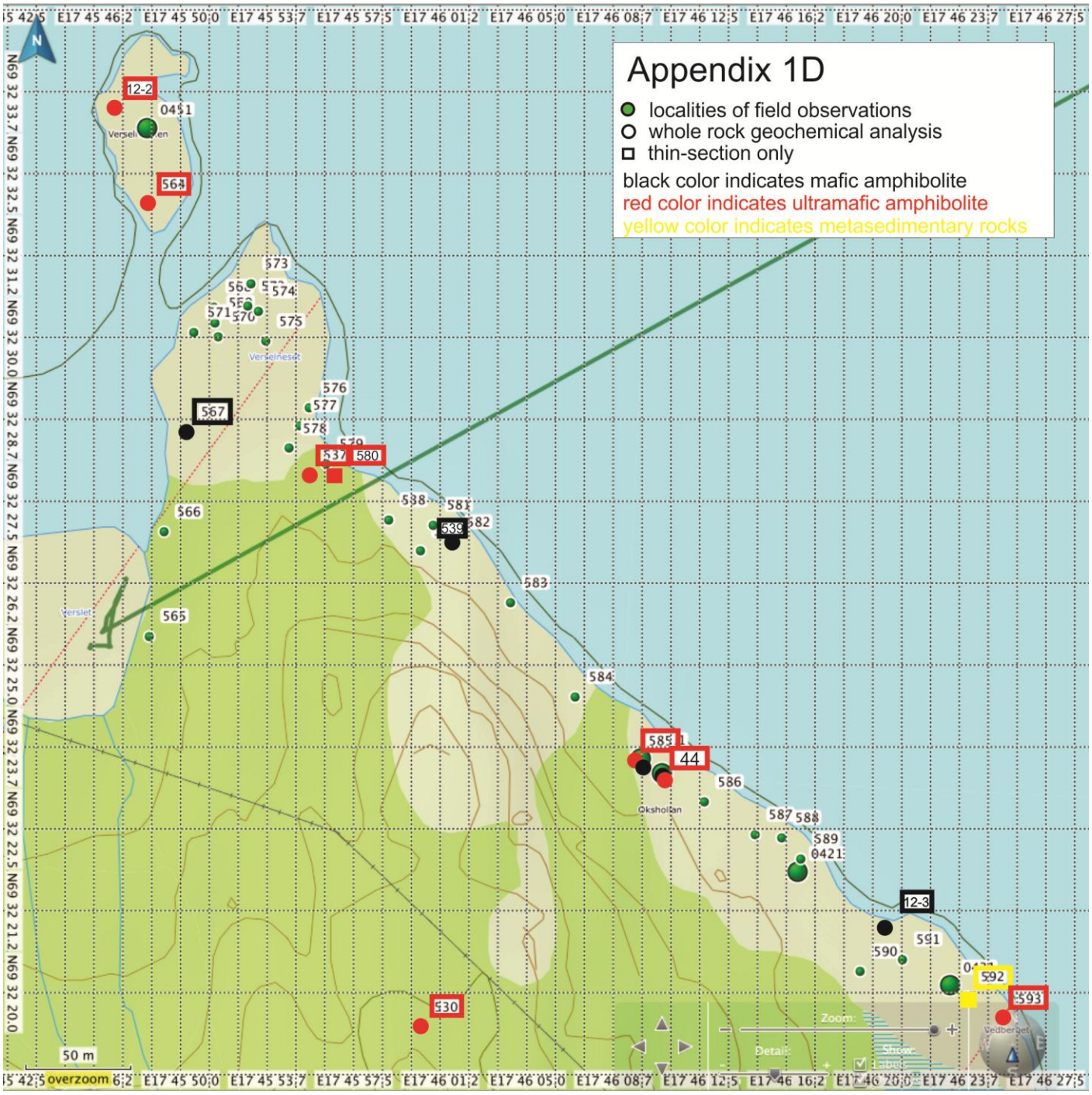
Appendix 1D
localities of field observations
whole rock geochemical analysis
thin-section only
black color indicates mafic amphibolite
red color indicates ultramafic amphibolite
yellow color indicates metasedimentary rocks
E17 45 42.5
E17 45 46.2
E17 45 50.0
E17 45 53.7
E17 45 57.5
E17 46 01.2
E17 46 05.0
E17 46 08.7
E17 46 12.5
E17 46 16.2
E17 46 20.0
E17 46 23.7
E17 46 27.5
N69 32 33.7
N69 32 32.5
N69 32 31.2
N69 32 30.0
N69 32 28.7
N69 32 27.5
N69 32 26.2
N69 32 25.0
N69 32 23.7
N69 32 22.5
N69 32 21.2
N69 32 20.0
12-2
564
567
580
44
12-3
530
50 m
overzoom 6.2

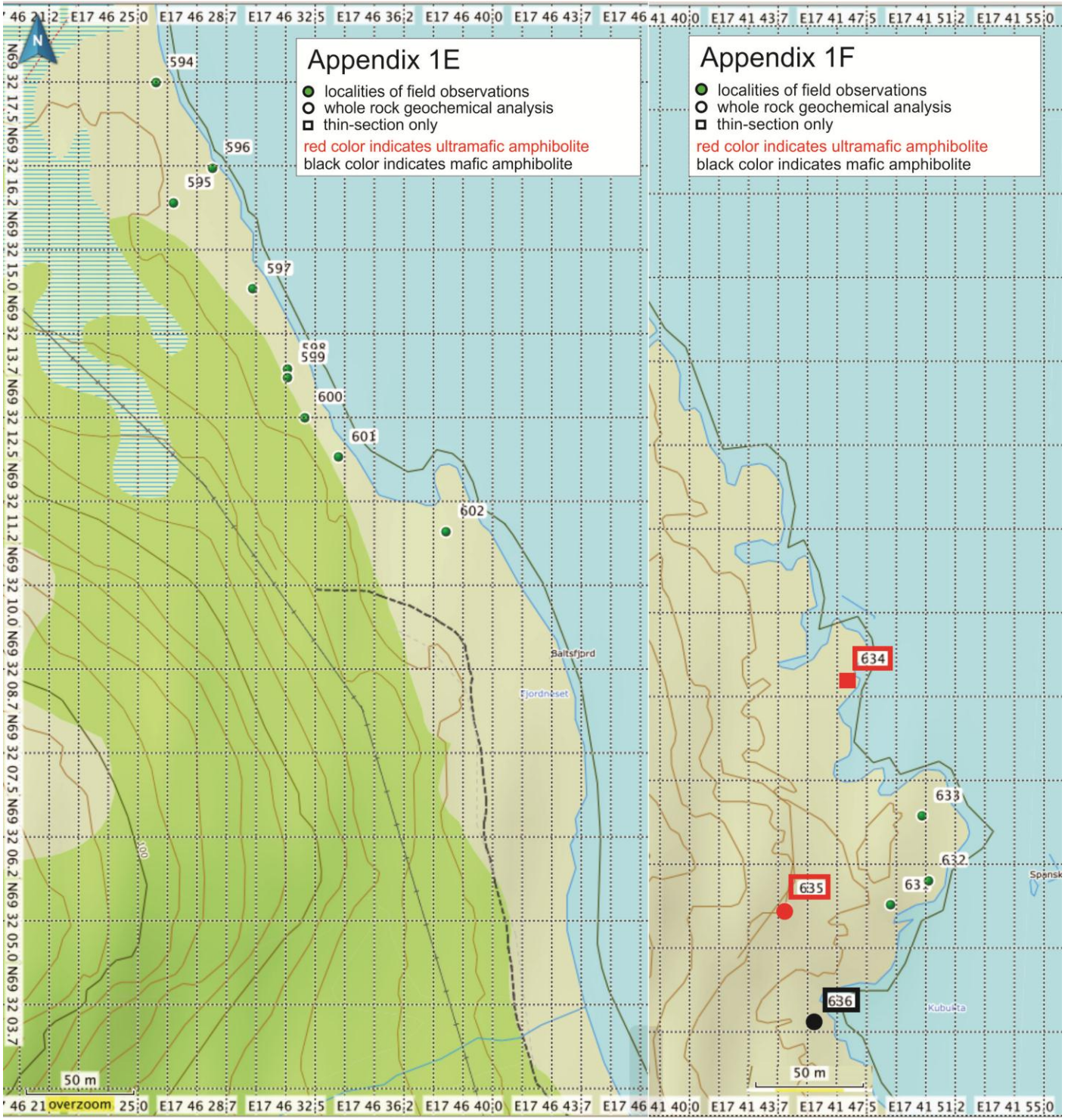
Appendix 1E
localities of field observations
whole rock geochemical analysis
thin-section only
red color indicates ultramafic amphibolite
black color indicates mafic amphibolite
Appendix 1F
localities of field observations
whole rock geochemical analysis
thin-section only
red color indicates ultramafic amphibolite
black color indicates mafic amphibolite
N
E17 46 25.0
E17 46 28.7
E17 46 32.5
E17 46 36.2
E17 46 40.0
E17 46 43.7
E17 41 40.0
E17 41 43.7
E17 41 47.5
E17 41 51.2
E17 41 55.0
N69 32 17.5
N69 32 16.2
N69 32 15.0
N69 32 13.7
N69 32 12.5
N69 32 11.2
N69 32 10.0
N69 32 08.7
N69 32 07.5
N69 32 06.2
N69 32 05.0
N69 32 03.7
594
595
596
597
599
600
601
602
634
633
632
635
636
Baltsfjord
Kjordneset
Kubukta
50 m
50 m
overzoom

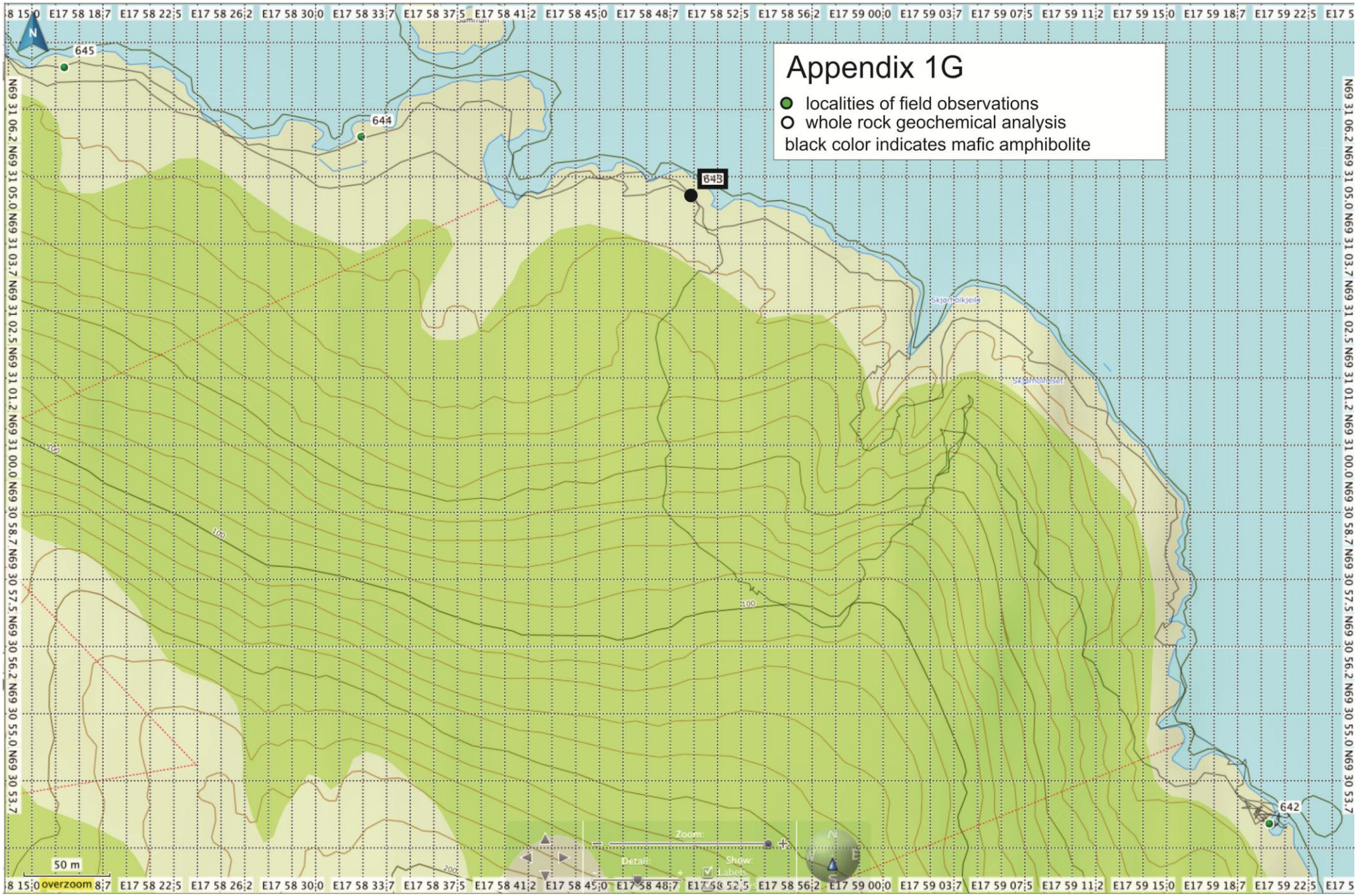
Appendix 1G
localities of field observations
whole rock geochemical analysis
black color indicates mafic amphibolite
645
644
645
642
Skjærholkjela
Skjærholmsset
50 m
overzoom
Zoom:
Detail:
Show:
Labels

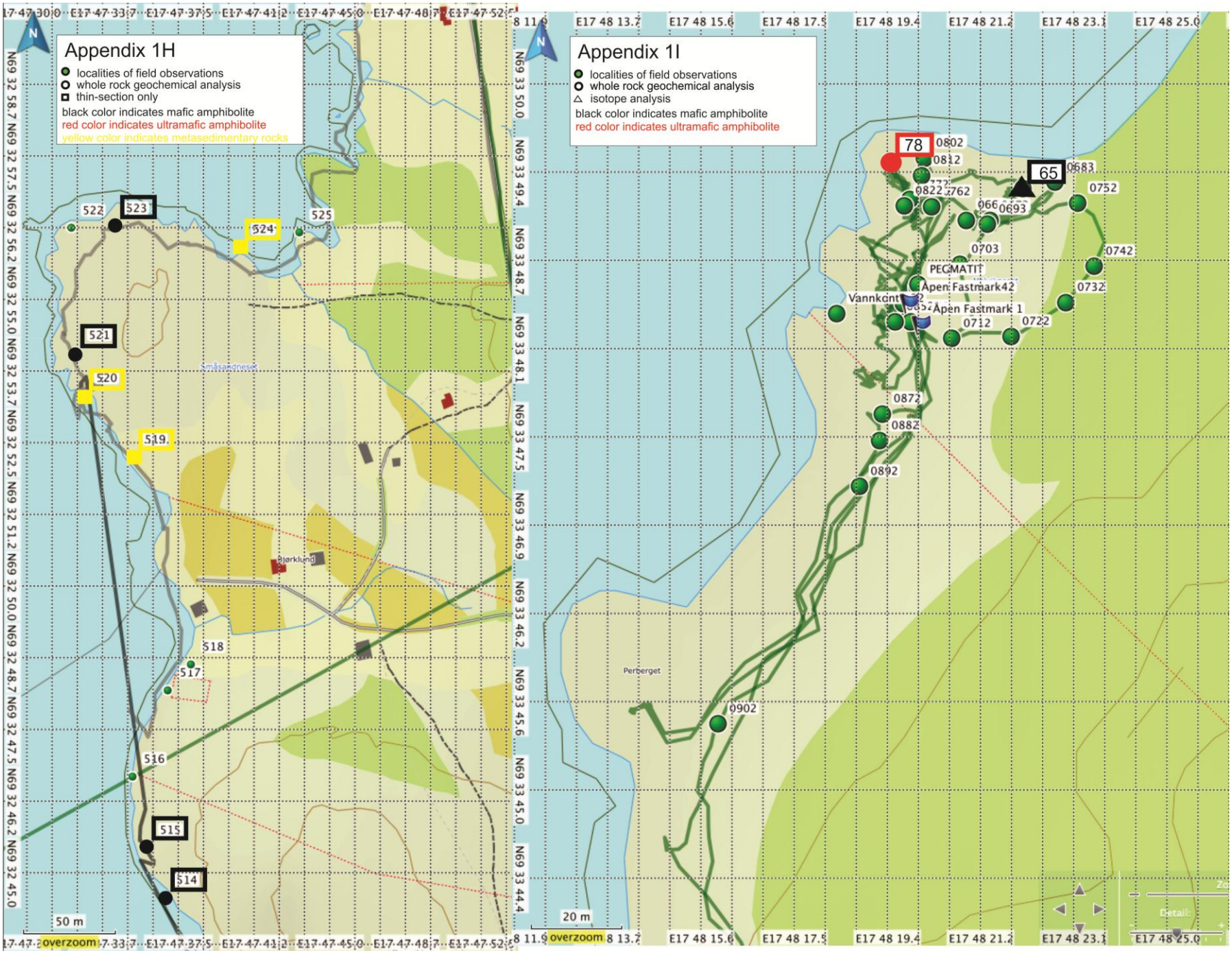
Appendix 1H
localities of field observations
whole rock geochemical analysis
thin-section only
black color indicates mafic amphibolite
red color indicates ultramafic amphibolite
yellow color indicates metasedimentary rocks
522
523
524
525
521
520
519
518
517
516
515
514
50 m
overzoom
Appendix 1I
localities of field observations
whole rock geochemical analysis
isotope analysis
black color indicates mafic amphibolite
red color indicates ultramafic amphibolite
78
65
0802
0812
0683
0752
0762
0693
0703
0742
0732
0712
0722
PEGMATITT
Åpen Fastmark42
Åpen Fastmark 1
0872
0882
0892
0902
Perberget
20 m
overzoom

Analytical technics			XRF	XRF	XRF	XRF	XRF	XRF	XRF	XRF	XRF	XRF	XRF
Element			SiO_2	TiO_2	Al_2O_3	Fe_2O_3	MnO	MgO	CaO	Na_2O	K_2O	P_2O_5	H_2O
Rock type	Sample	Lab	wt %	wt %	wt %	wt %	wt %	wt %	wt %	wt %	wt %	wt %	wt %
	514	UH	49.75	1.17	12.66	13.94	0.22	7.46	10.39	3.53	0.39	0.14	0.60
	515	UH	49.97	1.31	13.28	14.55	0.22	6.36	8.89	4.32	0.50	0.15	0.27
volcanoclastic/	521/1	UH	52.27	0.88	12.55	13.34	0.17	8.26	8.53	3.04	0.33	0.06	0.39
massive	521/2	UH	52.28	0.95	12.47	12.87	0.17	8.75	8.33	3.15	0.33	0.10	0.38
amphibolite from	523	UH	53.53	0.89	12.62	12.70	0.18	8.21	8.05	2.91	0.86	0.08	0.50
the supracrustal	636	UH	48.60	0.64	13.94	13.61	0.23	9.04	8.69	4.33	0.07	0.06	0.63
suite	637	UH	49.92	1.50	13.33	14.43	0.22	6.77	9.02	3.86	0.42	0.13	0.19
	638	UH	50.55	1.02	13.54	13.31	0.22	7.15	9.28	3.76	0.40	0.11	0.47
	639	UH	45.51	0.32	5.90	11.95	0.18	27.90	7.24	0.32	0.05	0.05	0.40
	646	UH	51.55	1.08	11.94	13.04	0.17	8.60	7.56	2.54	1.06	0.13	2.03
amphibolite	533	UH	51.06	0.92	13.38	12.67	0.25	6.73	10.20	3.32	0.87	0.14	0.30
enclaves in	536	UH	50.06	1.30	13.69	15.40	0.23	7.69	7.76	3.49	0.61	0.10	0.20
tonalitic gneiss	536	UH	50.06	1.30	13.69	15.40	0.23	7.69	7.76	3.49	0.61	0.10	0.20
amphibolite	539	UH	50.74	0.26	13.17	10.54	0.20	12.84	8.90	2.06	0.06	0.02	1.03
(metagabbroic	567	UH	48.31	1.44	10.93	15.23	0.32	9.30	10.50	2.25	0.89	0.13	0.50
rock) from the	627	UH	49.65	0.39	14.70	11.39	0.23	9.33	9.50	3.44	0.27	0.03	0.90
layered mafic-	44-2	UiT	43.00	0.37	12.74	8.60	0.16	8.16	8.85	3.32	0.12	0.05	14.51
ultramafic suite	65-2	UiT	47.40	1.27	13.66	12.56	0.38	5.84	7.43	3.85	0.43	0.21	6.91
	526	UH	44.52	0.25	5.87	11.50	0.18	31.36	4.73	0.23	0.09	0.02	0.79
	527/2	UH	43.01	0.22	5.53	10.50	0.16	28.20	5.27	0.51	1.68	0.02	4.43
	527/1	UH	42.00	0.27	5.75	11.00	0.17	28.03	5.90	0.45	1.20	0.02	4.69
	528	UH	42.43	0.16	9.79	12.02	0.20	24.79	7.22	0.56	0.12	0.02	2.21
	529	UH	39.58	0.11	11.01	12.35	0.16	26.89	5.82	0.13	0.08	0.02	3.41
	530/2	UH	44.63	0.37	5.02	11.96	0.18	28.72	5.93	0.37	0.09	0.03	2.18
	534	UH	44.29	0.22	5.40	11.65	0.22	26.55	7.30	0.74	0.11	0.02	3.06
	535/2	UH	40.47	0.38	5.70	12.51	0.30	26.46	6.30	0.41	0.15	0.04	6.74
hornblende	537	UH	48.25	0.08	6.71	10.03	0.19	23.39	8.69	0.81	0.04	0.02	1.28
peridotite, olivine	540	UH	41.89	0.05	4.95	10.02	0.17	36.48	3.49	0.26	0.65	0.01	1.36
hornblendite,	564/1	UH	42.00	0.59	8.65	12.97	0.27	24.31	7.73	0.60	0.13	0.06	2.29
spinel-bearing	593	UH	44.02	0.30	12.47	13.58	0.20	19.01	7.89	1.31	0.12	0.03	0.90
olivine pyroxene-	613	UH	43.17	0.14	8.88	9.72	0.17	23.44	8.01	0.88	0.17	0.02	4.97
hornblendite	635	UH	44.17	0.38	5.69	12.58	0.23	26.64	6.75	0.14	0.07	0.04	2.84
	641	UH	41.53	0.27	5.23	12.02	0.19	27.28	5.51	0.12	0.02	0.03	7.37
	643	UH	47.55	0.61	6.10	11.69	0.18	19.43	9.90	0.43	0.05	0.06	3.70
	646 k	UH	44.74	1.28	5.04	11.96	0.17	24.80	7.85		0.03	0.09	3.63
	s12-2-1	UiT	40.17	0.28	10.02	12.30	0.22	21.01	8.20	1.37	0.51	0.04	5.53
	65-1	UiT	47.94	0.65	7.06	9.75	0.24	11.14	22.49	0.19	0.02	0.09	0.11
	78-1	UiT	45.42	0.85	7.07	13.67	0.29	20.40	7.80	1.16	0.46	0.11	2.35
	585	UH	44.40	0.21	12.64	11.92	0.22	16.00	10.80	1.87	0.30	0.02	1.34
horblendite	s12-2-3	UiT	45.26	1.91	13.04	13.57	0.25	11.46	9.57	2.67	0.22	0.18	1.82
	44-1	UiT	46.37	0.23	11.93	11.96	0.24	15.28	10.14	1.83	0.22	0.03	1.58
greenstone	640	UH	51.80	0.63	12.99	11.11	0.21	7.10	6.70	5.15	0.18	0.08	3.92
glimmerite	s12-2-2	UiT	32.56	2.27	17.69	13.64	0.14	19.01	0.37	0.51	7.49	0.26	5.75
ultramafic xenolith	630	UH	48.180	0.257	7.598	12.900	0.547	9.145	16.730	1.110	0.713	0.119	2.077

n.a.=not analyzed

UH= University of Huelva

UiT= University of Tromsø

Note that for the samples analyzed in UiT all analysis have been processed by XRF technichs

Analytical technics			ICP-MS	ICP-MS	ICP-MS	ICP-MS	ICP-MS	ICP-MS	ICP-MS	ICP-MS	ICP-MS
Element			Li	Be	B	Sc	V	Cr	Co	Ni	Cu
Rock type	Sample	Lab	ppm	ppm	ppm	ppm	ppm	ppm	ppm	ppm	ppm
	514	UH	31.20	0.60	61.58	46.44	467.90	446.13	61.74	230.48	283.02
	515	UH	24.61	0.48	131.52	33.20	379.80	182.86	39.10	119.68	258.42
	521/1	UH									
volcanoclastic/	521/2	UH	25.38	0.32	314.69	41.34	286.98	674.58	51.26	244.95	117.30
massive amphibolite	523	UH	37.06	0.35	<0.01	52.92	404.27	669.59	65.59	<0.01	563.67
from the	636	UH	64.74	0.39	342.89	86.27	575.34	665.00	88.09	378.10	53.26
supracrustal suite	637	UH	23.61	0.42	<0.01	39.31	412.32	117.22	47.71	<0.01	473.01
	638	UH	18.74	0.40	<0.01	47.13	431.35	269.20	53.07	<0.01	433.45
	639	UH	n.a.	n.a.	n.a.	n.a.	n.a.	n.a.	n.a.	n.a.	n.a.
	646	UH	39.05	1.04	198.74	32.53	365.53	541.43	53.72	349.36	<0.01
amphibolite	533	UH	n.a.	n.a.	n.a.	n.a.	n.a.	n.a.	n.a.	n.a.	n.a.
enclaves in tonalitic	536	UH	n.a.	n.a.	n.a.	n.a.	n.a.	n.a.	n.a.	n.a.	n.a.
gneiss	536	UH	n.a.	n.a.	n.a.	n.a.	n.a.	n.a.	n.a.	n.a.	n.a.
amphibolite	539	UH	46.25	0.03	159.74	50.74	305.47	1037.73	64.97	216.05	<0.01
(metagabbroic rock)	567	UH	n.a.	n.a.	n.a.	n.a.	n.a.	n.a.	n.a.	n.a.	n.a.
from the layered	627	UH	28.83	0.16	233.08	50.16	306.97	518.71	49.20	268.36	143.58
mafic-ultramafic	44-2	UiT	n.a.	n.a.	n.a.	n.a.	n.a.	n.a.	n.a.	n.a.	n.a.
suite	65-2	UiT	n.a.	n.a.	n.a.	n.a.	n.a.	n.a.	n.a.	n.a.	n.a.
	526	UH	17.06	0.10	202.43	16.90	148.29	1522.59	89.15	2949.93	<0.01
	527/2	UH	39.01	0.91	194.44	23.11	173.61	2592.38	106.80	2896.27	<0.01
	527/1	UH	14.89	0.21	<0.01	19.83	194.56	2807.67	94.52	<0.01	<0.01
	528	UH	8.52	<0.01	159.63	21.29	141.34	1347.15	59.31	1108.02	<0.01
	529	UH	8.38	<0.01	<0.01	39.13	196.43	1269.66	77.96	<0.01	202.97
	530/2	UH	n.a.	n.a.	n.a.	n.a.	n.a.	n.a.	n.a.	n.a.	n.a.
	534	UH	6.82	0.31	95.87	23.04	168.89	2358.00	100.45	1629.12	<0.01
	535/2	UH	n.a.	n.a.	n.a.	n.a.	n.a.	n.a.	n.a.	n.a.	n.a.
hornblende	537	UH	n.a.	n.a.	n.a.	n.a.	n.a.	n.a.	n.a.	n.a.	n.a.
peridotite, olivine	540	UH	3.60	<0.01	<0.01	3.31	15.75	655.67	22.89	<0.01	<0.01
hornblendite, spinel-	564/1	UH	10.93	0.37	3.17	28.47	249.73	1765.68	113.56	4506.22	<0.01
bearing olivine	593	UH	n.a.	n.a.	n.a.	n.a.	n.a.	n.a.	n.a.	n.a.	n.a.
pyroxene-	613	UH	n.a.	n.a.	n.a.	n.a.	n.a.	n.a.	n.a.	n.a.	n.a.
hornblendite	635	UH	n.a.	n.a.	n.a.	n.a.	n.a.	n.a.	n.a.	n.a.	n.a.
	641	UH	1.77	0.07	7.19	18.56	151.29	1812.19	98.42	2619.11	33.20
	643	UH	5.94	0.25	<0.01	26.10	231.93	1418.67	76.41	1780.15	0.30
	646 k	UH	n.a.	n.a.	n.a.	n.a.	n.a.	n.a.	n.a.	n.a.	n.a.
	s12-2-1	UiT	n.a.	n.a.	n.a.	n.a.	n.a.	n.a.	n.a.	n.a.	n.a.
	65-1	UiT	n.a.	n.a.	n.a.	n.a.	n.a.	n.a.	n.a.	n.a.	n.a.
	78-1	UiT	n.a.	n.a.	n.a.	n.a.	n.a.	n.a.	n.a.	n.a.	n.a.
	585	UH	n.a.	n.a.	n.a.	n.a.	n.a.	n.a.	n.a.	n.a.	n.a.
horblendite	s12-2-3	UiT	n.a.	n.a.	n.a.	n.a.	n.a.	n.a.	n.a.	n.a.	n.a.
	44-1	UiT	n.a.	n.a.	n.a.	n.a.	n.a.	n.a.	n.a.	n.a.	n.a.
greenstone	640	UH	5.02	0.06	8.17	22.26	187.39	2471.15	103.40	2646.12	109.27
glimmerite	s12-2-2	UiT	n.a.	n.a.	n.a.	n.a.	n.a.	n.a.	n.a.	n.a.	n.a.
ultramafic xenolith	630	UH	14.976	7.067	429.758	22.639	192.181	2680.371	78.690	1991.083	431.501

n.a.=not analyzed

UH= University of Huelva

UiT= University of Tromsø

Note that for the samples analyzed in UiT all analysis have been processed by XRF technichs

Analytical technics			ICP-MS	ICP-MS	ICP-MS	ICP-MS	ICP-MS	ICP-MS	ICP-MS	ICP-MS	ICP-MS	ICP-MS
Element			Zn	Ga	Ge	As	Se	Rb	Sr	Y	Zr	Nb
Rock type	Sample	Lab	ppm	ppm	ppm	ppm	ppm	ppm	ppm	ppm	ppm	ppm
	514	UH	160.87	50.54	4.35	0.74	3.67	11.89	275.78	25.46	12.29	11.58
	515	UH	113.54	34.45	3.32	0.63	2.77	3.90	155.17	20.14	11.61	10.25
volcanoclastic/	521/1	UH										
massive	521/2	UH	98.97	22.74	2.64	0.62	2.27	4.17	114.07	16.30	40.23	3.45
amphibolite from	523	UH	170.56	173.60	4.63	0.80	3.26	30.49	171.97	21.17	13.14	5.49
the supracrustal	636	UH	190.48	22.68	4.78	4.64	4.38	2.22	145.98	33.79	58.81	2.54
suite	637	UH	151.24	53.64	4.02	1.23	4.02	3.27	156.64	25.45	10.57	5.81
	638	UH	173.65	77.45	4.33	0.87	3.23	12.35	269.46	21.57	10.37	7.64
	639	UH	n.a.	n.a.	n.a.	n.a.	n.a.	n.a.	n.a.	n.a.	n.a.	n.a.
	646	UH	115.50	178.41	3.41	1.11	2.94	27.38	111.35	20.48	23.78	1.88
amphibolite	533	UH	n.a.	n.a.	n.a.	n.a.	n.a.	n.a.	n.a.	n.a.	n.a.	n.a.
enclaves in	536	UH	n.a.	n.a.	n.a.	n.a.	n.a.	n.a.	n.a.	n.a.	n.a.	n.a.
tonalitic gneiss	536	UH	n.a.	n.a.	n.a.	n.a.	n.a.	n.a.	n.a.	n.a.	n.a.	n.a.
amphibolite	539	UH	76.68	17.59	2.53	0.11	1.96	1.22	77.58	16.18	14.01	0.36
(metagabbroic	567	UH	n.a.	n.a.	n.a.	n.a.	n.a.	n.a.	n.a.	n.a.	n.a.	n.a.
rock) from the	627	UH	183.53	16.17	2.35	0.21	2.27	5.02	87.58	18.74	10.63	0.63
layered mafic-	44-2	UiT	n.a.	n.a.	n.a.	n.a.	n.a.	n.a.	n.a.	19.00	22.00	0.00
ultramafic suite	65-2	UiT	n.a.	n.a.	n.a.	n.a.	n.a.	n.a.	n.a.	24.00	87.00	13.00
	526	UH	22.67	5.09	2.45	0.20	1.04	3.60	49.55	6.95	12.41	0.90
	527/2	UH	64.98	13.88	2.47	0.32	1.31	246.81	24.42	9.19	10.65	1.76
	527/1	UH	68.05	8.94	2.75	0.40	1.14	155.72	21.78	7.36	7.50	0.95
	528	UH	23.76	4.23	1.97	0.10	0.83	1.01	24.15	7.34	9.80	0.30
	529	UH	32.47	3.56	2.89	0.10	1.42	2.54	68.97	12.02	11.15	0.26
	530/2	UH	n.a.	n.a.	n.a.	n.a.	n.a.	n.a.	n.a.	n.a.	n.a.	n.a.
	534	UH	90.15	5.41	2.47	0.58	1.16	1.33	21.17	7.81	12.37	0.44
	535/2	UH	n.a.	n.a.	n.a.	n.a.	n.a.	n.a.	n.a.	n.a.	n.a.	n.a.
hornblende	537	UH	n.a.	n.a.	n.a.	n.a.	n.a.	n.a.	n.a.	n.a.	n.a.	n.a.
peridotite, olivine	540	UH	<0.01	3.88	0.62	<0.01	0.75	22.73	5.11	0.67	1.68	0.15
hornblendite,	564/1	UH	98.45	8.54	3.83	0.37	2.05	2.04	31.96	13.65	28.24	4.13
spinel-bearing	593	UH	n.a.	n.a.	n.a.	n.a.	n.a.	n.a.	n.a.	n.a.	n.a.	n.a.
olivine pyroxene-	613	UH	n.a.	n.a.	n.a.	n.a.	n.a.	n.a.	n.a.	n.a.	n.a.	n.a.
hornblendite	635	UH	n.a.	n.a.	n.a.	n.a.	n.a.	n.a.	n.a.	n.a.	n.a.	n.a.
	641	UH	55.30	4.46	2.52	0.39	1.01	0.17	25.27	6.36	2.69	0.82
	643	UH	63.26	6.95	2.79	0.92	1.82	0.29	24.61	11.05	2.74	2.28
	646 k	UH	n.a.	n.a.	n.a.	n.a.	n.a.	n.a.	n.a.			
	s12-2-1	UiT	n.a.	n.a.	n.a.	n.a.	n.a.	n.a.	n.a.	9.00	19.00	3.00
	65-1	UiT	n.a.	n.a.	n.a.	n.a.	n.a.	n.a.	n.a.	12.00	37.00	3.00
	78-1	UiT	n.a.	n.a.	n.a.	n.a.	n.a.	n.a.	n.a.	12.00	53.00	4.00
	585	UH	n.a.	n.a.	n.a.	n.a.	n.a.	n.a.	n.a.			
horblendite	s12-2-3	UiT	n.a.	n.a.	n.a.	n.a.	n.a.	n.a.	n.a.			
	44-1	UiT	n.a.	n.a.	n.a.	n.a.	n.a.	n.a.	n.a.	16.00	10.00	1.00
greenstone	640	UH	66.76	8.38	2.70	0.36	1.30	0.33	57.53	8.84	5.45	0.97
glimmerite	s12-2-2	UiT	n.a.	n.a.	n.a.	n.a.	n.a.	n.a.	n.a.	4.00	148.00	20.00
ultramafic xenolith	630	UH	191.930	21.866	2.702	0.761	2.428	10.028	50.890	25.223	12.176	34.510

n.a.=not analyzed

UH= University of Huelva

UiT= University of Tromsø

Note that for the samples analyzed in UiT all analysis have been processed by XRF technichs

Analytical technics			ICP-MS	ICP-MS	ICP-MS	ICP-MS	ICP-MS	ICP-MS	ICP-MS	ICP-MS	ICP-MS	ICP-MS
Element			**Mo**	**Cd**	**Sn**	**Sb**	**Cs**	**Ba**	**La**	**Ce**	**Pr**	**Nd**
Rock type	**Sample**	**Lab**	**ppm**	**ppm**	**ppm**	**ppm**	**ppm**	**ppm**	**ppm**	**ppm**	**ppm**	**ppm**
	514	**UH**	0.88	0.58	0.33	0.02	0.05	150.25	13.05	29.43	3.82	16.80
	515	**UH**	0.25	0.59	0.27	<0.01	0.04	94.68	9.32	21.25	2.88	13.16
	521/1	**UH**										
volcanoclastic/	**521/2**	**UH**	0.68	0.27	0.35	0.02	0.25	58.97	4.75	11.72	1.74	8.26
massive amphibolite	**523**	**UH**	0.75	0.67	0.21	0.03	1.84	682.35	8.23	18.83	2.66	12.37
from the	**636**	**UH**	0.70	0.37	0.33	0.32	0.17	14.31	2.58	7.63	1.28	6.93
supracrustal suite	**637**	**UH**	0.41	0.19	0.41	0.10	0.04	170.67	8.09	19.55	2.89	13.82
	638	**UH**	0.14	0.08	0.24	<0.01	0.14	266.49	8.37	19.26	2.70	12.38
	639	**UH**	n.a.	n.a.	n.a.	n.a.	n.a.	n.a.	n.a.	n.a.	n.a.	n.a.
	646	**UH**	0.49	0.07	0.38	0.04	1.46	774.42	13.11	29.29	3.68	15.87
	533	**UH**	n.a.	n.a.	n.a.	n.a.	n.a.	n.a.	n.a.	n.a.	n.a.	n.a.
amphibolite enclaves	**536**	**UH**	n.a.	n.a.	n.a.	n.a.	n.a.	n.a.	n.a.	n.a.	n.a.	n.a.
in tonalitic gneiss	**536**	**UH**	n.a.	n.a.	n.a.	n.a.	n.a.	n.a.	n.a.	n.a.	n.a.	n.a.
amphibolite	**539**	**UH**	0.56	0.12	0.07	0.02	0.02	36.22	0.65	1.53	0.25	1.59
(metagabbroic rock)	**567**	**UH**	n.a.	n.a.	n.a.	n.a.	n.a.	n.a.	n.a.	n.a.	n.a.	n.a.
from the layered	**627**	**UH**	0.53	0.18	0.24	0.02	0.06	24.07	0.99	2.38	0.37	2.09
mafic-ultramafic	**44-2**	**UiT**	n.a.	n.a.	n.a.	n.a.	n.a.	n.a.	n.a.	n.a.	n.a.	n.a.
suite	**65-2**	**UiT**	n.a.	n.a.	n.a.	n.a.	n.a.	n.a.	n.a.	n.a.	n.a.	n.a.
	526	**UH**	0.85	0.10	0.23	0.04	0.04	14.96	0.74	1.86	0.30	1.70
	527/2	**UH**	0.30	0.10	1.29	0.03	13.74	41.31	1.46	3.28	0.45	2.24
	527/1	**UH**	0.10	0.10	0.44	<0.01	8.79	15.64	0.89	2.18	0.34	1.88
	528	**UH**	0.20	0.11	0.15	<0.01	0.03	12.32	0.53	1.21	0.18	0.96
	529	**UH**	0.43	0.08	0.07	<0.01	0.06	9.07	0.32	0.72	0.12	0.72
	530/2	**UH**	n.a.	n.a.	n.a.	n.a.	n.a.	n.a.	n.a.	n.a.	n.a.	n.a.
	534	**UH**	0.40	0.06	0.30	0.03	0.07	2.75	0.56	1.44	0.26	1.56
	535/2	**UH**	n.a.	n.a.	n.a.	n.a.	n.a.	n.a.	n.a.	n.a.	n.a.	n.a.
hornblende	**537**	**UH**	n.a.	n.a.	n.a.	n.a.	n.a.	n.a.	n.a.	n.a.	n.a.	n.a.
peridotite, olivine	**540**	**UH**	<0.01	<0.01	0.11	<0.01	2.30	26.44	0.30	0.52	0.06	0.26
hornblendite, spinel-	**564/1**	**UH**	0.41	0.03	0.32	<0.01	0.11	5.84	3.85	10.59	1.64	8.10
bearing olivine	**593**	**UH**	n.a.	n.a.	n.a.	n.a.	n.a.	n.a.	n.a.	n.a.	n.a.	n.a.
pyroxene-	**613**	**UH**	n.a.	n.a.	n.a.	n.a.	n.a.	n.a.	n.a.	n.a.	n.a.	n.a.
hornblendite	**635**	**UH**	n.a.	n.a.	n.a.	n.a.	n.a.	n.a.	n.a.	n.a.	n.a.	n.a.
	641	**UH**	<0.01	0.06	0.09	0.04	0.04	0.67	1.02	2.60	0.41	2.21
	643	**UH**	<0.01	0.18	0.25	0.21	0.03	2.94	2.59	7.37	1.21	6.27
	646 k	**UH**	n.a.	n.a.	n.a.	n.a.	n.a.	n.a.	n.a.	n.a.	n.a.	n.a.
	s12-2-1	**UiT**	n.a.	n.a.	n.a.	n.a.	n.a.	n.a.	n.a.	n.a.	n.a.	n.a.
	65-1	**UiT**	n.a.	n.a.	n.a.	n.a.	n.a.	n.a.	n.a.	n.a.	n.a.	n.a.
	78-1	**UiT**	n.a.	n.a.	n.a.	n.a.	n.a.	n.a.	n.a.	n.a.	n.a.	n.a.
	585	**UH**	n.a.	n.a.	n.a.	n.a.	n.a.	n.a.	n.a.	n.a.	n.a.	n.a.
horblendite	**s12-2-3**	**UiT**	n.a.	n.a.	n.a.	n.a.	n.a.	n.a.	n.a.	n.a.	n.a.	n.a.
	44-1	**UiT**	n.a.	n.a.	n.a.	n.a.	n.a.	n.a.	n.a.	n.a.	n.a.	n.a.
greenstone	**640**	**UH**	0.28	0.19	0.15	0.02	0.03	13.05	1.45	3.58	0.57	3.07
glimmerite	**s12-2-2**	**UiT**	n.a.	n.a.	n.a.	n.a.	n.a.	n.a.	n.a.	n.a.	n.a.	n.a.
ultramafic xenolith	**630**	**UH**	1.471	0.512	2.847	0.011	0.044	52.572	4.714	11.411	1.542	6.251

n.a.=not analyzed

UH= University of Huelva

UiT= University of Tromsø

Note that for the samples analyzed in UiT all analysis have been processed by XRF technichs

Analytical technics			ICP-MS	ICP-MS	ICP-MS	ICP-MS	ICP-MS	ICP-MS	ICP-MS	ICP-MS	ICP-MS	ICP-MS
Element			Tb	Dy	Ho	Er	Tm	Yb	Lu	Hf	Ta	W
Rock type	Sample	Lab	ppm	ppm	ppm	ppm	ppm	ppm	ppm	ppm	ppm	ppm
	514	UH	0.84	4.94	1.00	2.75	0.39	2.30	0.35	0.93	0.83	0.74
	515	UH	0.68	3.96	0.81	2.17	0.32	1.86	0.28	0.73	0.68	0.18
	521/1	UH										
volcanoclastic/	521/2	UH	0.51	3.05	0.64	1.76	0.26	1.56	0.24	1.24	0.37	0.76
massive amphibolite	523	UH	0.70	4.12	0.86	2.31	0.34	1.98	0.31	0.76	0.45	<0.01
from the	636	UH	0.82	5.59	1.29	3.83	0.58	3.69	0.56	1.84	0.46	0.22
supracrustal suite	637	UH	0.82	4.89	1.02	2.79	0.41	2.41	0.37	0.76	0.67	0.02
	638	UH	0.71	4.13	0.86	2.35	0.34	2.03	0.31	0.81	0.56	<0.01
	639	UH	n.a.	n.a.	n.a.	n.a.	n.a.	n.a.	n.a.	n.a.	n.a.	n.a.
	646	UH	0.65	3.80	0.80	2.22	0.33	1.98	0.29	0.78	0.19	<0.01
amphibolite	533	UH	n.a.	n.a.	n.a.	n.a.	n.a.	n.a.	n.a.	n.a.	n.a.	n.a.
enclaves in tonalitic	536	UH	n.a.	n.a.	n.a.	n.a.	n.a.	n.a.	n.a.	n.a.	n.a.	n.a.
gneiss	536	UH	n.a.	n.a.	n.a.	n.a.	n.a.	n.a.	n.a.	n.a.	n.a.	n.a.
amphibolite	539	UH	0.38	2.64	0.62	1.83	0.28	1.76	0.27	0.60	0.15	0.07
(metagabbroic rock)	567	UH	n.a.	n.a.	n.a.	n.a.	n.a.	n.a.	n.a.	n.a.	n.a.	n.a.
from the layered	627	UH	0.44	3.08	0.73	2.10	0.32	1.99	0.30	0.62	0.11	<0.01
mafic-ultramafic	44-2	UiT	n.a.	n.a.	n.a.	n.a.	n.a.	n.a.	n.a.	n.a.	n.a.	n.a.
suite	65-2	UiT	n.a.	n.a.	n.a.	n.a.	n.a.	n.a.	n.a.	n.a.	n.a.	n.a.
	526	UH	0.23	1.34	0.30	0.79	0.12	0.70	0.11	0.46	0.07	0.13
	527/2	UH	0.27	1.72	0.38	1.02	0.16	0.92	0.14	0.46	0.39	0.10
	527/1	UH	0.25	1.45	0.31	0.84	0.13	0.72	0.11	0.37	0.11	0.28
	528	UH	0.18	1.27	0.30	0.88	0.14	0.85	0.14	0.37	0.06	0.07
	529	UH	0.25	1.86	0.47	1.46	0.24	1.45	0.23	0.45	0.04	0.07
	530/2	UH	n.a.	n.a.	n.a.	n.a.	n.a.	n.a.	n.a.	n.a.	n.a.	n.a.
	534	UH	0.24	1.48	0.32	0.87	0.13	0.76	0.12	0.48	0.14	1.01
	535/2	UH	n.a.	n.a.	n.a.	n.a.	n.a.	n.a.	n.a.	n.a.	n.a.	n.a.
hornblende	537	UH	n.a.	n.a.	n.a.	n.a.	n.a.	n.a.	n.a.	n.a.	n.a.	n.a.
peridotite, olivine	540	UH	0.04	0.15	0.05	0.09	0.03	0.09	0.02	0.12	0.02	<0.01
hornblendite, spinel-	564/1	UH	0.47	2.71	0.57	1.53	0.23	1.30	0.20	1.13	0.39	0.17
bearing olivine	593	UH	n.a.	n.a.	n.a.	n.a.	n.a.	n.a.	n.a.	n.a.	n.a.	n.a.
pyroxene-	613	UH	n.a.	n.a.	n.a.	n.a.	n.a.	n.a.	n.a.	n.a.	n.a.	n.a.
hornblendite	635	UH	n.a.	n.a.	n.a.	n.a.	n.a.	n.a.	n.a.	n.a.	n.a.	n.a.
	641	UH	0.22	1.27	0.27	0.71	0.11	0.60	0.10	0.23	0.07	0.06
	643	UH	0.39	2.23	0.46	1.22	0.18	1.03	0.15	0.23	0.21	<0.01
	646 k	UH	n.a.	n.a.	n.a.	n.a.	n.a.	n.a.	n.a.	n.a.	n.a.	n.a.
	s12-2-1	UiT	n.a.	n.a.	n.a.	n.a.	n.a.	n.a.	n.a.	n.a.	n.a.	n.a.
	65-1	UiT	n.a.	n.a.	n.a.	n.a.	n.a.	n.a.	n.a.	n.a.	n.a.	n.a.
	78-1	UiT	n.a.	n.a.	n.a.	n.a.	n.a.	n.a.	n.a.	n.a.	n.a.	n.a.
	585	UH	n.a.	n.a.	n.a.	n.a.	n.a.	n.a.	n.a.	n.a.	n.a.	n.a.
horblendite	s12-2-3	UiT	n.a.	n.a.	n.a.	n.a.	n.a.	n.a.	n.a.	n.a.	n.a.	n.a.
	44-1	UiT	n.a.	n.a.	n.a.	n.a.	n.a.	n.a.	n.a.	n.a.	n.a.	n.a.
greenstone	640	UH	0.29	1.74	0.37	0.96	0.15	0.82	0.13	0.37	0.09	0.32
glimmerite	s12-2-2	UiT	n.a.	n.a.	n.a.	n.a.	n.a.	n.a.	n.a.	n.a.	n.a.	n.a.
ultramafic xenolith	630	UH	0.515	3.386	0.765	2.519	0.459	3.501	0.593	0.616	5.709	0.908

n.a.=not analyzed

UH= University of Huelva

UiT= University of Tromsø

Note that for the samples analyzed in UiT all analysis have been processed by XRF technichs

ICP-MS	**Analytical technics**			ICP-MS	ICP-MS	ICP-MS	ICP-MS
Tl	**Element**			**Pb**	**Bi**	**Th**	**U**
ppm	**Rock type**	**Sample**	**Lab**	**ppm**	**ppm**	**ppm**	**ppm**
<0.01		**514**	**UH**	19.76	<0.01	1.94	0.45
<0.01		**515**	**UH**	20.30	<0.01	1.18	0.13
		521/1	**UH**				
<0.01	**volcanoclastic/**	**521/2**	**UH**	<0.01	<0.01	0.55	0.58
0.00	**massive amphibolite**	**523**	**UH**	5.91	<0.01	1.20	0.14
<0.01	**from the**	**636**	**UH**	<0.01	0.04	0.39	0.51
<0.01	**supracrustal suite**	**637**	**UH**	1.72	<0.01	0.55	0.01
<0.01		**638**	**UH**	<0.01	<0.01	0.86	0.01
n.a.		**639**	**UH**	n.a.	n.a.	n.a.	n.a.
<0.01		**646**	**UH**	<0.01	<0.01	1.96	0.69
n.a.	**amphibolite**	**533**	**UH**	n.a.	n.a.	n.a.	n.a.
n.a.	**enclaves in tonalitic**	**536**	**UH**	n.a.	n.a.	n.a.	n.a.
n.a.	**gneiss**	**536**	**UH**	n.a.	n.a.	n.a.	n.a.
<0.01	**amphibolite**	**539**	**UH**	3.65	<0.01	<0.01	<0.01
n.a.	**(metagabbroic rock)**	**567**	**UH**	n.a.	n.a.	n.a.	n.a.
<0.01	**from the layered**	**627**	**UH**	<0.01	0.02	0.10	0.25
n.a.	**mafic-ultramafic**	**44-2**	**UiT**	n.a.	n.a.	n.a.	n.a.
n.a.	**suite**	**65-2**	**UiT**	n.a.	n.a.	n.a.	n.a.
<0.01		**526**	**UH**	<0.01	<0.01	<0.01	<0.01
1.54		**527/2**	**UH**	<0.01	<0.01	<0.01	0.02
0.90		**527/1**	**UH**	<0.01	<0.01	<0.01	<0.01
<0.01		**528**	**UH**	<0.01	<0.01	<0.01	<0.01
<0.01		**529**	**UH**	<0.01	<0.01	<0.01	<0.01
n.a.		**530/2**	**UH**	n.a.	n.a.	n.a.	n.a.
<0.01		**534**	**UH**	<0.01	0.01	<0.01	<0.01
n.a.		**535/2**	**UH**	n.a.	n.a.	n.a.	n.a.
n.a.	**hornblende**	**537**	**UH**	n.a.	n.a.	n.a.	n.a.
<0.01	**peridotite, olivine**	**540**	**UH**	<0.01	<0.01	<0.01	<0.01
<0.01	**hornblendite, spinel-**	**564/1**	**UH**	<0.01	<0.01	0.58	<0.01
n.a.	**bearing olivine**	**593**	**UH**	n.a.	n.a.	n.a.	n.a.
n.a.	**pyroxene-**	**613**	**UH**	n.a.	n.a.	n.a.	n.a.
n.a.	**hornblendite**	**635**	**UH**	n.a.	n.a.	n.a.	n.a.
<0.01		**641**	**UH**	<0.01	<0.01	0.02	<0.01
<0.01		**643**	**UH**	<0.01	<0.01	0.12	<0.01
n.a.		**646 k**	**UH**	n.a.	n.a.	n.a.	n.a.
n.a.		**s12-2-1**	**UiT**	n.a.	n.a.	n.a.	n.a.
n.a.		**65-1**	**UiT**	n.a.	n.a.	n.a.	n.a.
n.a.		**78-1**	**UiT**	n.a.	n.a.	n.a.	n.a.
n.a.		**585**	**UH**	n.a.	n.a.	n.a.	n.a.
n.a.	**horblendite**	**s12-2-3**	**UiT**	n.a.	n.a.	n.a.	n.a.
n.a.		**44-1**	**UiT**	n.a.	n.a.	n.a.	n.a.
<0.01	**greenstone**	**640**	**UH**	<0.01	<0.01	0.04	<0.01
n.a.	**glimmerite**	**s12-2-2**	**UiT**	n.a.	n.a.	n.a.	n.a.
0.282	**ultramafic xenolith**	**630**	**UH**	<0.01	0.224	0.976	2.805

n.a.=not analyzed

UH= University of Huelva

UiT= University of Tromsø

Note that for the samples analyzed in UiT all analysis have been processed by XRF technichs

Appendix 3. Chemical analysis of minerals, page 1

Amphibole

Measured contents of major oxides, wt %									
Sample№	**593**	**593**	**593**	**593**	**593**	**593**	**593**	**585**	**585**
Analysis№	**15**	**21**	**12**	**13**	**14**	**16**	**20**	**3**	**1**
SiO_2	44.305	44.691	44.747	44.761	44.999	45.008	45.262	45.275	45.517
Al_2O_3	13.71	13.651	13.499	13.018	13.292	13.813	12.986	13.989	12.951
TiO_2	0.619	0.441	0.424	0.422	0.428	0.386	0.453	0.38	0.24
Cr_2O_3	0.05	0.023	0.016	0.037	0.072	0	0	0.076	0.129
FeO[a]	9.557	9.352	9.648	9.661	9.572	9.478	9.638	10.842	11.259
MgO	15.441	15.453	15.673	15.624	15.895	15.452	16.094	13.722	14.436
MnO	0.115	0.177	0.128	0.169	0.089	0.132	0.205	0.229	0.209
NiO	0.107	0.049	0.097	0.016	0.012	0.088	0	0.05	0.019
CaO	11.144	11.22	11.104	10.885	11.019	11.004	10.756	11.213	11.126
BaO	0.072	0	0.106	0.116	0.111	0.169	0.3	0.164	0
Na_2O	1.999	2.023	2.092	2.09	2.119	2.042	2.026	1.966	1.969
K_2O	0.186	0.203	0.191	0.18	0.217	0.198	0.195	0.44	0.348
Total	97.305	97.283	97.725	96.979	97.825	97.77	97.915	98.346	98.203
Number of cations per formula[c]									
Si	6.25	6.30	6.28	6.33	6.30	6.31	6.32	6.41	6.42
Al IV[b]	1.75	1.70	1.72	1.67	1.70	1.69	1.68	1.59	1.58
Al VI	0.53	0.57	0.52	0.50	0.50	0.59	0.45	0.74	0.57
Ti	0.07	0.05	0.04	0.04	0.05	0.04	0.05	0.04	0.03
Cr	0.01	0.00	0.00	0.00	0.01	0.00	0.00	0.01	0.01
Fe	1.13	1.10	1.13	1.14	1.12	1.11	1.12	1.28	1.33
Mg	3.25	3.25	3.28	3.29	3.32	3.23	3.35	2.89	3.03
Mn	0.01	0.02	0.02	0.02	0.01	0.02	0.02	0.03	0.02
Ni	0.01	0.01	0.01	0.00	0.00	0.01	0.00	0.01	0.00
Total T + C si	13.00	13.00	13.00	13.00	13.00	13.00	13.00	13.00	13.00
Ca	1.68	1.70	1.67	1.65	1.65	1.65	1.61	1.70	1.68
Ba	0.00	0.00	0.01	0.01	0.01	0.01	0.02	0.01	0.00
Na	0.31	0.30	0.32	0.35	0.34	0.34	0.38	0.29	0.32
Total B site	2.00	2.00	2.00	2.00	2.00	2.00	2.00	2.00	2.00
Na	0.23	0.25	0.24	0.23	0.23	0.22	0.17	0.25	0.22
K	0.03	0.04	0.03	0.03	0.04	0.04	0.03	0.08	0.06
Total A site	0.27	0.28	0.28	0.26	0.27	0.25	0.21	0.33	0.28

[a]FeO expresses total iron

[b]Al IV (Al in tetrahedral site) is calculated as the difference between 8.0 cations (full tetrahedral occupancy) and the number of Si cations

[c]Formula calculated on the basis of 13 cations (T+C sites)

Appendix 3. Chemical analysis of minerals, page 2

Amphibole

Measured contents of major oxides, wt %									
Sample№	**585**	**613**	**535_2**	**535_2**	**641**	**526**	**526**	**526**	**641**
Analysis№	**2**	**1**	**3**	**4**	**3**	**11**	**10**	**9**	**8**
SiO_2	45.584	46	47.128	48.809	48.825	48.963	49.35	49.371	49.426
Al_2O_3	13.23	10.451	10.548	10.703	8.675	9.687	9.289	8.887	8.06
TiO_2	0.38	0.339	0.593	0.538	0.162	0.499	0.551	0.487	0.356
Cr_2O_3	0.201	0.373	0.337	0.39	0.464	0.227	0.171	0	0.391
FeO[a]	10.484	7.923	5.552	5.72	5.931	5.141	4.635	4.998	5.561
MgO	14.517	16.958	18.073	17.168	19.088	19.012	19.387	19.304	18.862
MnO	0.177	0.226	0.215	0.203	0.166	0.118	0.063	0.135	0.073
NiO	0.037	0	0.08	0	0.072	0	0.1	0.053	0.074
CaO	11.319	11.83	12.957	12.425	11.874	12.281	12.899	12.633	12.174
BaO	0.033	0.078	0.196	0.019	0.142	0	0	0.255	0
Na_2O	1.896	2.392	1.165	1.079	1.412	1.202	1.08	0.995	1.388
K_2O	0.273	0.315	0.325	0.325	0.315	0.285	0.287	0.194	0.169
Total	98.131	96.885	97.169	97.379	97.126	97.415	97.812	97.312	96.534
Number of cations per formula[c]									
Si	6.43	6.58	6.65	6.85	6.81	6.80	6.84	6.88	6.96
Al IV[b]	1.57	1.42	1.35	1.15	1.19	1.20	1.16	1.12	1.04
Al VI	0.63	0.34	0.41	0.62	0.24	0.38	0.36	0.34	0.29
Ti	0.04	0.04	0.06	0.06	0.02	0.05	0.06	0.05	0.04
Cr	0.02	0.04	0.04	0.04	0.05	0.02	0.02	0.00	0.04
Fe	1.24	0.95	0.66	0.67	0.69	0.60	0.54	0.58	0.65
Mg	3.05	3.61	3.80	3.59	3.97	3.93	4.01	4.01	3.96
Mn	0.02	0.03	0.03	0.02	0.02	0.01	0.01	0.02	0.01
Ni	0.00	0.00	0.01	0.00	0.01	0.00	0.01	0.01	0.01
Total T + C si	13.00	13.00	13.00	13.00	13.00	13.00	13.00	13.00	13.00
Ca	1.71	1.81	1.96	1.87	1.77	1.83	1.92	1.88	1.83
Ba	0.00	0.00	0.01	0.00	0.01	0.00	0.00	0.01	0.00
Na	0.29	0.18	0.03	0.13	0.22	0.17	0.08	0.10	0.17
Total B site	2.00	2.00	2.00	2.00	2.00	2.00	2.00	2.00	2.00
Na	0.23	0.48	0.29	0.16	0.16	0.15	0.21	0.17	0.21
K	0.05	0.06	0.06	0.06	0.06	0.05	0.05	0.03	0.03
Total A site	0.28	0.54	0.35	0.22	0.22	0.20	0.26	0.20	0.24

[a]FeO expresses total iron

[b]Al IV (Al in tetrahedral site) is calculated as the difference between 8.0 cations (full tetrahedral occupancy) and the number of Si cations

[c]Formula calculated on the basis of 13 cations (T+C sites)

Appendix 3. Chemical analysis of minerals, page 3

Amphibole

Measured contents of major oxides, wt %									
Sample№	**526**	**605**	**605**	**531a**	**531a**	**529**	**605**	**529**	**529**
Analysis№	**2**	**4**	**3**	**9**	**5**	**2**	**10**	**3**	**13**
SiO_2	49.766	50.269	50.993	52.66	52.933	53.11	53.124	53.403	53.449
Al_2O_3	8.909	8.21	8.705	6.59	4.891	8.518	3.871	8.031	7.987
TiO_2	0.468	0.088	0.195	0.344	0.084	0.422	0.182	0.421	0.363
Cr_2O_3	0.113	0.014	0.112	0.574	0.054	0.074	0.278	0.095	0.032
FeO[a]	4.899	9.184	9.22	4.956	4.278	5.02	5.12	4.855	4.686
MgO	19.45	15.766	15.663	19.079	21.13	18.156	20.923	18.168	19.516
MnO	0.125	0.219	0.247	0.121	0.104	0.12	0.174	0.079	0.135
NiO	0.071	0	0.139	0.086	0.073	0.061	0.008	0.102	0.08
CaO	12.437	12.246	11.642	11.39	12.497	12.003	12.389	12.02	12.638
BaO	0.049	0	0	0.132	0.069	0	0.024	0	0.098
Na_2O	1.047	0.853	0.89	1.12	1.022	0.446	1.321	0.571	0.525
K_2O	0.231	0.201	0.397	0.272	0.126	0.179	0.112	0.146	0.19
Total	97.565	97.05	98.203	97.324	97.261	98.109	97.526	97.891	99.699
Number of cations per formula[c]									
Si	6.89	7.15	7.14	7.29	7.32	7.27	7.37	7.34	7.21
Al IV[b]	1.11	0.85	0.86	0.71	0.68	0.73	0.63	0.66	0.79
Al VI	0.34	0.53	0.58	0.37	0.12	0.65	0.01	0.64	0.48
Ti	0.05	0.01	0.02	0.04	0.01	0.04	0.02	0.04	0.04
Cr	0.01	0.00	0.01	0.06	0.01	0.01	0.03	0.01	0.00
Fe	0.57	1.09	1.08	0.57	0.49	0.57	0.59	0.56	0.53
Mg	4.01	3.34	3.27	3.94	4.35	3.71	4.33	3.72	3.92
Mn	0.01	0.03	0.03	0.01	0.01	0.01	0.02	0.01	0.02
Ni	0.01	0.00	0.02	0.01	0.01	0.01	0.00	0.01	0.01
Total T + C si	13.00	13.00	13.00	13.00	13.00	13.00	13.00	13.00	13.00
Ca	1.84	1.87	1.75	1.69	1.85	1.76	1.84	1.77	1.83
Ba	0.00	0.00	0.00	0.01	0.00	0.00	0.00	0.00	0.01
Na	0.15	0.13	0.25	0.30	0.15	0.24	0.16	0.23	0.17
Total B site	2.00	2.00	2.00	2.00	2.00	2.00	2.00	2.00	2.00
Na	0.13	0.10	-0.01	0.00	0.13	-0.12	0.20	-0.08	-0.03
K	0.04	0.04	0.07	0.05	0.02	0.03	0.02	0.03	0.03
Total A site	0.17	0.14	0.06	0.04	0.15	-0.09	0.22	-0.05	0.00

[a]FeO expresses total iron

[b]Al IV (Al in tetrahedral site) is calculated as the difference between 8.0 cations (full tetrahedral occupancy) and the number of Si cations

[c]Formula calculated on the basis of 13 cations (T+C sites)

Amphibole

Measured contents of major oxides, wt %										
Sample№	**527**	**527**	**527**	**531a**	**529**	**613**	**605**	**531a**	**605**	**605**
Analysis№	**3**	**6**	**5**	**7**	**1**	**2**	**12**	**4**	**18**	**16**
SiO_2	53.67	54.063	54.385	55.172	55.546	56.189	56.606	58.572	58.612	58.852
Al_2O_3	5.401	5.013	3.771	5.407	6.465	3.149	0.749	1.555	0.938	0.911
TiO_2	0.243	0.207	0.161	0	0.287	0.166	0	0.02	0.063	0.014
Cr_2O_3	0.222	0.107	0.212	0.074	0.071	0.007	0.058	0.027	0	0.072
FeO[a]	4.621	4.63	4.143	4.537	4.39	5.631	4.101	3.59	4.372	4.172
MgO	19.503	19.308	21.874	19.566	19.161	20.236	22.365	21.533	22.254	21.414
MnO	0.122	0.184	0.127	0.073	0.158	0.115	0.265	0.208	0.226	0.135
NiO	0.098	0.08	0.104	0.063	0.129	0.047	0.059	0.128	0.069	0.029
CaO	11.7	11.407	12.268	11.587	12.265	11.899	12.241	12.009	12.197	11.707
BaO	0.097	0.107	0.137	0	0	0.039	0	0	0.103	0
Na_2O	1.073	0.996	0.839	0.989	0.366	0.747	0.256	0.34	0.324	0.331
K_2O	0.206	0.134	0.087	0.166	0.112	0.092	0.037	0.03	0.053	0.065
Total	96.956	96.236	98.108	97.634	98.95	98.317	96.737	98.012	99.211	97.702
Number of cations per formula[c]										
Si	7.46	7.55	7.41	7.58	7.53	7.69	7.78	7.95	7.87	8.01
Al IV[b]	0.54	0.45	0.59	0.42	0.47	0.31	0.22	0.05	0.13	-0.01
Al VI	0.35	0.38	0.02	0.45	0.56	0.19	-0.10	0.20	0.02	0.15
Ti	0.03	0.02	0.02	0.00	0.03	0.02	0.00	0.00	0.01	0.00
Cr	0.02	0.01	0.02	0.01	0.01	0.00	0.01	0.00	0.00	0.01
Fe	0.54	0.54	0.47	0.52	0.50	0.64	0.47	0.41	0.49	0.47
Mg	4.04	4.02	4.44	4.00	3.87	4.13	4.58	4.35	4.45	4.34
Mn	0.01	0.02	0.01	0.01	0.02	0.01	0.03	0.02	0.03	0.02
Ni	0.01	0.01	0.01	0.01	0.01	0.01	0.01	0.01	0.01	0.00
Total T + C si	13.00	13.00	13.00	13.00	13.00	13.00	13.00	13.00	13.00	13.00
Ca	1.74	1.71	1.79	1.70	1.78	1.74	1.80	1.75	1.75	1.71
Ba	0.01	0.01	0.01	0.00	0.00	0.00	0.00	0.00	0.01	0.00
Na	0.25	0.29	0.20	0.30	0.22	0.25	0.20	0.25	0.24	0.29
Total B site	2.00	2.00	2.00	2.00	2.00	2.00	2.00	2.00	2.00	2.00
Na	0.04	-0.02	0.02	-0.03	-0.12	-0.06	-0.13	-0.17	-0.16	-0.21
K	0.04	0.02	0.02	0.03	0.02	0.02	0.01	0.01	0.01	0.01
Total A site	0.07	0.01	0.04	0.00	-0.10	-0.04	-0.12	-0.16	-0.15	-0.20

[a]FeO expresses total iron

[b]Al IV (Al in tetrahedral site) is calculated as the difference between 8.0 cations (full tetrahedral occupancy) and the number of Si cations

[c]Formula calculated on the basis of 13 cations (T+C sites)

Appendix 3. Chemical analysis of minerals, page 5

Spinel

Measured contents of major oxides, wt %									
Sample№	**593**	**529**	**593**	**529**	**593**	**593**	**526**	**535_2**	**535_2**
Analysis№	**24**	**6**	**22**	**7**	**23**	**25**	**14**	**6**	**8**
SiO_2	0	0.009	0.016	0.03	0.033	0.033	0.035	0.037	0.048
Al_2O_3	60.838	63.435	61.602	63.425	61.443	61.329	57.818	58.346	58.195
TiO_2	0	0	0.029	0.029	0	0.025	0.033	0	0
Cr_2O_3	0.416	1.548	0.353	1.286	0.148	0.128	5.896	4.995	5.475
FeO[a]	27.826	18.739	27.014	19.076	27.035	27.161	18.254	21.026	21.025
MgO	11.462	15.898	11.594	15.987	11.383	11.749	16.623	14.363	14.511
MnO	0.112	0.131	0.122	0.107	0.16	0.122	0.161	0.406	0.344
NiO	0.456	0.246	0.443	0.326	0.416	0.257	0.379	0.204	0.219
CaO	0.036	0	0.021	0.001	0.007	0.026	0.035	0.067	0.092
BaO	0	0.032	0.096	0	0	0	0	0	0.249
Na_2O	0	0	0.011	0.003	0	0	0	0	0.013
K_2O	0.006	0.022	0	0.001	0	0	0.007	0	0.002
Total	101.152	100.07	101.301	100.271	100.633	100.83	99.241	99.445	100.175
Number of cations per formula[d]									
Al	1.91	1.94	1.92	1.93	1.93	1.92	1.80	1.84	1.83
Cr	0.01	0.03	0.01	0.03	0.00	0.00	0.12	0.11	0.12
Fe3+[b]	0.09	0.03	0.07	0.04	0.07	0.08	0.07	0.06	0.06
Fe2+[C]	0.53	0.38	0.53	0.37	0.54	0.53	0.33	0.41	0.41
Mg	0.45	0.61	0.46	0.62	0.45	0.47	0.66	0.57	0.58
Mn	0.00	0.00	0.00	0.00	0.00	0.00	0.00	0.01	0.01
Ni	0.01	0.01	0.01	0.01	0.01	0.01	0.01	0.00	0.00

[a]FeO expresses total iron

[b]Fe3+ is calculated as the difference between 2.0 cations (full B site occupancy) and the number af Al and Cr cations

[c]Fe3+ is calculated as the differnce between total number of Fe cations and Fe3+

[d]Formula calculated on basis of 3 cations

Appendix 3. Chemical analysis of minerals, page 6

Spinel

Measured contents of major oxides, wt %					
Sample№	**529**	**535_2**	**526**	**526**	**529**
Analysis№	**8**	**5**	**16**	**15**	**12**
SiO_2	0.078	0.084	0.087	0.103	0.215
Al_2O_3	62.654	57.854	57.447	57.978	64.677
TiO_2	0	0.061	0.069	0	0
Cr_2O_3	1.447	5.001	5.37	5.96	0.688
FeO[a]	19.313	20.778	19.119	19.358	18.012
MgO	16.181	14.731	16.509	15.986	17.098
MnO	0.141	0.354	0.167	0.186	0.177
NiO	0.321	0.166	0.605	0.437	0.306
CaO	0.017	0.046	0.04	0.055	0.001
BaO	0	0.013	0	0.069	0
Na_2O	0	0	0.002	0.054	0
K_2O	0	0.028	0.016	0.007	0
Total	100.159	99.116	99.441	100.193	101.174
Number of cations per formula[c]					
Al	1.92	1.83	1.79	1.80	1.94
Cr	0.03	0.11	0.11	0.12	0.01
Fe3+[b]	0.05	0.07	0.09	0.07	0.04
Fe2+[C]	0.36	0.40	0.33	0.36	0.34
Mg	0.63	0.59	0.65	0.63	0.65
Mn	0.00	0.01	0.00	0.00	0.00
Ni	0.01	0.00	0.01	0.01	0.01

[a]FeO expresses total iron

[b]Fe3+ is calculated as the difference between 2.0 cations (full B site occupancy) and the number af Al and Cr cations

[c]Fe3+ is calculated as the differnce between total number of Fe cations and Fe3+

[d]Formula calculated on basis of 3 cations

Olivine

Measured contents of major oxides, wt %										
Sample№	**593**	**593**	**593**	**593**	**641**	**531a**	**641**	**535_2**	**535_3**	**535_4**
Analysis№	**11**	**1**	**11**	**10**	**5**	**10**	**6**	**2**	**1**	**8**
SiO_2	36.773	37.07	37.261	37.711	38.808	38.973	39.083	39.2	39.363	39.448
Al_2O_3	0	0.015	0	0.003	0.025	0.007	0.064	0.047	0.053	0
TiO_2	0	0.011	0	0	0.013	0.011	0.015	0.093	0	0.032
Cr_2O_3	0.004	0	0	0.026	0.022	0	0	0	0.035	0
FeO[a]	30.85	30.687	31.092	31.355	21.814	19.352	21.701	17.659	18.202	18.41
MgO	32.815	31.948	32.916	32.858	39.875	41.925	40.259	42.809	42.477	42.465
MnO	0.293	0.368	0.253	0.303	0.367	0.344	0.457	0.651	0.649	0.387
NiO	0.267	0.259	0.211	0.29	0.329	0.315	0.506	0.213	0.131	0.258
CaO	0	0	0	0	0.034	0.042	0.006	0.011	0.055	0
BaO	0.11	0.087	0.05	0.032	0.013	0.08	0	0.189	0	0
Na_2O	0	0	0	0	0.011	0	0	0.003	0	0
K_2O	0	0	0	0	0	0	0.009	0.008	0.007	0.018
Total	112.112	101.445	112.783	112.578	106.311	111.049	108.091	102.875	101.965	109
Number of cations per formula[b]										
Si	0.99	1.00	0.99	1.00	0.99	0.99	0.99	0.99	1.00	1.00
Al	0.00	0.00	0.00	0.00	0.00	0.00	0.00	0.00	0.00	0.00
Fe	0.69	0.69	0.69	0.69	0.47	0.41	0.46	0.37	0.38	0.39
Mg	1.31	1.29	1.31	1.30	1.52	1.59	1.52	1.61	1.60	1.60
Mn	0.01	0.01	0.01	0.01	0.01	0.01	0.01	0.01	0.01	0.01
Ni	0.01	0.01	0.00	0.01	0.01	0.01	0.01	0.00	0.00	0.01
Mg#[c]	0.65	0.65	0.65	0.65	0.77	0.79	0.77	0.81	0.81	0.80

[a]FeO expresses total iron

[b]Formula calculated on basis of 3 cations

[c]Mg# calculated as Mg/(Mg+Fe)

Olivine

Measured contents of major oxides, wt %									
Sample№	**529**	**527**	**527**	**526**	**526**	**526**	**526**	**526**	**526**
Analysis№	**4**	**7**	**8**	**7**	**8**	**6**	**1**	**5**	**4**
SiO_2	39.647	39.829	39.848	39.992	40.003	40.047	40.151	40.374	40.541
Al_2O_3	0.012	0.027	0.013	0.006	0	0.018	0	0	0
TiO_2	0	0.032	0	0	0	0.057	0.057	0.04	0
Cr_2O_3	0.018	0	0.005	0.025	0.026	0	0	0	0.049
FeO[a]	19.509	16.735	16.771	14.479	14.414	13.878	14.011	14.41	14.244
MgO	41.958	44.378	44.315	45.565	46.278	46.075	46.448	46.435	46.18
MnO	0.244	0.403	0.375	0.237	0.227	0.237	0.219	0.152	0.284
NiO	0.172	0.311	0.313	0.338	0.231	0.387	0.422	0.295	0.26
CaO	0.014	0.034	0.036	0.015	0	0	0.048	0	0
BaO	0	0	0.221	0	0.128	0	0	0	0
Na_2O	0	0	0.006	0	0	0	0	0	0
K_2O	0	0.016	0	0	0	0	0.021	0.04	0
Total	105.574	108.749	109.903	107.657	109.307	106.699	102.356	106.706	105.558
Number of cations per formula[b]									
Si	1.00	0.99	0.99	1.00	0.99	0.99	0.99	0.99	1.00
Al	0.00	0.00	0.00	0.00	0.00	0.00	0.00	0.00	0.00
Fe	0.41	0.35	0.35	0.30	0.30	0.29	0.29	0.30	0.29
Mg	1.58	1.65	1.64	1.69	1.70	1.70	1.71	1.70	1.70
Mn	0.01	0.01	0.01	0.00	0.00	0.00	0.00	0.00	0.01
Ni	0.00	0.01	0.01	0.01	0.00	0.01	0.01	0.01	0.01
Mg#[c]	0.79	0.83	0.82	0.85	0.85	0.86	0.86	0.85	0.85

[a]FeO expresses total iron

[b]Formula calculated on basis of 3 cations

[c]Mg# calculated as Mg/(Mg+Fe)

Orthopyroxene

Measured contents of major oxides, wt %									
Sample№	**593**	**593**	**593**	**641**	**529**	**529**	**641**	**529**	**641**
Analysis№	**19**	**17**	**18**	**2**	**9**	**10**	**4**	**11**	**1**
SiO_2	53.478	53.516	53.546	53.976	54.524	55.145	55.3	55.517	55.817
Al_2O_3	2.339	2.007	2.272	1.912	2.65	2.185	1.204	2.222	1.357
TiO_2	0.009	0	0.034	0.001	0.071	0.063	0	0	0
Cr_2O_3	0.002	0	0.008	0.074	0	0.005	0.096	0.046	0
FeO[a]	18.024	17.756	17.97	13.518	12.524	12.444	13.51	12.453	13.316
MgO	26.002	26.144	25.434	29.014	29.565	30.348	29.336	30.533	29.633
MnO	0.317	0.23	0.309	0.488	0.284	0.313	0.527	0.26	0.446
NiO	0.053	0.094	0.045	0	0.049	0.076	0.016	0.029	0.104
CaO	0.098	0.125	0.139	0.715	0.263	0.123	0.124	0.143	0.148
BaO	0	0.009	0.241	0.014	0	0.042	0	0.042	0
Na_2O	0.018	0	0	0.046	0.037	0.014	0	0	0
K_2O	0.002	0	0.005	0	0	0	0	0	0
Total	100.345	99.882	100.008	99.773	99.967	100.762	100.115	101.245	100.821
Number of cations per formula[b]									
Si	0.97	0.97	0.98	0.97	0.97	0.97	0.99	0.97	0.99
Al	0.05	0.04	0.05	0.04	0.06	0.05	0.03	0.05	0.03
Fe	0.27	0.27	0.27	0.20	0.19	0.18	0.20	0.18	0.20
Mg	0.70	0.71	0.69	0.78	0.78	0.80	0.78	0.80	0.78
Mn	0.00	0.00	0.00	0.01	0.00	0.00	0.01	0.00	0.01
Ni	0.00	0.00	0.00	0.00	0.00	0.00	0.00	0.00	0.00
Mg#[c]	0.72	0.72	0.72	0.79	0.81	0.81	0.79	0.81	0.80

[a]FeO expresses total iron

[b]Formula calculated on basis of 2 cations

[c]Mg# calculated as Mg/(Mg+Fe)

Orthopyroxene

Measured contents of major oxides, wt %									
Sample№	**531a**	**527**	**531a**	**527**	**526**	**526**	**531a**	**526**	**605**
Analysis№	**3**	**2**	**1**	**1**	**12**	**13**	**2**	**3**	**15**
SiO_2	56.025	56.116	56.152	56.419	56.491	56.547	56.654	56.655	57.824
Al_2O_3	0.581	0.816	0.558	0.99	1.157	1.018	0.516	1.122	0
TiO_2	0	0	0.017	0.138	0.049	0	0	0.043	0
Cr_2O_3	0.015	0.032	0.046	0.063	0.063	0.019	0.027	0.043	0
FeO[a]	12.154	11.084	11.818	11.019	9.55	9.359	12.317	9.414	14.714
MgO	30.611	31.763	30.639	31.744	32.035	33.118	30.485	32.401	22.439
MnO	0.383	0.36	0.396	0.374	0.298	0.278	0.42	0.29	0.909
NiO	0.124	0	0.01	0.072	0.047	0.167	0.043	0	0.086
CaO	0.156	0.124	0.148	0.123	0.087	0.106	0.19	0.174	0.327
BaO	0.105	0.086	0	0.014	0.091	0	0	0.067	0.014
Na_2O	0.008	0	0	0	0.002	0.004	0	0.017	0.001
K_2O	0.022	0.015	0.011	0.009	0.019	0.013	0.022	0.006	0.005
Total	100.184	100.401	99.8	100.965	99.889	100.629	100.676	100.232	96.319
Number of cations per formula[b]									
Si	0.99	0.98	1.00	0.99	0.99	0.98	1.00	0.99	1.11
Al	0.01	0.02	0.01	0.02	0.02	0.02	0.01	0.02	0.00
Fe	0.18	0.16	0.18	0.16	0.14	0.14	0.18	0.14	0.24
Mg	0.81	0.83	0.81	0.83	0.84	0.86	0.80	0.84	0.64
Mn	0.01	0.01	0.01	0.01	0.00	0.00	0.01	0.00	0.01
Ni	0.00	0.00	0.00	0.00	0.00	0.00	0.00	0.00	0.00
Mg#[c]	0.82	0.84	0.82	0.84	0.86	0.86	0.82	0.86	0.73

[a]FeO expresses total iron

[b]Formula calculated on basis of 2 cations

[c]Mg# calculated as Mg/(Mg+Fe)

Magnetite

Measured contents of major oxides, wt %				
SampleNo	**535_2**	**605**	**526_Ox**	**527**
AnalysisNo	**7**	**9**	**17**	**4**
SiO_2	0.062	0.098	0.118	0.306
Al_2O_3	0.804	0.024	1.1	0.5
TiO_2	0.828	1.33	1.069	0.95
Cr_2O_3	4.248	3.26	4.869	3.394
FeO[a]	84.519	87.666	84.424	84.547
MgO	0.553	0.234	1.088	0.571
MnO	0.256	0.154	0.131	0.149
NiO	0.175	0.283	0.493	0.296
CaO	0.055	0.114	0.027	0.293
BaO	0.02	0.064	0	0.152
Na_2O	0.021	0.016	0	0
K_2O	0	0	0.014	0
Total	91.541	94.638	93.356	91.159
Number of cations per formula[b]				
Al	0.04	0.00	0.05	0.02
Ti	0.02	0.04	0.03	0.03
Cr	0.13	0.10	0.15	0.11
Fe	2.76	2.83	2.69	2.79
Mg	0.03	0.01	0.06	0.03
Mn	0.01	0.01	0.00	0.00
Ni	0.01	0.01	0.02	0.01

[a]FeO expresses total iron

[b]Formula calculated on basis of 3 cations

Chlorite				Phlogopite				
Measured contents of major oxides, wt %								
SampleNo	**531a**	**605**	**605**	**SampleNo**	**605**	**527**	**527**	**605**
AnalysisNo	**6**	**5**	**6**	**AnalysisNo**	**1**	**12**	**11**	**2**
SiO_2	30.34	31.29	31.545	**SiO_2**	39.861	39.912	40.106	40.416
Al_2O_3	20.02	16.152	16.005	**Al_2O_3**	16.311	14.779	14.523	17.411
TiO_2	0.032	0.03	0.036	**TiO_2**	1.215	0.388	0.457	0.973
Cr_2O_3	0.289	0.648	0.384	**Cr_2O_3**	0.187	0.142	0.237	0.12
FeO[a]	4.413	6.936	7.098	**FeO**[a]	11.711	4.202	4.282	12.487
MgO	30.816	30.594	30.848	**MgO**	12.667	25.544	25.257	14.646
MnO	0.085	0.05	0.005	**MnO**	0.141	0.005	0.003	0.17
NiO	0.228	0.131	0.139	**NiO**	0.142	0.15	0.209	0.136
CaO	0.067	0	0	**CaO**	0.041	0.022	0	0.024
BaO	0.009	0	0	**BaO**	0.072	0.038	0.141	0.168
Na_2O	0.02	0	0	**Na_2O**	0.118	0.46	0.519	0.041
K_2O	0.011	0.03	0.007	**K_2O**	8.525	7.981	8.17	8.634
F	0	0	0	**F**	0	0	0	0
Cl	0	0.017	0.024	**Cl**	0	0.094	0.089	0.044
Total	86.33	85.874	86.086	**Total**	90.991	93.696	93.973	95.26

[a]FeO expresses total iron

Appendix 3. Chemical analysis of minerals, page 13

Serpentine

Measured contents of major oxides, wt %									
Sample№	**605**	**605**	**605**	**605**	**605**	**527**	**605**	**527**	**641**
Analysis№	**14**	**7**	**8**	**11**	**13**	**9**	**17**	**10**	**7**
SiO_2	38.5	38.547	38.977	39.08	39.439	41.013	41.381	41.617	42.342
Al_2O_3	0.028	0	0.047	0	0.05	0.388	0.622	0.023	0.055
TiO_2	0.035	0	0	0	0	0	0	0.009	0.045
Cr_2O_3	0.019	0.011	0	0.02	0.013	0.027	0.007	0	0.053
FeO[a]	19.106	19.302	16.676	19.844	15.397	10.009	12.964	6.072	3.65
MgO	21.651	24.873	27.994	24.196	24.477	33.104	26.233	37.566	39.544
MnO	0.634	0.718	0.562	0.777	0.517	0.253	0.347	0.202	0.075
NiO	0.035	0.078	0.142	0.066	0.175	0.166	0.037	0.071	0.397
CaO	0.079	0.143	0.086	0.183	0.134	0.228	0.163	0.103	0.043
BaO	0.051	0.056	0	0	0.108	0	0	0.077	0.033
Na_2O	0.02	0	0.015	0.029	0.012	0.022	0.037	0	0
K_2O	0.023	0.038	0.013	0.024	0	0.046	0.017	0	0.005
F	0	0	0	0	0	0	0	0	0
Cl	0	0.043	0.128	0.072	0.093	0.127	0.069	0.096	0.046
Total	80.181	83.799	84.611	84.275	80.394	85.354	81.861	85.814	86.278

[a]FeO expresses total iron

Appendix 4. Initial U-Th-Pb ID TIMS data

Sample №[1]		**63/2 357/27**	**63/2 357/28**
Weight	**[μg]**	1	1
U	**[ppm]**	141	69
Th/U[2]		0.17	0.21
Pbcom	**[ppm]**		0.43
Pbcom[2]	**[pg]**	1.5	2.5
^{206}Pb/^{204}Pb[4]		1702	533
^{207}Pb/^{235}U[5]		4.30043	4.31207
2 σ[5]	**[abs]**	0.01542	0.03018
^{206}Pb/^{238}U[5]		0.29485	0.29445
2 σ[5]	**[abs]**	0.00072	0.00090
rho		0.79	0.61
^{207}Pb/^{206}Pb[5]		0.10578	0.10621
2 σ[5]	**[abs]**	0.00024	0.00060
^{206}Pb/^{238}U[5]	**[Ma]**	1665.7	1663.7
2 σ[5]	**[abs]**	3.6	4.5
^{207}Pb/^{235}U[5]	**[Ma]**	1693.4	1695.7
2 σ[5]	**[abs]**	2.9	5.8
^{207}Pb/^{206}Pb	**[Ma]**	1727.9	1735.4
2 σ	**[abs]**	4.1	10.3
Disc.[6]	**[%]**	4.1	4.7

[1]Characteristics of samples are given in section 6.1

[2]Th/U ratio inferred from 208/206 ratio and the age of sample

[3]Pbcom=total common Pb in sample (initial+blank)

[4]Data corrected for fractionation and blank

[5]Data corrected for fractionation, spike, blank, initial common Pb; error calculated by propagating the main sources of uncertainty

[6]Degree of discordance